The 11th
Tamura Memorial Symposium
~ Frontiers in Nanoscience ~

December 3–5, 2011

Osaka Prefecture University, Sakai, Osaka, Japan

Abstracts

Sponsors

The Taro Tamura Memorial Fund
The Murata Science Foundation
Osaka Prefecture University

The 11th Tamura Memorial Symposium

Frontiers in Nanoscience

December 3-5, 2011
Department of Physical Science,
Osaka Prefecture University, Sakai, Japan

Tamura Memorial Symposium is intended to promote international research exchanges between Japan and the United States, based on the will of the late Professor Tamura of the University of Texas at Austin. It is a biennial international symposium held alternating between the University of Texas at Austin and Japanese institutions.

The Tamura Memorial Symposium in honor of Dr. Taro Tamura, entitled "Frontiers in Nano Science" organized jointly by the Osaka Prefecture University and the University of Texas at Austin Departments of Physics and Astronomy, will be held on December 3rd – 5th at Osaka Prefecture University. This is the 11th symposium in memory of Dr. Taro Tamura.

Topics include:

- Quantum Dynamics, Quantum Control in Nanomaterials
- Optical Phenomena, Ultrafast Relaxation Processes in Nanomaterials
- Molecular Magnetism and Strongly Correlated Nanomaterials
- Spintronics in Nanomaterials
- Nonequilibrium Transport in Nanosystems

Committee members

S. Tanaka – Osaka Prefecture University, Japan (**Chair**)
K. Mizoguchi – Osaka Prefecture University, Japan
Y. Hosokoshi – Osaka Prefecture University, Japan
Y. Kubota – Osaka Prefecture University, Japan
K. Kanki – Osaka Prefecture University, Japan
Y. Kayanuma – Osaka Prefecture University, Japan
L. Reichl – The University of Texas at Austin, USA
C. -K. Shih – The University of Texas at Austin, USA
T. Petrosky – The University of Texas at Austin, USA

Sponsors

The Taro Tamura Memorial Fund,
The Murata Science Foundation,
Osaka Prefecture University.

CONTENTS

Saturday December 3, 2011

Sunday December 4, 2011

9:00 – 11:50

Session 3: Molecular Magnetism and Strongly Correlated Nanomaterials

Chairperson: A. MacDonald (*The Univ. of Texas*)

9:00 – 9:40 O-9 ***Strongly correlated fulleride superconductors***
Kosmas Prassides, *Durham University, UK*

9:40 – 10:20 O-10 ***Application of Nano-Interfaces of Molecular Spins toward Organic Electronics***
Kunio Awaga, *Nagoya University, JAPAN*

(10:20 – 10:30 *Coffee break*)

Chairperson: Y. Kubota (*Osaka Pref. Univ.*)

10:30 – 11:10 O-11 ***Study of Charge Ordering in Strongly Correlated Molecular Conductor System by Synchrotron Radiation X-ray Diffraction***
Hiroshi Sawa, *Nagoya University, JAPAN*

11:10 – 11:50 O-12 ***Arrangements and Magnetism of O_2-O_2 Dimer Adsorbed in Microprous Coordination Polymers***
Tatsuo C. Kobayashi, *Okayama University, JAPAN*

(11:50 – 13:20 *Lunch time*)

Chairperson: Y. Hosokoshi (*Osaka Pref. Univ.*)

13:20 – 14:00 O-13 ***Thermodynamic Properties of the Spin-Liquid State in Organic Charge Transfer Salts***
Yasuhiro Nakazawa, *Osaka University, JAPAN*

14:00 – 14:40 O-14 ***Magnetic Properties of the Organic S=1/2 Spin Triangle TNN***
Yasu Takano, *University of Florida, USA*

(14:40 – 15:00 *Coffee break*)

15:00 – 18:00

Session 4: Nonequilibrium Transport in Nanosystems

Chairperson: K. Shih (*The Univ. of Texas*)

15:00 – 15:40 O-15 ***Fractal Sturcture of Transport Coefficients in 1D Protein Chain***
Tomio Petrosky, *The University of Texas, USA*

15:40 – 16:20 O-16 ***Response theory around a non-equilibrium steady state in terms of full-counting statistics***
Hisao Hayakawa, *Kyoto University, JAPAN*

(16:20 – 16:40 *Coffee break*)

Chairperson: T. Petrosky (*The Univ. of Texas*)

16:40 – 17:20 O-17 ***Resonant States of a Quantum Dot System and Breaking of Time-Reversal Symmetry***
Naomichi Hatano, *The University of Tokyo, JAPAN*

17:20 – 18:00 O-18 ***Nonequilibrium transport of one-dimensional molecular chain***
Satoshi Tanaka, *Osaka Prefecture University, JAPAN*

19:00 –

Banquet (@ Hotel Dai-ichi Sakai)

Monday December 5, 2011

9:00 – 12:00

Session 5: Spintronics in Nanomaterials

Chairperson: L. Reichl (*The Univ. of Texas*)

9:00 – 9:40 O-19 ***Spontaneous Quantum Hall States in Graphene Bilayers***
Allan MacDonald, *The University of Texas, USA*

9:40 – 10:20 O-20 ***Theoretical design of topological insulators and superconductors***
Naoto Nagaosa, *The University of Tokyo, JAPAN*

(10:20 – 10:30 *Coffee break*)

Chairperson: T. Ono (*Osaka Pref. Univ.*)

10:30 – 11:10 O-21 ***Ferrimagnetism Induced by Spontaneous Atomic Ordering in Epitaxial Double-Perovskite Films***
Akira Ohtomo, *Tokyo Institute of Technology, JAPAN*

11:10 – 11:50 O-22 ***Applications of Spin-Transfer-Torque in Spintronics***
Maxim Tsoi, *The University of Texas, USA*

11:50 – 12:00

Closing Remarks, L. Reichl, *The University of Texas, USA*

Poster session

16:50 – 18:20, Saturday December 3, 2011. *Chairperson*: H. Yamaguchi (*Osaka Pref. Univ.*)

P-1 ***Effect of Born and unitary impurity scattering on the Kramer-Pesch shrinkage of a vortex core in an s-wave superconductor***
N. Hayashi, *Osaka Prefecture University*

P-2 ***Simulation of Scanning Tunneling Microscopy with Molecular Tips***
S. Saiki and N. Hayashi, Osaka Prefecture University

P-3 ***Phase-sensitive Flux-flow Resistivity in Unconventional Superconductors***
Y. Higashi, Y. Nagai, M. Machida, and N. Hayashi, *Osaka Prefecture University*

P-4 ***Numerical analysis on stability of a time oscillating discrete state coupled with a continuum***
K. Noba, *Osaka Prefecture University*

P-5 ***Complex Eigenvalue Problem of Floquet Hamiltonian of Driven Friedrichs Model***
N. Yamada, S. Tanaka, K. Noba, and T. Petrosky, *Osaka Prefecture University*

P-6 ***Complex Eigenvalue Problem of Liouvillian forWeakly Coupled One-dimensional Quantum Lorentz Gas***
K. Hashimoto, Y. Sakaguchi, K. Kanki, S. Tanaka, and T. Petrosky, *Osaka Prefecture University*

P-7 ***Photo-induced relaxation dynamics of spin-electron coupled systems***
W. Koshibae, N. Furukawa, and N. Nagaosa, *RIKEN*

P-8 ***Scattering control of Bloch electrons under an oscillating external field***
Y. Mizumoto and Y. Kayanuma, *Osaka Prefecture University*

P-9 ***Spectroscopy of quasi-particle bound states around a pair of half-quantum vortices in triplet p-wave ($p_x \pm ip_y$) superconductors***
Y. Niwa, M. Kato, and K. Maki, *Osaka Prefecture University*

P-10 ***Double Cluster Model Study of NiO 2p X-ray Photoemission Spectroscopy and Resonant Inelastic X-ray Scattering***
A. Hariki and T. Uozumi, *Osaka Prefecture University*

P-11 ***Non-phenomenological Impurity Model Analysis of Resonant Inelastic X-ray Scattering for 3d System***
Y. Kawano and T. Uozumi, *Osaka Prefecture University*

P-12 ***A Non-phenomenological Framework for X-ray Spectroscopy Analysis - Theoretical Scheme and Application to 3d Systems -***
T. Uozumi, *Osaka Prefecture University*

P-13 ***Raman Scattering Emission from Silicon High-Q Photonic Crystal Nanocavities***
Y. Takahashi, R. Terawaki, M. Chihara, T. Asano, Y. Inui, and S. Noda, *Osaka Prefecture University*

P-14 ***Role of non-radiative relaxation process in formation of organic nano-particles by liquid laser ablation***
I. Akimoto, M. Ohata, N. Ozaki and G. Ping, *Wakayama University*

P-15 ***Structural change of single-walled carbon nanotubes induced by soft x-ray irradiation***
K. Asai, T. Murakami, and C. Itoh, *Wakayama University*

P-16 ***Free exciton luminescence of anthracene nanocrystals***
M. Yamashita, T. Kawai, and K. Mizoguchi, *Osaka Prefecture University*

Oral Presentations

Dynamic Control of Quantum Structures

L.E. Reichl
Center for Complex Quantum Systems
The University of Texas at Auatin
reichl@mail.utexas.edu

When intense laser radiation interacts with nanometer scale structures, such as carbon nanotubes or graphene stripes, the energy band structure is largely destroyed. However, the Floquet-Bloch (FB) band structure remains intact, because such systems maintain discrete time and space translational invariance. As the intensity of the radiation is increased, the FB band structure is altered significantly. It is known that when intense laser radiation interacts with matter, it changes the topological structure and dynamical behavior of the matter-radiation *phase space*. The structural changes to the phase space can include regions of chaos and the appearance of dynamic potential wells that trap classical orbits and create locally bound quantum states. These *light-induced dynamical structures* are robust because of the time-translational invariance of such systems.

In this talk, we describe the changes induced in the band structure of spatially periodic systems, such as single walled carbon nanotubes, by intense laser radiation and discuss the possibility of using these structural changes to control their dynamical properties.

1. Han Hsu and L.E. Reichl, "Floquet-Bloch states, quasienergy bands, and high-order harmonic generation for single-walled carbon nanotubes under intense laser fields," Phys.Rev. B **74** 115406 (2006).

2. Han Hsu and L.E. Reichl, "Selection rule for the optical absorption of graphene nanoribbons," Phys.Rev. B **76** 045418 (2007).

3. B.P. Holder and L. E. Reichl, "Stimulated-Raman-adiabatic passage-like transitions in a harmonically modulated optical lattice," Phys. Rev. A **76** 013420 (2007).

4. Wenjun Li and L.E. Reichl, "Transport in Strongly Driven Heterostructures and Bound-state-induced Dynamics Processes," Phys. Rev. B **62** 8269 (2000).

5. G.A., Luna-Acosta, Kyungsun Na, L.E. Reichl, and A. Krokhin, "Band structure and quantum Poincare sections of a classically chaotic quantum rippled channel," Phys. Rev. E **53** 3271 (1996).

6. Analahba Roy and L.E. Reichl, "Quantum control of interacting bosons in a periodic optical lattice," Physica E **42** 1627 (2010).

Nontrivial role of a quantum phase in driven dynamics

Yosuke Kayanuma
Research Organization for the 21st Century, Osaka Prefecture University, and JST-CREST, Japan
kayanuma@pe.osakafu-u.ac.jp

Recent advances in nano physics and the ultrafast laser physics made it possible to investigate peculiar *coherent* quantum dynamics under external driving fields. The technique of coherent control of quantum systems is prerequisite also for realization of the ideas of quantum information processing. In this presentation, I would like to review some recent studies, experimental as well as theoretical, of nonadiabatic coherent controls, and then report our proposal of a new scheme for coherent control of Bloch electrons.

The keyword of my talk is the quantum phase interference in repeated level-crossings under driving fields. This is related with the old topic of the Landau-Zener transition [1]. The effect of phase interference in nonadiabatic transitions under repeated level crossings in driven quantum system [2] has been realized in superconducting qubits [3] recently. This effect may be utilized for the qubit control as a *correlated Landau-Zener gate* [4].

It was shown that the so called dynamic localization (DL) [5] and the coherent destruction of tunneling (CDT) [6] are understood from a unified view point of the Mach-Zehnder destructive interference in the time-domain [7]. The experimental observations of DL and CDT have recently been achieved in the BEC loaded in optical lattices [8].

We have recently proposed a new type of coherent control scheme for Bloch band named a dynamical band-gap collapse. It is shown that a band gap in one-dimensional insulators may be collapsed to zero by applying a monochromatic oscillating field [9]. As shown in Fig.1, the CDT and the dynamical band-gap collapse are regarded as a result of destructive interference (Mach-Zehnder interferometry) *in the real space* (a) and *in the momentum space* (b), respectively, under the repeated level crossings.

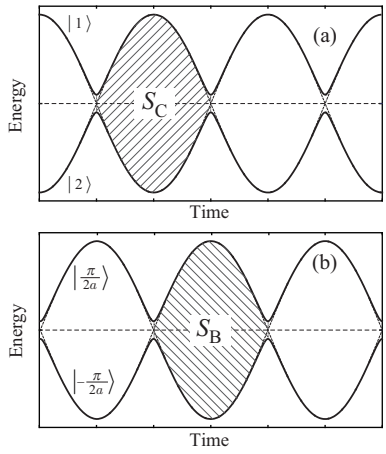

Figure 1: The schematic plot of the time-evolution of the adiabatic energies for the two-site model (a) and the tight binding model at the gap states $k = \pm\pi/2a$ in the Bloch band (b). The dynamical phase is the hatched area divided by $\hbar$.

References

[1] L. Landau, *Phys. Z. Sowjetunion* **2** (1932) 46, C. Zener, *Rroc. R. Soc. London* Ser. A **137** (1932) 696. See also, E. Majorana, *Il Nuovo Cimento* **9** (1932) 43.

[2] Y. Kayanuma, *Phys. Rev. A* **50** (1994) 843.

[3] M. Sillampää *et. al.*, *Phys. Rev. Lett.* **96** (2006) 187002, and S. N.Schevchenko, S. Ashhab and F. Nori, *Phys. Rep.* (2010) 1.

[4] K. Saito and Y. Kayanuma, *Phys. Rev. B* **70** (2004) 201304(R).

[5] D. H. Dunlap and V. M. Kenkre, *Phys. Rev. B* **34** (1986) 3625.

[6] F. Grossmann *et. al.*, *Phys. Rev. Lett.* **67** (1991) 516.

[7] Y. Kayanuma and K. Saito, *Phys. Rev. A* **77** (2008) 010101(R).

[8] E. Kierig *et. al. Phys. Rev. Lett.* **100** (2008) 190405, and A. Eckardt *et. al. Phys. Rev. A* **79** (2010) 013611.

[9] Y. Mizumoto and Y. Kayanuma, *Phys. Rev. B* **81** (2010) 233202.

Optically engineered quantum interference of delocalized excitons in solid parahydrogen

Hiroyuki Katsuki
Department of Photo-molecular Science, Institute for Molecular Science,
Aichi, 444-8585 Japan
katsuki@ims.ac.jp

Coherent control is a technique to manipulate the quantum states of atomic and molecular systems.[1,2] By combining ultrashort lasers and pulse shaping techniques, it is now possible to perform various manipulation of the amplitude and phase distribution within a wave packet of isolated atoms and molecules in the gas phase.[3-6] However, coherent control of wavefunctions in the condensed phase still remains challenging due to fast decoherence. Coherent control in the condensed phase is of great interest not only from the viewpoint of fundamental science but also for the application to the quantum information technology.

Here, we demonstrate the coherent control of ro-vibrational wavefunctions of solid para-H_2. Solid para-H_2 is often classified as a quantum solid because of the weak intermolecular interaction and large zero-point lattice motion. It is known from the previous spectroscopic studies that the ro-vibratinal quantum number of each molecule is still well defined even in the crystal. Because of the long coherence lifetime of excited states, solid para-H_2 is an ideal system to demonstrate the quantum coherent control in the condensed phase. Due to the weak but non-negligible intermolecular interactions between p-H_2 molecules, the rotational and vibrational excited states of solid p-H_2 form band structures. As a result, wavefunctions of excited states are delocalized in the crystal. We tried to demonstrate the manipulation of such delocalized quantum states within the crystal.

Experiments are performed based on CARS scheme. Combining two femtosecond pulses with 600 nm (pump) and 800 nm (Stokes), a ro-vibrational wave packet is generated by impulsive Raman excitation. After some delay τ, another pair of pump and Stokes pulses generates second wave packet. By precisely tuning the delay τ, we can create various mixtures of ground state wave function and (v=1, k=0, J=0) and (v=1, k=0, J=2) excited state wavefunctions within the p-H_2 crystal, where k is the wave vector of the excited state. The amplitude of the overlapped wave packet is retrieved as Anti-Stokes scattering by irradiating the probe pulse. Using a narrowband ps probe pulse, the Anti-Stokes scattering signal from different excited states can be spectrally resolved. The fringe structure of each frequency component observed by scanning the delay τ carries the amplitude and phase information of each excited state. High controllability of the vibrational coherence even after τ~500 ps is demonstrated, which might be useful for storing and retrieving quantum information in the condensed phase.[7]

References:
[1] P. Brumer and M. Shapiro, J. Chem. Phys., **84**, 4103 (1986).
[2] D. J. Tannor and S. A. Rice, J. Chem. Phys., **83**, 5013 (1985).
[3] H. Katsuki et al., Phys. Rev. Lett. **102**, 103602 (2009).
[4] H. Katsuki et al., Phys. Rev. A **76**, 013403 (2007).
[5] K. Ohmori et al., Phys. Rev. Lett. **96**, 093002 (2006).
[6] H. Goto et al., Nature Physics **7**, 383 (2011).
[7] H. Katsuki et al., submitted.

Photonic quantum circuits and their application

Shigeki Takeuchi
Research Institute for Electronic Science, Hokkaido University, Japan
The Institute for Scientific and Industrial Research, Osaka University, Japan
takeuchi@es.hokudai.ac.jp

In this talk, we report our recent effort for making photonic quantum circuits and discuss their possible applications.

The first example is `an entanglement filter'[1]. The ability to filter quantum states is a key capability in quantum information science and technology, where one-qubit filters, or polarizers, have found wide application. Filtering on the basis of entanglement requires extension to multi-qubit filters with qubit-qubit interactions. We demonstrate an optical entanglement filter that passes a pair of photons if they have the desired correlations of their polarization. Such a device has been proposed for photonic qubits[2], however, the technical requirements to build such a device, an optical circuit with two ancillary photons and multiple quantum gates, requiring both quantum interference and classical interference in several nested interferometers, have been lacking. We demonstrate an entanglement filter by combining two key recent technological approaches---a displaced-Sagnac architecture[3] and partially polarizing beam splitters[4]. The entangling capability of the filter was verified, distinguishing it from classical ones.

The second example is the optical quantum circuit of a Knill-Laflamme-Milburn (KLM) CNOT gate[5]. This photonic quantum circuit combines two efficient `artificial' nonlinear elements. We developed a stable architecture to realize the required four-photon network of nested multiple interferometers, and found that the average gate fidelity of our experimental quantum CNOT gate is $0.82 \pm 0.01$[6]. This result confirms the first step in the KLM `recipe' for all-optical quantum computation, and should be useful for on-demand entanglement generation and purification.

We will also briefly introduce our recent activities on the realization of solid state quantum using diamond nano-crystals coupled to tapered optical fibers and microsphere resonators [7-10]

This work was supported in part by Grant-in-Aid from JSPS, Quantum Cybernetics project, JST-CREST project, FIRST Program of JSPS, Special Coordination Funds for Promoting Science and Technology, and the GCOE program, and Research Foundation for Opto-Science and Technology.

References

1 R. Okamoto, J. O'Brien, H. F. Hofmann, T. Nagata, K. Sasaki and S. Takeuchi, **Science** 323, 483, (2009)
2. H. F. Hofmann and S. Takeuchi, **Phys. Rev. Lett.** 88, 147901 (2009).
3. T. Nagata, R. Okamoto, J. O'Brien, K. Sasaki and S. Takeuchi, **Science** 316, 726 (2007).
4. R. Okamoto, H. F. Hofmann, S. Takeuchi and K. Sasaki, **Phys. Rev. Lett.** 95, 210506 (2005).
5. E. Knill, R. Laflamme, and G. J. Milburn, **Nature** 409, 46 (2001).
6. R. Okamoto, J. L. O'Brien, H. F. Hofmann and S. Takeuchi, **PNAS**, 108, 10067 (2011).
7. H. Takashima, T. Asai, K. Toubaru, M. Fujiwara, K. Sasaki, and S. Takeuchi, **Opt. Exp.** 18, 15169 (2010).
8. A. Tanaka, T. Asai, K. Toubaru, H. Takashima, M. Fujiwara, R. Okamoto, and S. Takeuchi, **Opt. Exp.** 19, 422 (2011).
9. M. Fujiwara, K. Toubaru and S. Takeuchi, **Opt. Exp.** 19, 8596 (2011).
10. M. Fujiwara, K. Toubaru, T. Noda, H. Q. Zhao, and S. Takeuchi, **Nano Lett.**, 11, 4362 (2011).

Coherent Control of Quantum Emitters

C.K. Shih
Department of Physics, The University of Texas, Austin, TX 78712 USA
Shih@physics.utexas.edu

Semiconductor nanostructures such as quantum dots (QDs) have offered unique opportunities to investigate sophisticated quantum optical effects in a solid-state system. These include quantum interference, Rabi oscillations, as well as photon antibunching, and were previously only observable in isolated atoms or ions. In addition, QDs can be readily integrated into optical microcavities, making them attractive for a number of applications, particularly for quantum information processing and high efficiency quantum light sources. Recent successful demonstrations of resonant fluorescence of single quantum emitters have further open a new door toward coherently control of solid-state quantum emitters in microcavities. This talk will focus on these new recent developments.

Quantum Electrodynamics in Single Quantum Dot and Photonic Crystal Nanocavity Coupled Systems

A Yasuhiko Arakawa
Institute for Nano Quantum Information Electronics, The University of Tokyo
4-6-1 Komaba, Meguro-ku, Tokyo, 153-8505, Japan
E-mail: arakawa@iis.u-tokyo.ac.jp

One of the most ultimate goals in the field of the semiconductor lasers is to realize ultra-small lasers consisting of an optical cavity with the size of a wavelength of light and a single (artificial) atom. Since a single atom laser using a single trapped gas atom was demonstrated [1], various efforts have been devoted toward realization of such single emitter laser in solid-state materials. Combination of a single semiconductor quantum dot (QD) [2] with a semiconductor photonic crystal nanocavity is one of the best systems for this purpose. The coupled single-quantum-dot-2D/3D-photonic-crystal-nanocavity system provides with an excellent platform to investigate solid state cavity quantum electro-dynamics (Cavity-QED). In the strong coupling regime, reversible exchange of a single quantum between a single quantum dot and the nanocavity is well-preserved. Though the coexistence of vacuum Rabi oscillation and laser oscillation seems to be contradictory, it has recently been theoretically predicted that the strong-coupling effect could be sustained in laser oscillation [3].

In this presentation, we discuss recent advances in solid state cavity-QED in coupled single-quantum-dot-2D/3D-photonic-crystal-nanocavity systems. First, lasing oscillation in both weak- and strong-coupling regime in a single QD–nanocavity coupled system is demonstrated [4,5]. A high-quality semiconductor optical nanocavity and the strong single QD–field coupling enabled the lasing while maintaining the fragile coherent exchange of quanta. Furthermore, electron-phonon interaction under the cavity-QED conditions shows an asymmetric vacuum Rabi doublet and its temperature dependence, which is a unique phenomenon in solid state semiconductor systems [6]. Moreover, successful demonstration on spontaneous two photon emission from a single quantum dot with a high Q nanocavity is discussed [7]. Fabrication of a three dimensional photonic crystal nanocavity of a high Q-factor (~40,000) embedding quantum dots is also discussed, demonstrating lasing oscillation with systematic reduction of threshold with the increase of the Q-factor [8]. Purcell effect in the three dimensional photonic crystal nanocavity with a single quantum dot is observed with enhanced and suppressed factors of the spontaneous emission rate, respectively [9]. Finally we briefly mention a silicon-based three dimensional photonic crystal nanocavity.

This work is supported by MEXT Japan through the Creation of Innovation Centers for Advanced Interdisciplinary Research Areas Program and JSPS through FIRST Program.

References

1. J. McKeever, A. Boca, A. D. Boozer, J. R. Buck, and H. J. Kimble, Nature 425, 268 (2003).
2. Y. Arakawa and H. Sakaki: Appl. Phys. Lett., 40, 939 (1982)
3. E. D. Valle, F. P. Laussy, C. Tejedor, Phys. Rev. B 79, 235326 (2009).
4. M. Nomura, N. Kumagai, S. Iwamoto, Y. Ota, and Y. Arakawa, Opt. Express, 17, 15975 (2009).
5. M. Nomura, N. Kumagai, S. Iwamoto, Y. Ota, and Y. Arakawa, Nature Physics 6, 279, (2010).
6. Y. Ota, N. Kumagai, S. Ohkouchi, M. Shirane, M. Nomura, S.Ishida, S. Iwamoto, S. Yorozu and Y. Arakawa, arXiv:0908.0788 (2009)
7. Y. Ota, S. Iwamoto, N. Kumagai, and Y. Arakawa, Phys. Rev. Lett., in press (2011)
8. A. Tandaechanurat, S. Ishida, D. Guimard, M. Nomura, S. Iwamoto, and Y. Arakawa, Nature Photonics 5, 91 (2010)
9. A. Tandaechanurat, S. Ishida, D. Guimard, M. Nomura, S. Iwamoto, and Y. Arakawa, unpublished

Manipulating Coupling between Individual Nanoparticles

Xiaoqin (Elaine) Li*, Daniel Ratchford, and Farbod Shafiei
Physics Department, University of Texas-Austin, TX, 78717, U. S. A.
*elaineli@physics.utexas.edu

A key feature in complex nanostructures is that the coupling between individual components leads to new properties and functionalities. This coupling, in turn, sensitively depends on composition and geometry and the nanostructure. While this strong dependence on structure presents exciting opportunities to create nanomaterials with broadly tunable properties, it also poses serious challenges for fabrication and characterization. Small structural inhomogenieties in synthesized samples result in large variations in properties. Thus, the underlying relationship between structure and function is masked in ensemble measurements. To reveal intrinsic properties of nanostructures, experiments need to be performed on individual structures with well-defined composition and geometry.

We have taken the approach of nanomanipulation using atomic force microscope (AFM) to assemble structures consisting of multiple metallic and/or semiconductor nanoparticles. We then characterize the optical properties of the same structure using photoluminescence or scattering measurements. We discuss two specific examples.

In the first example, we determine the 3D relative orientation between two metallic nanoparticles. A gold nanosphere (150 nm in diameter) is placed within a few nanometers to the end of a gold nanorod (20 nm in diameter and 180 nm in length), the near field coupling between them introduces new features in the scattering spectra. Specifically, a Fano resonance emerges, due to the interference between a dark mode, corresponding to the quadrupole charge distribution on the rod, and the bright, dipole mode of the sphere. As the linear polarization of the incident and emission light are rotated, the scattering spectra evolve systematically, enabling us to determine the 3D relative orientation between these two plasmonic nanosparticles. Such information is difficult, if not impossible, to obtain via other techniques.

In the second example, we assemble a simple hybrid nanostructure consisting of a single CdSe/ZnS quantum dot and a gold nanoparticle. As the geometry of the structure is varied, coupling between the two changes accordingly. Both radiative and nonradiative decay rates of the quantum dot increase near the Au nanoparticle. In some cases, the nonradative energy transfer between the quantum dot and Au nanoparticle dominates and leads to a complete disappearance of luminescence blinking of the quantum dot. Two directly measured parameters, the total decay rate enhancement and photoluminescence intensity enhancement of the quantum dots, both sensitively depend on the size of the Au nanoparticle and the separation between the two components. The correlation between these two parameters for all assembled hybrid structures agrees well with simple analytical calculations.

Cooperative Phenomena in Nanocomposites Dynamically Controlled by Light-induced Force and Fluctuations

Takuya Iida

Nanoscience and Nanotechnology Research Center,
Research Organization for the Twenty-First Century, Osaka Prefecture University
Email address: t-iida@21c.osakafu-u.ac.jp

We theoretically study the optical response of nanocomposites (NCs) consisting of nanoparticles (NPs) assembled by light-induced force (LIF). There is a possibility that various types of cooperative phenomena can arise via light electromagnetic field since LIF depends on a variety of properties of excitation light such as wavelength, angular momentum, polarization and intensity distributions [1]. Based on such a mechanism, we are aiming at the construction of a new field "*Light-induced-force Nano Engineering*" for 'Fabrication', 'Observation', and 'Manipulation' of NCs (Fig. 1). In this contribution, as target materials of this engineering, we pay attention to metallic NCs with strong optical response due to localized surface plasmon (LSP) even at room temperature.

In order to evaluate assembling dynamics of metallic NPs by LIF, we have developed a new numerical method "Light-induced-force Nano-dynamics (LND) Method" based on the general expression of LIF [1] and Langevin equation. Here, I will show one of our results related to the control of configuration and optical response of NCs by LIF [2]. We have numerically evaluated the dynamics of gold nanoparticles under the self-consistently determined inter-object LIF and random force arising from thermal fluctuations by using our LND method (Fig 2). Due to the balance of trapping force (gradient force) toward high light intensity region and inter-object force modulated by light make an array of gold NPs parallel to the light polarization. As increase of the number of NPs N, we have found the drastic enhancement of light scattering efficiency arising from the collective effect of LSP in multiple NPs via light electromagnetic field (*Plasmonic Super Radiance*). Such optically-controlled cooperative phenomena of LSP would be the foundation of the high efficient light energy conversion systems [3], optical sensors [4], medical applications [5], single molecule detection [6] and so on.

Fig.1: Concept of "Light-induced Force Nano-engineering".

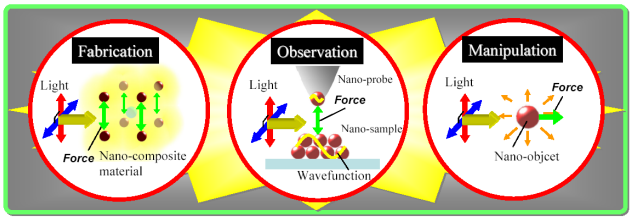

Fig.2: Control of configuration and optical response of localized surface plasmon in metallic nanocomposites assembled by light-induced force.

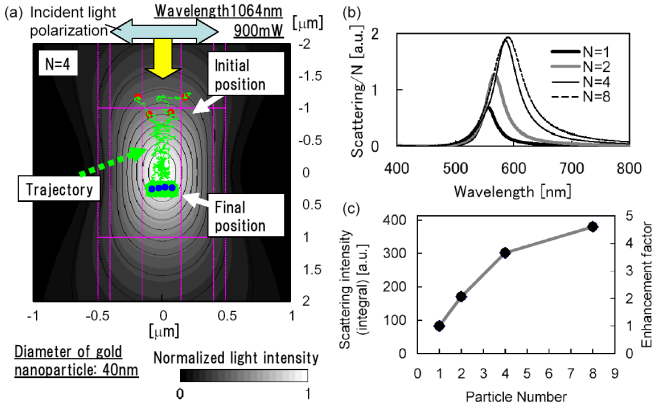

[1] T. Iida, H. Ishihara, *Phys. Rev. B*; **77**, 245319 (2008). See also, *Phys. Rev. Focus* **21**, St. 21 (2008).
[2] T. Iida, *CLEO/Eurepo-EQEC Technical Digest*; EI5.4 (2011). Other than this, 2 papers have been submitted.
[3] H. A. Atwater, A. Polman, *Nature Material* **9**: 205 (2010).
[4] S. Tokonami, et al., T. Iida, *CLEO/Europe-EQEC Technical Digest*; CH.P.10 (2011).
[5] C. Kojima, Y. Watanabe, H. Hattori, T. Iida, *J. Phys. Chem. C* **115**, 19091 (2011).
[6] T. Iida, Y. Aiba, H. Ishihara, *Appl. Phys. Lett.* **98**, 053108 (2011).

Strongly correlated fulleride superconductors

Kosmas Prassides
Department of Chemistry, Durham University, Durham DH1 3LE, United Kingdom
Email address: k.prassides@durham.ac.uk

A_3C_{60} (A = alkali metal) superconductors were known to adopt face-centred cubic (fcc) structures with their superconducting T_c increasing monotonically with increasing interfullerene spacing, reaching a 33 K maximum for $RbCs_2C_{60}$ – this physical picture had remained unaltered since 1992. Trace superconductivity (s/c fraction<0.1%) at 40 K under pressure was also reported in 1995 in multiphase samples with nominal composition Cs_3C_{60}. Despite numerous attempts by many groups worldwide, this remained unconfirmed and the structure and composition of the material responsible for superconductivity unidentified. Thus the possibility of enhancing fulleride superconductivity and understanding the structures and properties of these archetypal molecular solids had remained elusive. Here I will present our recent progress in this field in accessing high-symmetry hyperexpanded alkali fullerides in the vicinity of the Mott-Hubbard metal-insulator boundary and at previously inaccessible intermolecular separations. The physical picture that emerges for the alkali fullerides is that, contrary to long-held beliefs, they are the simplest members of the high-Tc superconductivity family. We demonstrated this by showing that in the two hyperexpanded Cs_3C_{60} polymorphs (fcc- and A15-structured) [1,2], superconductivity emerges upon applied pressure out of an antiferromagnetic insulating state and displays an unconventional behaviour – a superconductivity dome – explicable by the prominent role of strong electron correlations.

[1] Y. Takabayashi et al., *Science* **2009**, *323*, 1585-1590.
[2] A. Y. Ganin et al., *Nature* **2010**, *466*, 221-225.

Application of Nano-Interfaces of Molecular Spins toward Organic Electronics

Kunio Awaga

Research Center for Materials Science & Department of Chemistry & CREST, JST, Nagoya University, Nagoya 464-8602, Japan
E-mail: awaga@mbox.chem.nagoya-u.ac.jp

Organic semiconductors have received growing attention in recent years, and they currently represent perhaps the most mature and applicable systems in the field of organic electronics. Work in this field, however, has focused almost entirely on closed-shell molecules, and scant attention has been paid to molecules with unpaired electrons as building blocks for organic semiconductors, in contrast to the fact that many paramagnetic transition metal complexes and organic radicals have been studied extensively in the field of molecular metals and magnets. In this presentation, we will describe the nano-interfaces of paramagnetic species for optoelectronic conversion and electron storage.

Anomalous transient current of organic radical photocells. Thiazyl radicals are stable organic radicals, and possess strong intermolecular interactions in 3D network crystal structures. A disjoint diradical BDTDA (4,4'-bis(1,2,3,5-dithiadiazolyl)) forms highly oriented thin films, which are excellent examples of interactive radical dimers; the thin films contain alternating π-stacking that bridge the distance between the two electrodes. The ITO/BDTDA/Al cells exhibit a photocurrent with a high on/off ratio at negative bias voltages [1]. Furthermore, these films exhibit an anomalous transient current at zero-bias voltage, probably due to the imbalance between hole and electron mobilities, and space-charge triggered polarization in the samples [2]. We also report a highly efficient optoelectronic conversion in ITO/Polarization layer/Charge separation layer/Al photocells [3]. Theoretical analysis of this structure indicates the generation of a large transient current that is triggered by photogenerated space charges, and governed by the dielectric properties of the blocking layer.

Molecular Cluster batteries. Recently, we proposed rechargeable molecular cluster batteries (MCBs), in which the anode is Li metal and the cathode includes a transition metal cluster complex, such as Mn12 - a well-known single molecule magnet (Fig. 1) [4]. Mn12-MCBs operate as a rechargeable battery with an extremely large battery capacity. The XAFS analyses [5] on these batteries indicate that the large capacity can be understood as a combination of the redox change of the Mn ions and a capacitance effect at the electrode surface.

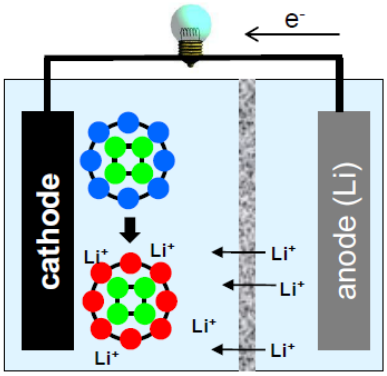

Figure 1

[1] A. Iwasaki, L. Hu, R. Suizu, K. Nomura, H. Yoshikawa, K. Awaga, Y. Noda, K. Kanai, Y. Ouchi, K. Seki, and H. Ito, (2009) *Angew. Chem. Int. Ed.*, **48**, 4022.
[2] L. Hu, A. Iwasaki, R. Suizu, H. Yoshikawa, K. Awaga, H. Ito, (2010) *Chem. Phys. Lett.* **484**, 177.
[3] L. Hu, Y. Noda, H. Ito, H. Kishida, A. Nakamura, K. Awaga, (2010) *Appl. Phys. Lett.* **96**, 243303.
[4] H. Yoshikawa, C. Kazama, K. Awaga, M. Satoh, J. Wada, (2007) *Chem. Commun*, 3169-3170.
[5] H. Yoshikawa, S. Hamanaka, Y. Miyoshi, Y. Kondo, S. Shigematsu, N. Akutagawa, M. Sato, T. Yokoyama, K. Awaga, (2009) *Inorg. Chem.*, **48,** 9057-9059.

Study of Charge Ordering in Strongly Correlated Molecular Conductor System by Synchrotron Radiation X-ray Diffraction

Hiroshi Sawa
Department of Applied Physics, Nagoya University, Japan
hiroshi.sawa@cc.nagoya-u.ac.jp

In a molecular crystal, on site *U* is not so large because the frontier orbital spreads on the whole of a molecule. However, the electron correlation described by U / t is not able to be neglected due to the small transfer integral *t* between molecules. In the case of a well-known classical molecular conductor α-(BEDT-TTF)$_2$I$_3$, the theoretical prediction pointed out first that the metal-insulator transition is based on electric charge ordering[1]. The flow of research of the molecular conductor as the superconductivity search by control of dimensionality was changed into of the electron correlation phenomena.

We first investigated the charge ordering phenomena of α-(BEDTTTF)$_2$I$_3$ using the conventional single crystal structure analysis by synchrotron radiation X-ray at Photon Factory in KEK[2]. The results show that the horizontal-stripe-type structure, which was suggested by the mean field theory [3], is established. We also find the charge disproportionation above the metal–insulator transition temperature and a significant change in the transfer integrals caused by the phase transition. The valence of a BEDT-TTF molecule is estimated by an empirical method based on the bond lengths in the molecule.

On the other hand, the X-ray is diffracted by the periodic electrons in a crystal. We tried to carry out the precise charge density analysis to quantitatively estimate the charges on the BEDT-TTF molecules using synchrotron radiation X-ray diffraction at SPring-8. The charge densities were calculated by the maximum entropy method (MEM). The charges of the molecules were estimated by the Bader's topological analysis. Using this method, the unit cell is divided by the zero flux point calculated by the gradient charge density, so called atomic basin, then we can count the electron number in this area.

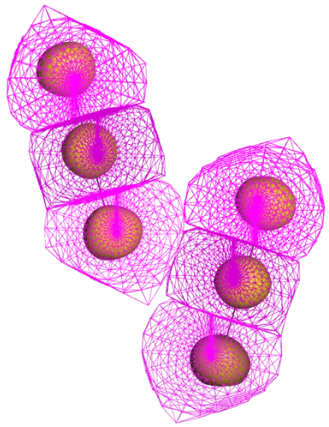

Fig.1. Atomic basin of two I_3 molecules.

First of all, in order to check the reliability of this method, the number of electrons of the closed shell I_3^- ion was counted. The error of the electron counting is about 1% in the metallic state and the insulating state (Fig.1). Using this method, we can calculate not only the charge of the molecules but also the charge disproportion on the molecule according to the distribution of the molecular orbital in the crystal. The precise charge density analysis for strongly correlated electron materials promises the new stage of the research of the structural material science.

1. H. Kino and H. Fukuyama: *J. Phys. Soc. Jpn.* 64 (1995) 1877.
2. T. Kakiuchi, Y. Wakabayashi, H. Sawa, *et al.*: *J. Phys. Soc. Jpn.* 76 (2007) 113702.
3. H. Seo: *J. Phys. Soc. Jpn.* 69 (2000) 805.

Arrangements and Magnetism of O_2-O_2 Dimer Adsorbed in Microporous Coordination Polymers

T. C. Kobayashi[1,2], A. Hori[2], Y. Kubota[3], M. Takata[2], A. Matsuo[4], K. Kindo[4], R. Matsuda[5], S. Kitagawa[2,5,6]

[1] *Graduate School of Natural Science and Technology, Okayama University, Okayama 700-8530, Japan*
[2] *Harima Institute, RIKEN SPring-8 Center, Sayo-gun, Hyogo 679-5198, Japan*
[3]*Graduate School of Science, Osaka Prefecture University, Sakai, Osaka 599-8531, Japan*
[4]*ISSP, University of Tokyo, Kashiwa, Chiba 277-9531, Japan*
[5]*Kitagawa Integrated Pore Project, ERATO, JST, Shimogyo-ku, Kyoto 600-8815, Japan*
[6]*Institute for Integrated Cell-Material Sciences, Kyoto University, Sokyo-ku, Kyoto 606-8501, Japan*
kobayashi@science.okayama-u.ac.jp

Molecular oxygen is known as a magnetic molecule with S = 1. The magnetic properties of liquid and solid O_2 have been investigated a long time ago. Ten years ago, we found that the adsorbed O_2 forms O_2-O_2 dimer in the microporous coordination polymer and revealed the anomalous magnetic properties which cannot be explained by the S = 1 Heisenberg AF dimer model.[1] We found two typical systems of O_2-O_2 dimer in $Cu_2(pzdc)_2(pyz)$: pzdc = 2,3-prazinedicarboxylate and pyz = pyrazine (CPL-1) [1] and Cu-trans-1,4- cyclohexanedicarboxylic acid (Cu-CHD) [2] and some candidates.

The magnetization process of adsorbed O_2 shows metamagnetic behavior with one step while the temperature dependence of the susceptibility shows a broad peak.[1-3] These magnetic properties are explained consistently by "O_2-O_2 dimer model" taking into account the spin-dependent intermolecular potential which was calculated by some researchers. The magnetic interaction depends on the molecular arrangement and is considered to be dominant in the molecular arrangement. In this model, we treated the energy gap $\Delta_{s\text{-}t}$ between the singlet ground state (S_{dim} = 0) and the excited triplet (S_{dim} = 1) and the $\Delta_{t\text{-}q}$ between the triplet and the quintet (S_{dim} = 2) as independent parameters, considering the excited states at different arrangement. To our knowledge, the effect of spin-dependent intermolecular potential has never previously been observed in liquid and solid O_2.

We investigated the arrangement of O_2 adsorbed in Cu-CHD by x-ray powder diffraction. It was found that the O_2-O_2 dimer varies from the planar rectangular parallel H-geometry to the shifted S-geometry with increasing temperature. This result demonstrates that the thermally excited quintet state (S_{dim} = 2) has S-geometry. [2,4]

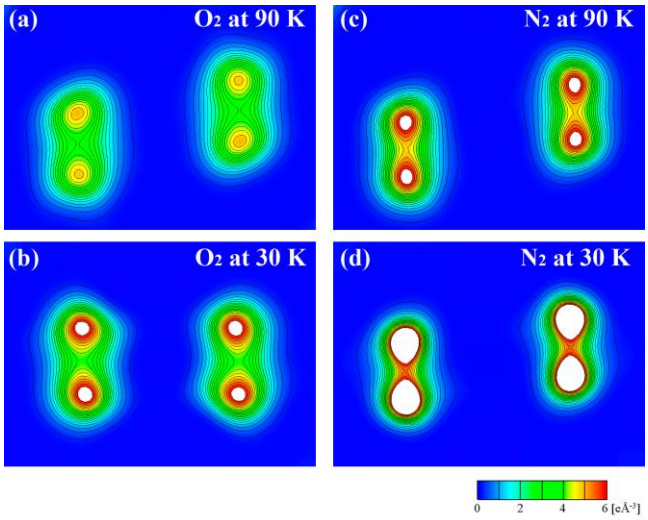

Fig. 1. Section of MEM charge densities of O_2 and N_2 adsorbed in Cu-CHD.

References

[1] R. Kitaura *et al*., Science **298** (2002) 2358.
[2] A. Hori *et al*., (in preparation).
[3] W. Mori *et al*., Mol. Cryst. Liq. Cryst. **306** (1997) 1.
[4] T. C. Kobayashi *et al*., Prog. Theor. Phys. Suppl. **159**, 271 (2005).

Thermodynamic Properties of the Spin-Liquid State in Organic Charge Transfer Salts

Yasuhiro Nakazawa[1], Satoshi Yamashita[2], Reizo Kato[2]

[1]Department of Chemistry, Graduate School of Science,
Osaka University, Machikaneyama 1-1, Osaka 560-0043, JAPAN
nakazawa@chem.sci.osaka-u.ac.jp

[2] RIKEN, Wako Saitama 351-0198, JAPAN

Low-temperature magnetic properties of frustrated systems with *S*-1/2 are attracting interests in condensed matter science, because formation of long-range orderings is prohibited by geometric restriction and an appearance of novel quantum mechanical ground states is expected in them. Organic charge transfer compounds of κ-(BEDT-TTF)$_2$Cu$_2$(CN)$_3$ and EtMe$_3$Sb[Pd(dmit)$_2$]$_2$ where BEDT-TTF is bisethylenedithiotetrathiafulvalene and dmit is 1,3-dithiole-2-thione-4,5-dithiolate are known to give unique viewpoints in frustration physics. These compounds are Mott insulating systems in which one electron or hole localizes on each molecular dimer. The dimers are arranged in triangle structures in a donor or acceptor layer and therefore ideal two dimensional spin systems of molecular dimers are constructed. The two compounds show peculiar thermodynamic properties characteristic of spin-liquids ground states at low temperatures.

In this presentation, we discuss heat capacity data of single crystal samples of these organic charge transfer compounds. From the ^{13}C-NMR measurements, both compounds do not show any long-range orderings down to about 30 mK. We have performed heat capacity measurements by the standard thermal relaxation calorimetry technique down to 75-100 mK and observed that the low temperature heat capacities give a distinct *T*-linear term of which electronic heat capacity coefficient γ is about 10-20 mJK^{-2}mol^{-1}. The *T*-linear term is insensitive to external magnetic fields up to about 8 T. This fact indicates that the ground state is a spin-liquid and there are dense gapless type excitations from the liquid like ground states. The magnitude of γ roughly scales to the magnetic susceptibility extrapolated down to 0 K. We also observed that these salts show broad hump structures in temperature dependences of C_pT^{-1} around 5.7 K in κ-(BEDT-TTF)$_2$Cu$_2$(CN)$_3$ and 3.7 K in EtMe$_3$Sb[Pd(dmit)$_2$]$_2$, which cannot be observed in other salts with ordered ground state.

In order to study chemical pressure effects of the electronic properties, thermodynamic measurements of deuterated sample are also performed. In the case of κ-(BEDT-TTF)$_2$Cu$_2$(CN)$_3$, deuteration of BEDT-TTF molecule do not give any change of heat capacity in this low temperature region. On the other hand, EtMe$_3$Sb[Pd(dmit)$_2$]$_2$ was found to be very sensitive deuteration of cation site. The variation of spin-liquid ground state with a parameter of *t'/t* is discussed.

References

[1] S. Yamashita, Y. Nakazawa, M. Oguni, Y. Oshima, H. Nojiri, Y. Shimizu, K. Miyagawa and K. Kanoda, *Nature Physics* **4**, 459-462 (2008) .
[2] S. Yamashita, T. Yamamoto and Y. Nakazawa, *Physica* B **405**, S237-S239 (2010).

Magnetic Properties of the Organic $S = \frac{1}{2}$ Spin Triangle TNN

Y. Takano
Department of Physics, University of Florida
K. Takada, S. Iisaka, H. Yamaguchi, T. Ono, Y. Hosokoshi
Department of Physics, Osaka Prefecture University
J.-H. Park, T. P. Murphy
National High Magnetic Field Laboratory, Tallahassee
H. Nakano
Graduate School of Material Science, University of Hyogo
Y. Shimura, T. Sakakibara
Institute for Solid State Physics, University of Tokyo

Molecular magnets are attracting much attention because of a rich variety of quantum-mechanical phenomena they exhibit, as well as potential applications. Among them, molecules containing three $S = 1/2$ spins coupled by antiferromagnetic Heisenberg exchange are the simplest yet non-trivial because their ground states comprise states of opposite scalar spin chirality. This extra degree of freedom can lead to a permanent electric dipole moment and an orbital magnetic moment, making these nanoscale magnets promising candidates for qubits in quantum computing and multiferroic components in spintronics.

Tris[4-(4'-(1-oxyl-3-oxide-4,4,5,5-tetramethylimidazolin-2-yl)-2-yl)phenyl]amine, also known as TNN, is a completely organic molecule possessing a threefold rotational symmetry which incorporates three identical radicals, whose $S = 1/2$ spins are coupled antiferromagnetically with each other with an exchange J of about 6 K. The perfect symmetry of TNN makes it a particularly attractive system in which to study the role of spin chirality in a molecular magnet. TNN can be forced to form a crystal that is stable at room temperature by mixing it with acetonitrile, rendering it amenable to studies with macroscopic probes.

Using specific-heat, magnetic-susceptibility, magnetization, magnetic-torque, and magnetocaloric-effect measurements, we have investigated the magnetism of TNN in such a crystal in magnetic fields at low temperatures. The results provide a solid foundation on which to explore the rich physics of this novel molecular magnet.

Fractal Structure of Transport Coefficients in 1D Protein Chain

Tomio Petrosky

Center for Complex Quantum Systems, The University of Texas at Austin,
Department of Physical Science, Osaka Prefecture University

The spectrum of the Liouville-von Neumann operator (the Liovillian) of a one-dimensional protein chain, such as the α helix, is analyzed for the resonance states. The system is described by Davydov's Hamiltonian that consists of an exiton coupled with phonon in the protein chain. We assume that the phonon is in a thermal equilibrium with a given temperature *T*. Imaginary part of the spectrum gives transport coefficients, such as the decay rate of irreversible process that approaches to a thermal equilibrium. An important dimensionless parameter of the system is $R = \pi^{-1}\sin^{-1}(b_p/b_e)$ where b_p is the band-width of the energy spectrum of the phonon, while b_e is the band-width of the energy spectrum of the exiton. Depending on *R* being a rational number or an irrational number, the structure of the imaginary component of the spectrum of the Liovillian drastically changes with a self-similar structure (see Fig.1). Hence we have a fractal structure of the spectrum of the Liovillian. This structure is quite similar to the well-known Hofstader's butterfly for Hamiltonian spectrum of a two-dimensional tight-binding model of an electron imbedded in a constant magnetic field. However, the physical meaning is very different: our Liouvillian spectrum is associated to entropy production in irreversible process, while Hofstader's spectrum is associated to energy in reversible process. Moreover, the shape of our spectrum is like the alien Barutan in a Japanese TV character (Fig.2) rather than a butterfly. We will show that depending on the form of the potential the approach to equilibrium obeys an exponential law, or a power law.

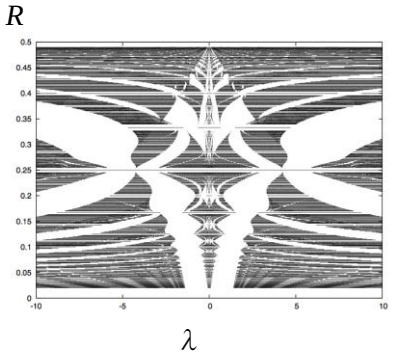

Fig.1: Fractal Structure of the spectrum λ

Fig.2: the alien Barutan

Response theory around a non-equilibrium steady state in terms of full-counting statistics

Hisao Hayakawa
Yukawa Institute for Theoretical Physics, Kyoto University,
Kyoto 606-8502, Japan
Email: hisao@yukawa.kyoto-u.ac.jp

Full-counting statistics is used for the analysis of mesoscopic quantum systems such as quantum dots. This is also a powerful tool to obtain the fluctuation theorem in quantum systems. Recently, Sagawa and Hayakawa[1] demonstrated that an extended Clausius equality for quasi-static transitions between nonequilibrium steady states of Markovian jump processes can be derived in terms of full counting statistics and the adiabatic approximation. The paper suggests that such a potential depends on the path of the process we consider. The assumption they used is only that the system does not have degenerated slowest mode. This is true in general for open dissipative systems, in which dissipation resolves the degeneracy of zero-eigen modes for Hamilton systems. As an application of the previous work [1], let us consider a response theory around a non-equilibrium steady state. This system, of course, contains dissipation, and thus, the Liouville operator is no longer Hermitian. With the aid of adiabatic approximation and full-counting statistics technique we can demonstrate the general framework of nonlinear response theory around a non-equilibrium steady state. Moreover, we can determine the response function, in general. In this talk, I will demonstrate (i) how to construct a non-equilibrium steady state in a granular system under a plane shear, and (ii) how to obtain the response function under this situation.

[1] T. Sagawa and H. Hayakawa, arXiv:1109.0796.

Resonant States of a Quantum Dot System and Breaking of Time-Reversal Symmetry

Naomichi Hatano

Institute of Industrial Science, University of Tokyo

We discuss complex-eigenvalue problems of the Hamiltonian and the Liouvillian of a T-shaped quantum dot system. We stress that each eigenstate with a complex eigenvalue breaks the time-reversal symmetry, although the corresponding Schrödinger and Liouville-von Neumann equations observe the time-reversal symmetry. The dissipation that occurs in electronic conduction through the quantum dot is associated with the breaking of the time-reversal symmetry. A complex eigenvalue always accompanies its complex-conjugate counterpart; the two complex eigenvalues recover the time-reversal symmetry as a pair.

We first show that a complex eigenvalue of the Hamiltonian with a negative imaginary part represents a decaying state, and thereby describes dissipation in quantum-mechanical electronic conduction. The complex-conjugate eigenvalue with a positive imaginary part represents a growing state. The former is called a resonant state and the latter an anti-resonant state. We show that they are defined as eigenstates of the stationary Schrödinger equation under a specific boundary condition.

We next show that the same argument applies to the complex-eigenvalue problem of the Liouvillian, which now can have mixed-state solutions. The mixed eigenstate with a negative imaginary part should describe the approach to equilibrium. We map the problem to the Schrödinger equation of two distinguishable particles, namely the ket particle and the bra particle. The mapping introduces an interaction between the two particles, which can lead us to eigenvalues that cannot be deduced from the pure-state solutions of the original Schrödinger equation.

References

[1] N. Hatano, K. Sasada, H. Nakamura, T. Petrosky: Prog. Theor. Phys. **77**, 187–222 (2008)
[2] K. Sasada, N. Hatano: J. Phys. Soc. Jpn. **77**, 025003 (2008)
[3] N. Hatano, T. Kawamoto, J. Feinberg: Pramana J. Phys. **73**, 553–564 (2009)
[4] N. Hatano: Prog. Theor. Phys. Suppl. **184**, 497–515 (2010)
[5] K. Sasada, N. Hatano, G. Ordonez: J. Phys. Soc. Jpn. **80**, 104707 (2011)
[6] N. Hatano, G. Ordonez: Int. J. Theor. Phys. **50**, 1105–1115 (2011)
[7] R. Nakano, N. Hatano, T. Petrosky: Int. J. Theor. Phys. **50**, 1134–1142 (2011); R. Nakano, T. Mori, N. Hatano, T. Petrosky: in preparation [8] H. Nakamura, N. Hatano, S. Garmon, T. Petrosky: Phys. Rev. Lett. **99**, 210404 (2007)
[0] S. Garmon, H. Nakamura, N. Hatano, T. Petrosky: Phys. Rev. B **80**, 115318 (2009)
[10] S.-P. Liew, N. Hatano: arXiv:1010.1336

Nonequilibrium transport of one-dimensional molecular chain

Satoshi Tanaka
Department of Physical Science, Osaka Prefecture University
Gakuen-cho 1-1, naka-ku, Sakai 599-8531, Japan

Exciton transport plays an important role as an energy transfer in many biomolecules with one-dimensional molecular chain, such as alpha-helix protein, DNA bases, and so on. Since these biomolecules exhibit various biological functions in far-from equilibrium, we have to clarify the exciton transport in non-equilibrium situation. [1]

In the present work, we theoretically investigate the transport process in the non-equilibrium stationary state of a molecular chain under a thermal force by different temperature thermal baths.(Fig.1) Our theory is based on the complex spectral representation of the Liouville operator which governs the microscopic dynamics, [2] where the non-equilibrium stationary state is obtained as the zero eigenstate of the Liouvillian. Following the concepts of the correlation dynamics, the nonequilibrium stationary state is represented by a superposition of components with various orders of correlations.

Any physical quantity is obtained by taking an expectation value in terms of the nonequilibrium stationary state. Since the non-equilibrium stationary state is derived as a solution of the eigenvalue problem of the Liouvillian, the transport quantities are evaluated rigorously based on microscopic dynamics, which is in contrast to a phenomenological method, such as usage of the Landauer formula.

We have revealed that an energy flow in the nonequilibrium stationary state is attributed to the first order correlation created out of the vacuum of correlation, and that the derived expression of the energy flow can be reduced to the form similar to the Landauer formula. In addition, we investigate the induced polarization appearing in the molecule due to the thermal force exerting on the molecule. Contrary to the energy flow, the induced polarization is described by the second order correlation, which cannot be reduced to Landauer formula.[3]

One of the advantage of our theory is that we can clarify the effect of the interaction of excitons on the nonequilibrium transport process. We have found that the repulsive interaction of the excitons can enhance the energy flow, as shown in Fig.2.

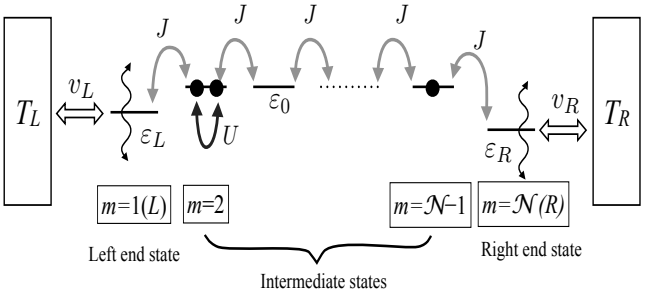

Fig.1 One-dimensional molecular chain coupled with different thermal baths at the both ends.

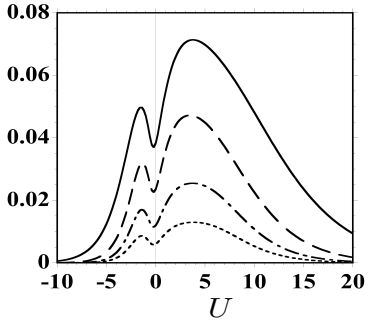

Fig.2 Energy flow as a function of the exciton interaction, U.

References

[1] J. Jortner and M. Ratener, *Molecular Electronics* (Blackwell Science, 1997)

[2] T. Petrosky and I. Prigogine, *Adv. Chem. Phys.* **99,** 1 (1997).

[3] S. Tanaka, K. Kanki, T. Petrosky, *Phys. Rev. E* **83,** 051118 (2011).

Spontaneous Quantum Hall States in Graphene Bilayers

Allan MacDonald, University of Texas at Austin

Graphene is a gapless semiconductor in which conduction and valence band wavefunctions differ only in the phase difference between their projections onto the two sublattices of the material's two-dimensional honeycomb crystal structure. I will discuss why[1] this circumstance creates openings for broken symmetry states. In bilayer graphene, conduction and valence band states are characterized by a layer pseudospin with zero polar angle, corresponding to symmetric occupation of the two layers, and an azimuthal angle that specifies the momentum dependent interlayer phase difference. The broken symmetry state of bilayer graphene forms a core in the band structure's momentum-space vortex texture, in which pseudospins near zero momentum spontaneously tilt toward the north or south poles. These states have large an energy gap and large momentum-space Berry curvatures that can give rise to quantized anomalous Hall effects. I will discuss what we can learn about these states from recent experiments, and comment briefly on the potential for pseudospin order[1] in other graphene-based two-dimensional electron systems.

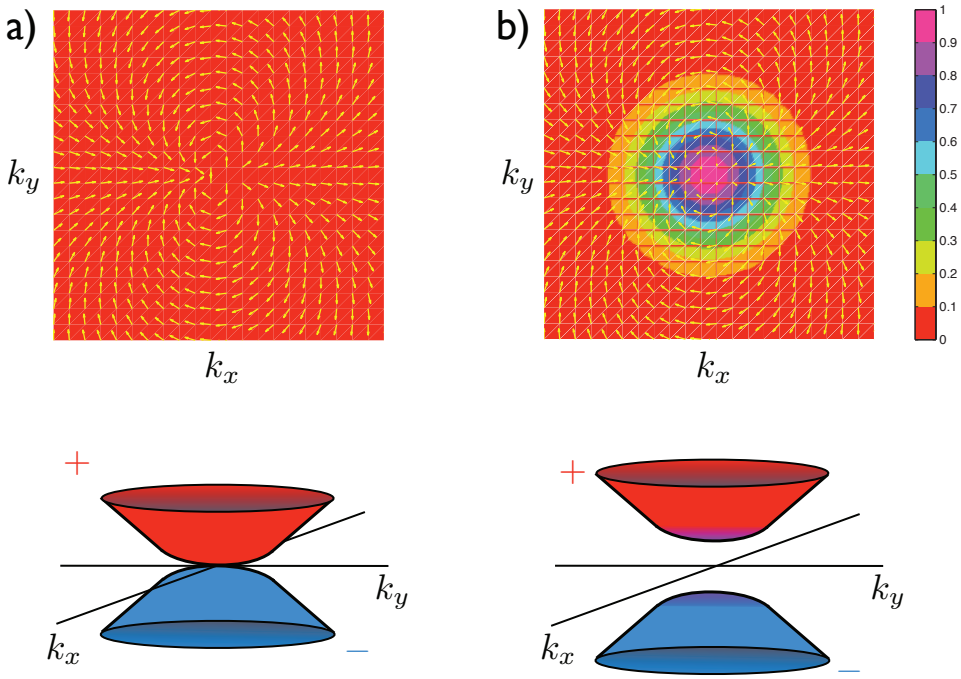

Figure 1: Pseudopin orientations and quasiparticle bands for bilayer graphene. In the ordered state the $\hat{x} - \hat{y}$ components of the quasiparticle pseudospins (yellow arrows) shorten while the polar component (color scale) develops a non-zero component. The quasiparticle energy bands (bottom panels) develop a gap between valence and conduction bands.

References

[1] A.H. MacDonald, Jeil Jung, and Fan Zhang, arXiv:1109.0307 and work cited therein.

Theoretical design of topological insulators and superconductors

Naoto Nagaosa
Department of Applied Physics, The University of Tokyo, Japan
nagaosa@ap.t.u-tokyo.ac.jp

Recently, the topological properties of electrons in solids attract much attention both from the scientific and technological viewpoints. Especially the topological insulator (TI) and superconductor (TS) are the new states of matter recently studied extensively. As for the TI, the relativistic spin-orbit interaction in the nonmagnetic system is indispensable. Up to now, several candidate materials have been proposed and actually confirmed experimentally to be TI's. However, all of these materials are based on the s- and p-orbitals. In this talk, I will discuss the possibility of TI in d-electron systems. In this case, we expect a variety of phenomena related to the magnetism, ferroelectricity, and superconductivity due to the many-body interactions, and the interplay between the topology and correlation can be studied in depth. Especially, the possible TI at the hetero-structures of transition metal oxides is studied in details [1]. As for the TS, we focus on the noncentrosymmetric superconductors with Rashba spin-orbit interaction. Also this can be realized in the superstructure of transition metal oxides such as LaAlO/SrTiO, where the superconductivity is actually observed. The possible topological phases and their physical properties are discussed. These works have been done in collaboration with S.Okamoto, D. Xiao, W. Zhu, Y. Ran, S. Nakosai, and Y. Tanaka.

[1] D. Xiao et al., arXiv:1106.4296.

Ferrimagnetism Induced by Spontaneous Atomic Ordering in Epitaxial Double-Perovskite Films

A. Ohtomo[1,*], S. Chakraverty[2], M. Kawasaki[2,3]
[1] Department of Applied Chemistry, Tokyo Institute of Technology, Tokyo 152-8552, Japan
[2] Correlated Electron Research Group (CERG) and Cross-Correlated Materials Research Group (CMRG), RIKEN Advanced Science Institute, Wako 351-0198, Japan
[3] Quantum-Phase Electronics Center and Department of Applied Physics, University of Tokyo, Tokyo 113-8656, Japan, and CREST, Japan Science and Technology Agency, Tokyo 102-0075, Japan
*aohtomo@apc.titech.ac.jp

Double-perovskite oxides $A_2B'B''O_6$ (*A* being an alkaline- or rare-earth, while *B'* and *B"* being different transition-metal elements), exhibiting high-Curie temperature ferromagnetism, have been attracting much attention not only for future spintronics applications but also for the challenge to atomically controlled oxide epitaxy. $Sr_2Fe^{3+}Mo^{5+}O_6$ and $Sr_2Cr^{3+}Re^{5+}O_6$ are well-known examples, where a large difference in the formal valence (*FV*) permits spontaneous ordering of transition-metal elements, thus facile to synthesize in a bulk form. Among the 3*d*-3*d* combinations, however, only a few are known to form double-perovskites such as $La_2Mn^{4+}B''O_6$ (*B"* = Co^{2+}, Ni^{2+}, Fe^{2+}), where difference in the ionic radius as well as *FV* is exceptionally large. Here we have studied two systems with identical *FV* of *B'* and *B"*, $La_2Cr^{3+}Fe^{3+}O_6$ (LCFO) [1] and $La_2V^{3+}Mn^{3+}O_6$ (LVMO) [2], both of which have never been reported to exist in ordered forms, neither in bulk nor in thin film form. These compounds are particularly interesting because of the possibility to explore ferromagnetism (expected from Kanamori-Goodenough rule for LCFO) or half-metallic antiferromagnetism (predicted by Pickett for LVMO [3]). However, recent experimental results contradict the theories and determination of their magnetic ground states is still under debate.

Using pulsed-laser deposition technique with single solid-solution targets, we have prepared a number of films on (111) $SrTiO_3$ substrates at a wide range of growth parameters (oxygen pressure and growth temperature) to study how the ordering as well as physical properties depend on the growth parameters. Surprisingly, highly ordered phases could reproducibly be stabilized for both compounds when grown at appropriate conditions. The highest ordered LCFO exhibited the degree of order ~90% and a saturation magnetization of ~2μ_B/f.u. at 5 K, from which the ground-state magnetic order of LCFO has been verified to be ferrimagnetic ($3d^3\downarrow 3d^5\uparrow$; S = -3/2 + 5/2 = 1). The ordered phase of LVMO was also ferrimagnetic with Mn^{3+} at a high-spin state ($3d^2\downarrow 3d^4\uparrow$; S = -1 + 2 = 1) in contrast to the theoretically calculated one; a spin-compensated state with Mn^{3+} at a low-spin state ($3d^2\downarrow 3d^2\uparrow$; S = 0). Our results present a wide opportunity to explore novel magnetic properties of "binary" transition-metal perovskites upon epitaxial stabilization of the ordered phase.

[1] S. Chakraverty, A. Ohtomo, M. Kawasaki *et al.*, Phys. Rev. B **84**, 132411 (2011).
[2] S. Chakraverty, A. Ohtomo, M. Kawasaki *et al.*, Phys. Rev. B **84**, 064436 (2011).
[3] W. E. Pickett, Phys. Rev. B **57**, 10613 (1998).

Applications of Spin-Transfer-Torque in Spintronics

Maxim Tsoi
Physics Department,
University of Texas at Austin, USA
tsoi@physics.utexas.edu

Spintronics is built on a complementary set of phenomena in which the magnetic configuration of a system influences its transport properties and vice versa. In ferromagnetic (F) systems these interconnections are exemplified by Giant Magnetoresistance (GMR) – where the system's resistance depends on the relative orientation of magnetic moments in constituent F-parts [1], and Spin Transfer Torque (STT) – in which an electrical current can perturb the system's magnetic state [2]. Recently, corresponding effects were proposed [3] to occur in systems where F-components are replaced with antiferromagnets (AFM), thus leading to antiferromagnetic GMR and STT effects.

In this talk I will focus on STT which may be the method of choice to control and manipulate magnetic moments in future spintronic devices. I will describe several experiments where transport currents alter the magnetic state in various solid state systems:

(i) In ferromagnetic/nonmagnetic (F/N) multilayers a dc electrical current can switch and/or drive its constituent F parts into high-frequency precession [4] which is of interest for microwave and magnetic recording technologies. Interestingly, application of high-frequency currents can also drive the multilayer, e.g. into STT-driven ferromagnetic [5] and parametric [6] resonances. The latter can be potentially used for reducing power and increasing speed of magnetic logic and memory devices.

(ii) In antiferromagnetic (AFM) systems I will focus on our experiments with exchange-biased spin valves [7] where extreme current densities were found to affect the exchange bias at F/AFM interfaces. As exchange bias is known to be associated with interfacial AFM magnetic moments, this observation can be taken as the first evidence of STT in AFM materials and the first step towards all-AFM spintronics [8].

In collaboration with (i) T. Staudacher, C. Wang, H. Seinige, (ii) Z. Wei, A. Sharma, J. Basset, A. S. Núñez, P. M. Haney, R. A. Duine, J. Bass, A. H. MacDonald. Supported in part by NSF Grant No. DMR-06-45377, DoE, and the Welch Foundation.

[1] M. N. Baibich *et al.*, Phys. Rev. Lett. **61**, 2472 (1988); G. Binasch *et al.*, Phys. Rev. B **39**, 4828 (1989); [2] J. C. Slonczewski, J. Magn. Magn. Mater. **159**, L1 (1996); L. Berger, Phys. Rev. B **54**, 9353 (1996); M. Tsoi *et al.*, Phys. Rev. Lett. **80**, 4281 (1998); [3] A. S. Núñez *et al.*, Phys. Rev. B **73**, 214426 (2006); [4] M. Tsoi *et al.*, Nature 406, 46 (2000); [5] A. A. Tulapurkar *et al.*, Nature **438**, 339 (2005); J. C. Sankey *et al.*, Phys. Rev. Lett. **96**, 227601 (2006); T. Staudacher and M. Tsoi, J. Appl. Phys. **109**, 07C912 (2011); [6] C. Wang *et al.*, to be published; [7] Z. Wei *et al.*, Phys. Rev. Lett. **98**, 116603 (2007); [8] A. H. MacDonald and M. Tsoi, Phil. Trans. R. Soc. A **369**, 3098 (2011).

Poster Presentations

Effect of Born and unitary impurity scattering on the Kramer-Pesch shrinkage of a vortex core in an *s*-wave superconductor

Nobuhiko Hayashi
NanoSquare Research Center (N2RC), Osaka Prefecture University,
1-2 Gakuen-cho, Naka-ku, Sakai 599-8570, Japan
n-hayashi@21c.osakafu-u.ac.jp

We theoretically investigate a non-magnetic impurity effect on the temperature dependence of the vortex core shrinkage (Kramer-Pesch effect) in a single-band *s*-wave superconductor [1]. The Born limit and the unitary limit scattering are compared within the framework of the quasiclassical theory of superconductivity.

The radius of a vortex core in type-II superconductors is one of the fundamental physical quantities which characterize a property of superconductivity. The temperature and magnetic field dependences of the core radius have been investigated theoretically and experimentally [2-5]. The low-temperature vortex core shrinkage, called the Kramer-Pesch effect [6], was theoretically investigated under the influence of non-magnetic impurities in the Born limit previously [2]. Here, we study the Kramer-Pesch effect both in the Born and unitary limits, and compare their results. It is found that the temperature dependence of the core shrinkage is stronger in the unitary limit than in the Born one, in the moderately clean regime where the mean free path is of the order of or larger than the coherence length. We elucidate that the impurity effect inside an *s*-wave vortex core is stronger in the Born limit than in the unitary limit.

[1] N. Hayashi, Y. Higashi, N. Nakai, H. Suematsu, arXiv:1110.5050.
[2] N. Hayashi, Y. Kato, M. Sigrist, J. Low Temp. Phys. 139 (2005) 79, arXiv:cond-mat/0411110.
[3] J. E. Sonier, J. Phys.: Condens. Matter 16 (2004) S4499.
[4] W. A. Atkinson, J. E. Sonier, Phys. Rev. B 77 (2008) 024514.
[5] P. Belova, K. B. Traito, E. Lähderanta, J. Appl. Phys. 110 (2011) 033911.
[6] L. Kramer, W. Pesch, Z. Phys. 269 (1974) 59.

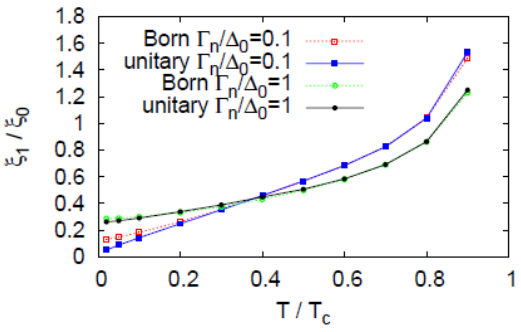

Fig. 1: Vortex core radius vs. temperature for different impurity strengths.

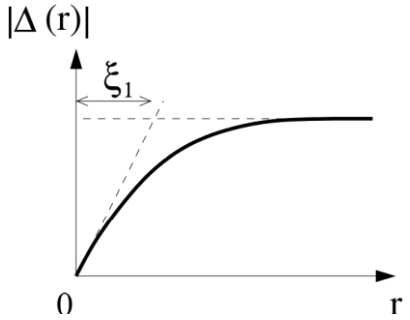

Fig. 2: Spatial profile of pair potential around a vortex core.

Simulation of Scanning Tunneling Microscopy with Morecular Tips

Sho Saiki and Nobuhiko Hayashi
Nanoscience and Nanotechnology Research Center (N2RC), Osaka Prefecture University

We report on numerical simulations for the Scanning Tunneling Microscopy (STM) with a molecular tip. Molecules are adsorbed on the top of metal tip, and it enables us to selectively observe a specific site of a sample molecule on a scale of single atom by charge-transfer interactions between the sample and tip molecules [1]. However, a qualitative analysis of experimental results would be insufficient, because this observation is dominated by quantum nature, and a complex mixture of multi-electron, dynamical, and chemical processes. In such a case, computational simulation analysis based on fundamental theory is expected to be effective, and an advanced theoretical analysis in this direction will play an important role in the development of physical science.

We have conducted tunneling current calculations based on Bardeen's perturbation theory [2, 3] in combination with a facilitating technique [4]. The electronic states of sample and tip molecules are obtained by means of the first principle LCAO-DV-Xα method [5]. The tunneling current is calculated by using those electronic states.

Here, we will show the simulation results for real-space STM imaging of the pentacene molecule observed with the CO molecular tip.

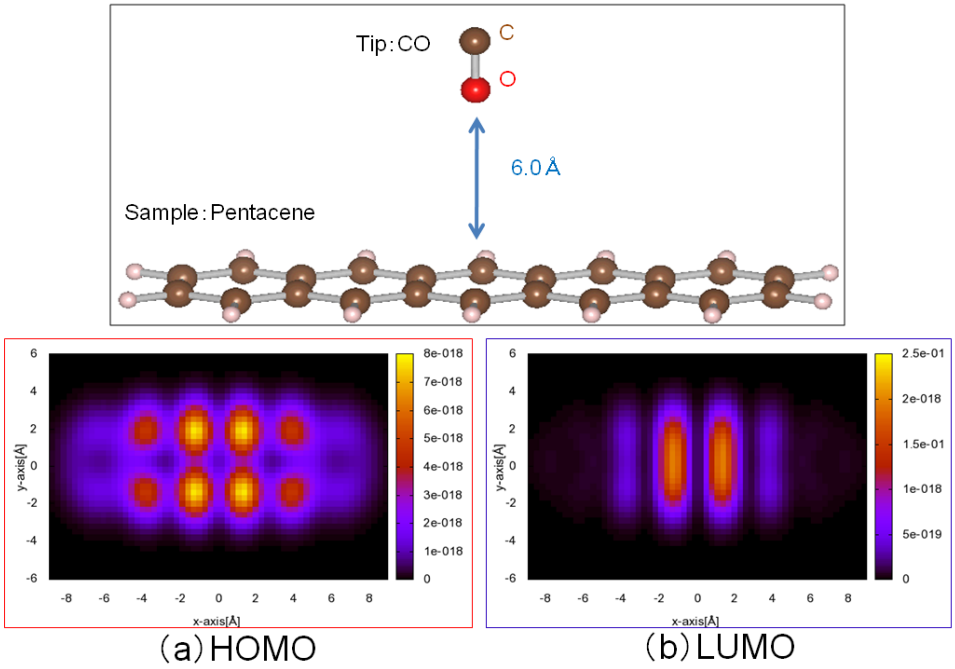

Figure 1: [Top] Simulation model of the pentacene molecule observed with the CO molecular tip. (a)HOMO level simulation image, Bias voltage -2.0[V]. (b)LUMO level simulation image, Bias voltage 1.2[V].

References

[1] T. Nishino et al., *Proc. Natl. Acad. Sci. U.S.A.* **102** (2005) 5659.

[2] J. Bardeen, *Phys. Rev. Lett.* **6** (1961) 57.

[3] M. Tsukada et al., *Sur. Sci. Rept.* **13** (1991) 265.

[4] C. J. Chen, *Phys. Rev. B* **42** (1990) 8841.

[5] H. Adachi et al., *J. Phy. Soc. Jpn.* **45** (1978) 875.

Phase-sensitive Flux-flow Resistivity in Unconventional Superconductors

Yoichi Higashi,
Department of Mathematical Sciences, Osaka Prefecture University
Yuki Nagai, Masahiko Machida,
CCSE, Japan Atomic Energy Agency
Nobuhiko Hayashi,
Nanoscience and Nanotechnology Research Center (N2RC), Osaka Prefecture University

The elucidation of the superconducting pair potential structure is of great importance for obtainingthe clue to the pairing mechanism in unconventional superconductors. The field-angle resolved thermal conductivity and specific heat measurements are powerful techniques, which can detect the anisotropy of pair potential amplitude [1], but they cannot probe the phase in the pair potential. However, it is crucial to probe the phase of the pair potential in order to discriminate unconventional superconductivity from conventional one [2]. Therefore, we theoretically propose that the field-angle dependence of the flux-flow resistivity $\rho_{\rm f}$ can be a new phase-sensitive probe [3]. We consider the following pair potential models: a line-node s-wave and a d-wave pair with the same anisotropy of the pair potential amplitude, but with a sign change only for the d-wave one. Our results reveal contrasting field-angle dependence of $\rho_{\rm f}$ between these two pair potential models [3] (see Fig. 1). To clarify its mechanism, we investigate the dependence of the quasiparticle scattering rate inside a vortex core on the Fermi wave vector $k_{\rm F}$. We also discuss the quasiparticle scattering process on a spherical Fermi surface.

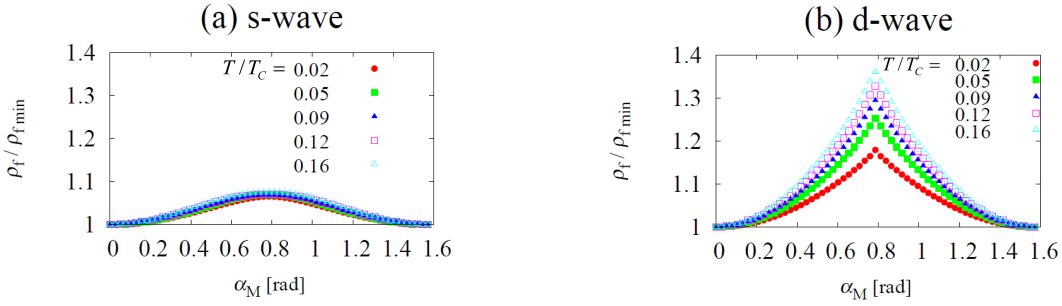

Figure 1: The field-angle ($\alpha_{\rm M}$) dependence of the flux-flow resistivity $\rho_{\rm f}$ in the case of (a) the line-node s-wave pair and (b) the d-wave pair. The data are plotted for each temperature T. $T_{\rm c}$ is the superconducting critical temperature. The vertical axis is normalized by minimum values $\rho_{\rm f\ min}$ for each temperature.

References

[1] Y. Matsuda, K. Izawa, I. Vekhter, *J. Phys.: Condens. Matter* **18** (2006) R705;
T. Sakakibara, A. Yamada, J. Custers, K. Yano, T. Tayama, H. Aoki, K. Machida, *J. Phys. Soc. Jpn.* **76** (2007) 051004.

[2] C. C. Tsuei, J. R. Kirtley, *Rev. Mod. Phys.* **72** (2000) 969;
T. Hanaguri, S. Nittaka, K. Kuroki, H. Takagi, *Science* **328** (2010) 474.

[3] Y. Higashi, Y. Nagai, M. Machida, N. Hayashi, *Physica C* **471** (2011) 828;
Y. Higashi, Y. Nagai, M. Machida, N. Hayashi, *J. Phys.: Conf. Ser.*, in press.

Numerical analysis on stability of a time oscillating discrete state coupled with a continuum

Kenichi Noba
Graduate School of Engineering, Osaka Prefecture University,
Sakai, Osaka 599-8531, Japan
Email address: noba@ms.osakafu-u.ac.jp

Numerical analysis of electron survival probability is presented for the system where a periodically driven discrete state is coupled with continuum states of the tight-binding model[1].

In discrete-continuum systems where a discrete state couples with continuum states, a discrete state is unstable and irreversibly decays into the ground state when the resonance condition is satisfied. The process of the decay of an unstable state can be modeled by the Friedrichs Hamiltonian or the Fano-Anderson Hamiltonian that is known to be an exactly solvable model[2-5]. However, physics becomes much richer and more interesting if the energies of the discrete-continuum system are driven by external fields. In a periodically driven system, for example, it is expected that the decay process is largely modified because the resonance condition can be repeatedly satisfied. It may be possible to control decay rates of unstable states by a suitable choice of external driving fields.

The purpose of this study is to investigate the decaying dynamics of an electron in a driven discrete-continuum system. For the system where a sinusoidally oscillating discrete state couples with continuum states of the tight-binding model, the stability of the discrete state is examined by analyzing the survival probability. For the local coupling case where the discrete state couples with one site of the tight-binding model, a closed form of equations is derived for the probability amplitude at the discrete state and the coupled site. These equations are numerically integrated to obtain the probabilities.

Numerical results clearly show peculiar decaying dynamics in the weak coupling case or in the large oscillation amplitude case. There appears a stable state without decay even if the discrete state is embedded inside the continuum for certain values of the amplitude and the frequency of the external field when the continuum band is relatively narrow. Also, unstable decaying states may appear even if there is no overlap between the energy of the discrete state and the continuum. The peculiar dynamics obtained here is closely related to coherent destruction of tunneling (CDT) found in the driven two-level system where the electron transition between two levels is suppressed[6,7]. The decay in the discrete-continuum system is suppressed as a result of vanishing reduced coupling constant at the resonance.

[1] K. Noba and K. Murayama, Phys. Rev. B 84, 014304 (2011).
[2] K. Friedrichs, Commun. Pure Appl. Math. 1, 361 (1948).
[3] U. Fano, Phys. Rev. 124, 1866 (1961).
[4] P.W. Anderson, Phys. Rev. 124, 41 (1961).
[5] T. Petrosky, I. Prigogine, and S. Tasaki, Physica A 173, 175 (1991).
[6] F. Grossmann, T. Dittrich, P. Jung, and P. Hanngi, Phys. Rev. Lett. 67,156 (1991).
[7] F. Grossmann, P. Jung, T. Dittrich, and P. Hanngi, Z. Phys. B 84, 315 (1991).

Complex Eigenvalue Problem of Floquet Hamiltonian of Driven Friedrichs Model

Nobuhisa Yamada, Satoshi Tanaka
Department of Physical Science, Osaka Prefecture University
Ken-ichi Noba
Department of Mathematical Science, Osaka Prefecture University
Tomio Petrosky
The Center for Complex Quantum Systems, University of Texas at Austin

Coherent dynamics of a quantum system driven by external fields has been paid much attention with an attempt to achieve a coherent control in a quantum system. The Floquet theorem is one of the powerful methods to investigate a time evolution of a periodically driven quantum system. There have been many works to study the time evolution of a quantum system consisting of several discrete states coupled with each other, and many interesting phenomena has been revealed, such as coherent destruction of tunneling[1], and so on[2, 3, 4]. On the other hand, there have been a few works to investigate the time evolution of an unstable quantum system with continuous spectrum under an external field. For this case, the system becomes nonintegrable due to a resonance singularity which causes irreversible decay. Therefore, it is interesting to investigate the possibility of controlling the irreversible decay by applied external fields.

In this work, we theoretically investigate a time evolution of a quantum system described by the Friedrichs Hamiltonian under a periodic external field. The Friedrichs model has been widely used to investigate the decaying process of an excited atom with spontaneous photon emission[5, 6]. However, continuous spectrum of the electron plays a role of the photon in our case. Here, we focus on the driven Friedrichs Hamiltonian written by

$$H = (\epsilon_d + A\cos\omega t)\,|d\rangle\langle d| + \sum_k \epsilon_k |k\rangle\langle k| + \lambda V \sum_k \left(|k\rangle\langle d| + |d\rangle\langle k|\right),$$

where $|d\rangle$ is a discrete state, $|k\rangle$ is a continuous state with the energy ϵ_k in terms of a box normalization, and V is the interaction between them with the coupling constant λ. Since the Hamiltonian is periodic in time, we use the Floquet theorem to consider the eigenvalue problem of a time-independent Floquet Hamiltonian. Here we concentrate on the behavior of the complex pole of the Green's function for the Floquet Hamiltonian. The imaginary part of the pole gives the decay rate of the discrete state.

We have shown that in the weak coupling case the location of the complex pole is given by

$$\sigma_d = \epsilon_d + \lambda^2 \sum_{n=-\infty}^{\infty} \Xi\left(\epsilon_d - n\hbar\omega\right) J_n^2\left(\frac{A}{\hbar\omega}\right),$$

where J_n is the nth-order Bessel function, and $\Xi(z) = \sum_k V^2/(z-\epsilon_k)$ is the self-energy part of the discrete state of the Friedrichs model. It is found from this expression that an unstable decaying state without an external field turns out to be stable by applying the external field when the imaginary part of the pole vanishes. This happens when $J_0(A/\hbar\omega) = 0$ and $\mathrm{Im}\ \Xi(\epsilon_d - n\hbar\omega) = 0$ for any $n(\neq 0)$. This condition is satisfied only when the bandwidth of the continuous band spectrum is smaller than $\hbar\omega$. This result is consistent with the numerical analysis presented in the previous article[7].

References

[1] F. Grossmann, T. Dittrich, P. Jung, and P. Hanggi, Phys. Rev. Lett. **67**, 516 (1991)

[2] D. H. Dunlap and V. M. Kenkre, Phys. Rev. B **34**, 3625 (1986)

[3] Y. Kayanuma, Phys. Rev. A **50** (1994)

[4] D. F. Martinez and L. E. Reichl, Phys. Rev. B **66**, 174306 (2002)

[5] K. Friedrichs, Commun. Pure Appl. Math. **1**, 361 (1948).

[6] T. Petrosky, I. Prigogine and S. Tasaki, Physica A **173** (1991) 175-242

[7] K.Noba and K. Murayama, Phys. Rev. B **84**, 014304 (2011)

Complex Eigenvalue Problem of Liouvillian for Weakly Coupled One-dimensional Quantum Lorentz Gas

Kazunari Hashimoto, Yoichiro Sakaguchi, Kazuki Kanki, Satoshi Tanaka
Department of Physical Science, Osaka Prefecture University
Tomio Petrosky
Center for Complex Quantum Systems, The University of Texas at Austin

We investigate non-equilibrium transport processes of the weakly coupled one-dimensional (1D) quantum Lorentz gas in terms of the complex spectral representation of the Liouville-von Neumann operator (the Liouvillian). The imaginary part of an eigenvalue of the Liouvillian gives a transport coefficient in an irreversible process. Unlike in a corresponding 1D classical system that has no imaginary component of the eigenvalue, the spectrum of the quantum system has an imaginary component through the forward scattering between particles. Hence, dissipation appears as a purely quantum effect in the 1D case. The low dimensionality of the system makes the theoretical analysis much simpler than that in a system in higher dimensions. Taking advantage of this simplicity, we can exactly solve the eigenvalue problem. This exact solution allows us to discuss non-equilibrium relaxation phenomena even in a non-hydrodynamic regime where the wavenumber associated with the spatial inhomogeneity is much larger than the inverse of the mean-free-length.

The Lorentz gas consists of a test particle and uniformly distributed environmental particles. We assume that the mass of the environmental particles is much heavier than the mass of the test particle. Interactions are taken into account only between the test particle and each of the environmental particles. We also assume that initially the environmental particles are in thermal equilibrium with temperature T in the Maxwell-Boltzmann distribution.

In a traditional approach, the transport process of the system was studied with the phenomenological Boltzmann equation[1, 2]. In this phenomenological approach, the imaginary part of the eigenvalue of the Boltzmann collision operator that corresponds to the imaginary part of the eigenvalue of the Liouvillian reaches a constant value in the large wavenumber limit (Fig.1.A). In contrast, the true transport coefficient obtained by the eigenvalues of the Liouvillian asymptotically vanishes for large wavenumbers (Fig.1.B). This implies that a wave packet with components of extremely large wave numbers propagates like a free particle. As a result, this wave packet spreads its width through the phase mixing in a first stage. Then, after certain time the propagation of the wave packet is superseded by diffusion.

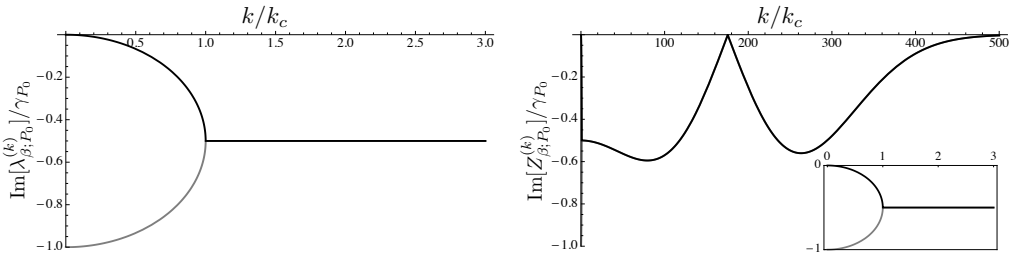

Figure 1: The dependence on wavenumber (k) of the imaginary part of the eigenvalues of the phenomenological Boltzmann collision operator(A) and Liouvillian(B). The k_c is the inverse of mean-free-length and the γ_{P_0} is the decay rate of the momentum distribution.

References

[1] R. Balescu, *Statistical Mechanics of Charged Particles*, (John Willey & Sons, 1963).

[2] Z. L. Zhang, *Doctoral dissertation*, The University of Texas at Austin, 1995.

Photo-induced relaxation dynamics of spin-electron coupled systems

W. Koshibae[1], N. Furukawa[2,3] and N. Nagaosa[1,4,5]
[1]Cross-Correlated Materials Research Group (CMRG), RIKEN, Wako 351-0198, Japan
[2]Aoyama-Gakuin University, 5-10-1, Fuchinobe, Sagamihara, Kanagawa 229-8558, Japan
[3]ERATO-Multiferroics, JST, c/o Dept. of Appl. Phys., University of Tokyo, Tokyo 113-8656, Japan
[4]Department of Applied Physics, University of Tokyo, Tokyo 113-8656, Japan
[5]Correlated Electron Research Group (CERG), RIKEN, Wako 351-0198, Japan

The anomalous and large cross-effect between electronic transport and external field is nothing more than the control of the excited electronic states and its relaxation by the external field. The colossal magnetoresistance in manganites is an example of the control of the spin, charge, and orbital ordering by external fields. In the spin-electron coupled systems, the time evolution of the nanoscaled electronic structure plays essential role for electronic phase transition by external fields.

We study quantum dynamics of the excited electronic states in the double-exchange model at half-filling by solving coupled equations for the quantum evolution of electrons and Landau-Lifshits-Gilbert equation for classical spins. The Hamiltonian is written as,

$$H = -t \sum_{<ij>,\sigma} \left(c_{i\sigma}^{\dagger} c_{j\sigma} + h.c. \right) - J_H \sum_i \left(\vec{\sigma}_{\alpha\beta} c_{i\alpha}^{\dagger} c_{i\beta} \right) \cdot \vec{S}_i + J \sum_{<ij>} \vec{S}_i \cdot \vec{S}_j + J_N \sum_{<ij>} \left(\vec{S}_i \cdot \vec{S}_j \right)^2 . \quad (1)$$

The localized spin $\vec{S}_i$ is considered to be a classical vector with a magnitude S. At half filling, the spin-electron coupled state of the model (1) shows a meta-stability between ferromagnetic metallic state and antiferromagnetic insulating one. Using finite size systems, we numerically investigate the photo-induced metal-insulator transition by calculating time evolution of the electronic states and local spin structure. The spatial and temporal evolutions of the system during the transition have been revealed including i) the threshold behavior with respect to the intensity and energy of light, ii) multiplication of particle-hole (p-h) pairs by a p-h pair of high energy, and iii) the space-time pattern formation such as (a) the stripe controlled by the polarization of light, (b) coexistence of metallic and insulating domains, and (c) dynamical spontaneous symmetry breaking associated with the spin spiral formation imposed by the conservation of total spin for small energy-dissipation rates.

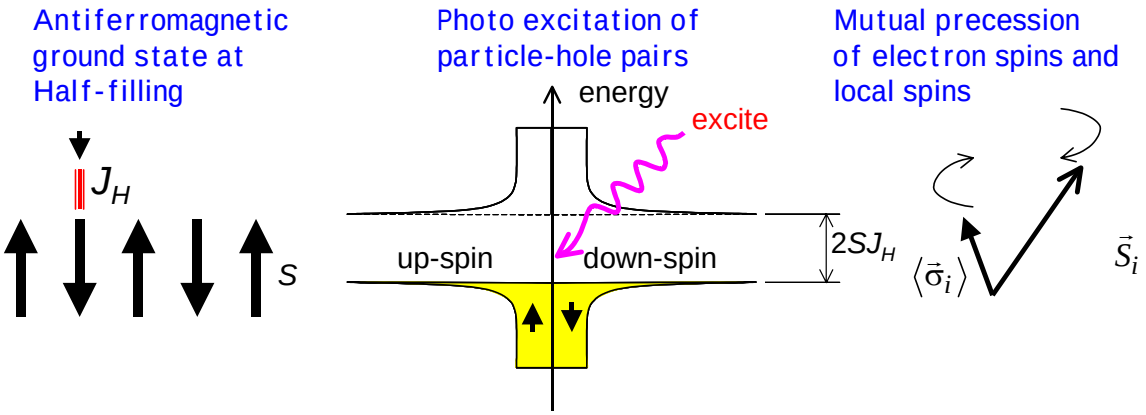

Fig. Schematic representation of the antiferromagnetic ground state and the interplay of electron and local spins for the relaxation dynamics.

Scattering control of Bloch electrons under an oscillating external field

Yoshihiko Mizumoto and Yosuke Kayanuma
The Research Organization for the 21st Century, Osaka Prefecture University and JST-CREST, Japan
mizumoto@pe.osakafu-u.ac.jp

The application of a periodic electric field causes modulation of quantum dynamics of electrons. The quantum dynamics under periodic field has been studied for a long time. Coherent destruction of tunneling [1] (CDT) and dynamical localization [2] (DL) are well-known examples. In CDT and DL, the wave packet motion is frozen under the periodic field with an appropriate condition of amplitude-frequency ratio in the two-level and one-dimensional system, respectively. Recently, these phenomena have been demonstrated experimentally [3,4] in the cold atoms with optical lattice systems. With the recent improvement of these quantum simulation techniques, importance of studying the quantum dynamics is much grown. In the recent study, we revealed that the band gap of one-dimensional Peierls systems collapses in the application of the electric field with certain condition [5].

The collapse corresponds to suppression of Bragg scattering caused by destructive interference between two states in momentum space.

In the present study, we examined potential scattering of Bloch electron under periodic external field with aim to control the potential scattering by external field. Consider a one-dimensional tight-binding model with half-bandwidth B and localized potentials V_j. The discrete system corresponds to solids and optical lattices. The model Hamiltonian of our system under the field with energy amplitude A and photon energy $\hbar\omega$ is written as,

$$H(t) = -(B/2)\sum_j \left[\exp\left(-i(A/\hbar\omega)\sin(\omega t)\right)|j\rangle\langle j+1| + (\text{H.c.})\right] + \sum_{j=-L+1}^{L-1} V_j|j\rangle\langle j|.$$

The quantum dynamics under the periodic field is described by the Floquet theory. According to the Floquet theory, the quasi-energy of Floquet states is conserved. Thus, for the incident energy ε_{k_I}, Floquet states correspond to the Houston states[6] with the quasi-energy $\varepsilon_k = \varepsilon_{k_I} \pm n\hbar\omega$ are the solutions of Schrödinger equation of the system in the potential-free region. The transmission and reflection coefficients are given by iteration of these Floquet states on the potential surface by means of the Green function. Figure 1 shows the results for the case of single-site potential. As shown in figures, the transmission spectrum has several structures. The origin of these structures is divided into three types; suppression of scattering by band gap collapse, resonance of scattering states with *anti-bound state*, and resonance with the band edge.

In the presentation, we show the calculation detail for the system with arbitrary-form potential, and discuss the dependence of the modulation on the parameters.

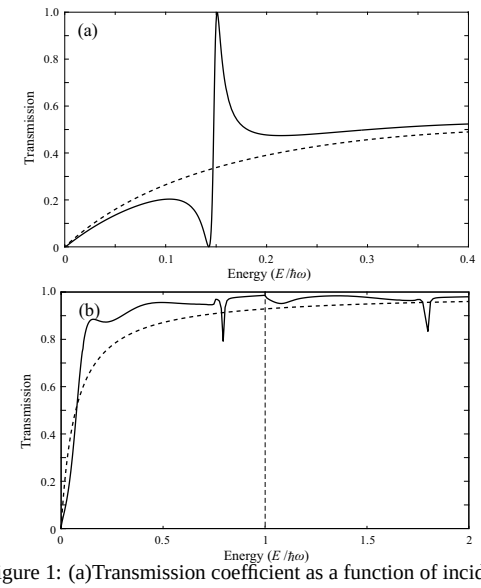

Figure 1: (a)Transmission coefficient as a function of incident energy. The dashed line shows one of field-free system. The parameters are $B/\hbar\omega = 0.5$, $V_0/\hbar\omega = 0.5$, $A/\hbar\omega = 0.5$. (b) Transmission coefficient for the case of parameters $B/\hbar\omega = 6.0$, $V_0/\hbar\omega = 1.0$, $A/\hbar\omega = 1.25$.

References

[1] F. Grossmann, et al., *Phys. Rev. Lett.* **67** (1991) 516.

[2] D. Dunlap and V. Kenkre, *Phys. Rev. B* **34** (1986) 3625.

[3] K. Kierig, et al., *Phys. Rev. Lett.* **100** (2008) 190405.

[4] K. Madison, et al., *Phys. Rev. Lett.* **81** (1998) 5093.

[5] Y. Mizumoto and Y. Kayanuma, *Phys. Rev. B* **81** (2010) 233202.

[6] W. Houston, *Phys. Rev.* **57** (1940) 184.

Spectroscopy of quasi-particle bound states around a pair of half-quantum vortices in triplet *p*-wave ($p_x \pm ip_y$) superconductors

Yuhei Niwa[A,B], Masaru Kato[A,B], Kazumi Maki[C]
Department of mathematical sciences Osaka Prefecture University[A], JST-CREST[B], USC[C]
1-1, Gakuen-cho, Naka-ku, Sakai, Osaka, 599-8531, Japan[A]
5, Sanbancho, Chiyoda-ku, Tokyo 102-0075, Japan[B]
Department of Physics and Astronomy, University of Southern California, Los-Angels, CA90089-0484, USA[C]
Email address: yuhei@ms.osakafu-u.ac.jp

Triplet *p*-wave superconductors such as Sr_2RuO_4 were discovered. Due to spin degree of freedom, it was suggested that a pair of half-quantum vortices (HQVs) can exist in triplet superconductors. It is found in phenomenological theory that a pair of HQVs is more stable than a singly quantized vortex in some cases. [1]

We study the spectroscopy of this half-quantum vortex states in chiral *p*-wave ($p_x \pm ip_y$) superconductors. For this purpose, we developed a new numerical method with Mathieu functions in elliptic coordinates where we put two vortex cores on each focus. [2]

Using this method, we have solved the Bogoliubov-de Gennes equations for a pair of HQVs and a pair of singly quantized vortices, and we have obtained the local density of state (LDOS) and magnetization. From each numerical result of the LDOS, we find that two bound states at two vortex cores interfere with each other for a pair of singly quantized vortices case, but don't interfere with each other for a pair of HQVs case. (Figure(a):a pair of singly quantized vortices, Figure(b): a pair of HQVs) Besides, because each half-quantum vortex consists of only up-spin or down-spin superconducting electrons independently, We find that spin magnetic moments are generated around the pair of HQVs.

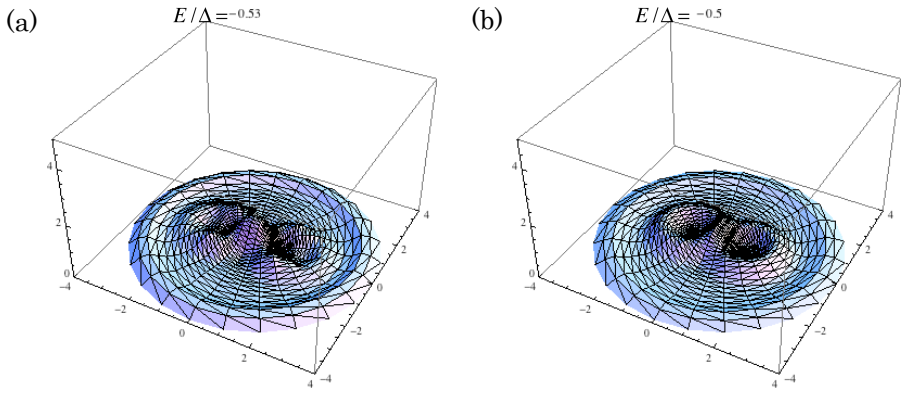

Fig. 1. The LDOS around a pair of singly quantized vortices at E/Δ=-0.53 (a) and a pair of HQVs at E/Δ=-0.5 (b) , where Δ is gap energy

Reference

[1] H.-Y.Kee and K.Maki, Europhys. Let. **80** 46003 (2007)
[2] Y. Niwa, M. Kato, K. Maki, Physica C **470** 1151 (2010)

Double Cluster Model Study of NiO 2p X-ray Photoemission Spectroscopy and Resonant Inelastic X-ray Scattering

Atsushi HARIKI and Takayuki UOZUMI
Department of Mathematical Sciences, Graduate School of Engineering,
Osaka Prefecture University, Japan
hariki@ms.osakafu-u.ac.jp

NiO is a prototype of charge transfer insulator and considered to be one of the most important compounds to understand electronic structure of strongly correlated systems, such as transition metal oxides. However, a simple conventional band theory cannot explain the insulating energy gap and the electronic structure of NiO seems to pose fundamental questions concerning the quantum many body problems. X-ray spectroscopy has great advantages to investigate electronic structure of strongly correlated systems. We can extract information on valence electrons through the spectral analyses using a proper theoretical model, and a variety of excitation processes available with different selection rules enables us to study a compound from different point of view. Since the 1990's, the so-called single impurity model as Anderson impurity model and charge transfer cluster model, which describe the essence of electronic structures, have greatly contributed to the interpretation of various X-ray spectra. Recently, remarkable progress in experimental resolution reveals several fine structures clearly, which are expected to be related with the insulating property of NiO. However, the single impurity models are not enough to interpret the fine structures essentially. For example, double peak structure observed at the $2p_{3/2}$ line in 2pXPS of NiO cannot be explained by the single impurity model. Although some phenomenological extensions were made recently [1], there seems to be still controversial.

In our study, we develop a full multiplet double cluster model including inter-metallic charge transfer effect, or non-local effect, which can be a trigger of various effects, such as a super exchange coupling, orbital and spin correlations and so on. The non-local effect in the final state of 2pXPS causes not only a direct d-d screening but also an indirect screening via oxygen sites. Calculated result by this model shows a double peak structure with appropriate hybridization strength V (D-D) =1.0eV, as a non local effect, and reproduces the high-resolution XPS spectra (see Fig.1). Moreover, we also perform a spectral analysis for the recent high resolution resonant inelastic X-ray scattering (RIXS) [2], which shows a good agreement with the experiment. Consequently, the fine structures observed in high-resolution 2pXPS and RIXS can be explained in the same footing, which will lead to further understanding of the electronic structure of NiO.

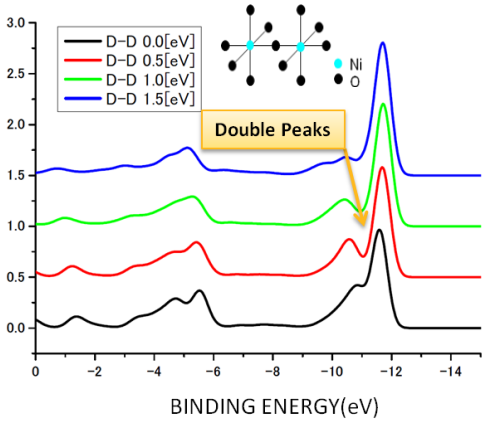

Fig.1: A full multiplet double cluster calculation.
Double-peak structure can be shown with V (D-D) =1.0eV.

[1] M.Taguchi, et al: Phys. Rev. Lett. **100** (2008), 206401.
[2] G.Ghiringhelli, et al: Phys. Rev. Lett. **102**(2009), 027401.

Non-phenomenological Impurity Model Analysis of Resonant Inelastic X-ray Scattering for 3d System

Yu KAWANO and Takayuki UOZUMI
Department of Mathematical Sciences, Graduate Scholl of Engineering,
Osaka Prefecture University, Japan
kawano@ms.osakafu-u.ac.jp

X-ray spectroscopy is a powerful tool to study electronic structure of 3d compounds. In early stage, the observed spectra, such as X-ray photoemission spectra (XPS) and X-ray absorption spectra (XAS), were successfully analyzed using a phenomenological MO_6-type charge transfer cluster model, for example. In these studies, the model analyses greatly contributed to the interpretation of basic spectral features and also to the determination of the so-called solid-state parameters, such as M3d-O2p hybridization V and 3d Coulomb repulsive energy U_{dd}. Recent years, experimental techniques are developing rapidly and high-energy resolution, less than 100meV, becomes available in resonant inelastic X-ray scattering (RIXS) measurements [1]. RIXS is the coherent second-order optical process, while XPS and XAS are the first-order optical process. Thus, we expect that the detailed analyses of relatively complicated RIXS process bring us more information about the electronic states. However, the conventional cluster model seems to be too simple to analyze the fine structures in the RIXS measurements.

For this aim, we developed a new theoretical framework based on the combination of Anderson impurity model with an LDA band structure calculation. Then, our model includes realistic valence band structure within the Slater-Koster LCAO scheme and has essentially only one adjustable parameter, U_{dd}, in contrast to the conventional phenomenological model.

In the session, we show the calculated RIXS for NiO and MnO, using our framework described above. Fig.1(a) is the result for NiO. Here we see a bunch of peaks due to d-d excitations in the RIXS final states and also see a broad band structure due to charge transfer excitations, which show good agreement with the experimental RIXS shown in Fig. 1(b). We also discuss the remarkable polarization dependence of the peak intensities and temperature effects.

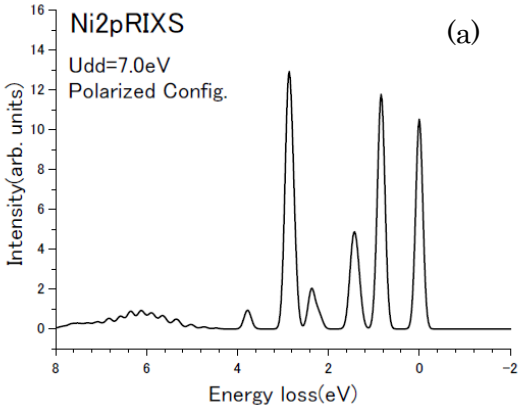

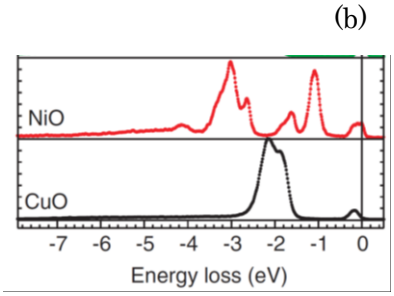

Fig.1 (a) NiO calculated RIXS. (b) NiO experimental RIXS from ref. [1].

[1]G.Ghiringhelli et al., Eur. Phys. J.,**169**(2009)199

A Non-phenomenological Framework for X-ray Spectroscopy Analysis - Theoretical Scheme and Application to 3d Systems -

Takayuki UOZUMI
Department of Mathematical Sciences, Graduate School of Engineering,
Osaka Prefecture University, Japan
uozumi@ms.osakafu-u.ac.jp

In the last two-decades, X-ray spectroscopy, using synchrotron radiations, has been a powerful technique to investigate the electronic structure of 3d and 4f systems. Among series of studies, experimentally observed core-level spectra, such as X-ray photoemission spectrum (XPS) and X-ray absorption spectrum (XAS), were analyzed by means of a phenomenological impurity model which includes several adjustable parameters. In studies of 3d transition metal oxides, for example, MO_6-type charge-transfer cluster model with full-multiplet interactions has been used as a standard theoretical model, and the so-called solid state parameters, M3d-O2p charge transfer energy Δ, hybridization strength V, crystal field 10Dq, and 3d Coulomb repulsive energy U_{dd} were successfully determined through the analyses of core-level spectra[1]. The collaborations between experiment and the impurity model analyses were very fruitful in the interpretation of fundamental structures of spectra and in making a rough plot of electronic structure in terms of the solid state parameters.

Nowadays, however, the experimental development goes further, in resolution for example, beyond the description of the simple impurity model, we are facing with a turning point to develop a new theoretical framework for the analyses of high-resolution spectra. In this context, there is an essential point required, i.e., the non-phenomenological scheme with realistic valence band structures, and such a framework enables us to derive more information about the electronic structure in low-energy scale through the analysis of fine spectral features, without possible ambiguities from the determination process of optimal values of adjustable parameters. For this aim, we develop a framework which combines full-multiplet Anderson impurity model with the LDA band structure calculation. The basic idea is straight forward; (i) Slater-Koster (SK) parameters are estimated from a least square fitting between LDA- and SK-LCAO energy dispersion curves, (ii) realistic valence band structure of host crystal without the impurity atom is calculated within the SK-LCAO scheme and is taken into account in the Anderson impurity model. Then, our new framework includes only U_{dd} as an adjustable parameter, since the other SK parameters are fixed in the LDA band mapping.

In the session, we describe our method in detail and show the results for MO (M=Ni, Co, Fe, Mn) system systematically. In NiO, for example, all the spectra of 2pXPS, 2pXAS, valence-band photoemission, and inverse photoemission are consistently reproduced within our framework with just one parameter U_{dd}. Moreover, we demonstrate another application of our framework to high-spin – low-spin transition of MO system under ultra high-pressure [2].

[1]T. Uozumi, et al. : J. Electron Spectrosc. and Relat. Phenom. **83** (1997) 9.,
[2]A. Mattila, et al. : Phys. Rev. Lett. **98** (2007) 196404.

Raman Scattering Emission from Silicon High-*Q* Photonic Crystal Nanocavities

Yasushi Takahashi[1,2], Ryo Terawaki[1], Masahiro Chihara[1], Takashi Asano[3], Yoshitaka Inui[3], and Susumu Noda[3]
[1]Nanoscience and Nanotechnology Research Center, Osaka Prefecture University, Japan
[2]PRESTO, Japan Science and Technology Agency (JST), Japan
[3]Department of Electronic Science and Engineering, Kyoto University, Japan
Author e-mail address: y-takahashi@21c.osakafu-u.ac.jp

Stimulated Raman scattering has been drawing attention in silicon (Si) photonics for developing optical amplifiers or lasers [1]. The continuous wave (cw) operation of Si Raman laser has been achieved using a Si rib waveguide with a reverse biased p-i-n diode structure, however, the laser threshold is as high as 20 mW, even in a high-*Q* ring cavity structure [2]. In addition, the laser cavity is longer than 1 cm. For practical applications such as CMOS-compatible Si photonic chips, it is important to decrease both the laser threshold and the cavity size. Nanocavities in two-dimensional photonic crystal slabs have high quality factors (*Q*) and small modal volumes (*V*) [3,4]. Their high *Q/V* values provide strong light-matter interaction, which enhances nonlinear optical phenomena. It has been shown numerically that pulse operation of a Si Raman laser could be possible without the p-i-n diode by using Si nanocavities with *Q* of ~10^4 [5]. We have already achieved the highest *Q* values of 3.9×10^6 for Si nanocavities [6], which may be capable of producing Si Raman lasers with cw operation. In preparation of constructing such a device, we have experimentally investigated how the nanocavity *Q* enhances spontaneous Raman scattering.

Figure 1 shows the scanning electron microscope (SEM) images for measured nanocavities. These four nanocavities have different *Q* factors but have the same photonic parameters in air hole radius of 100 nm, lattice constant of 370 nm, and slab thickness of 200 nm. The cavities were excited through the excitation waveguide next to the cavity. The light coupled into the nanocavity interacts strongly with the vibrational mode of the optical phonon in Si due to the large *Q/V*. As a result, Raman scattering is efficiently generated, which was spectrally measured. Figure 2 shows the relation between the coupled pump power into the cavity and detected Raman emission power for four nanocavities. It is noted that a few hundred nanowatt is sufficient for obtaining the Raman peak in the hetero nanocavities. The efficiency for producing the Raman scattering is almost enhanced in proportion to the *Q* factors of nanocavities. These are very encouraging results for creating nanocavity Si Raman lasers.

Reference

[1] R. Claps, *et. al.*, Electronics Letters, IEE **38**, 1352-1354 (2002).
[2] H. Rong, *et. al.*, Nature Photon. **1**, 232-237 (2007).
[3] Y. Akahane *et. al.*, Nature **425**, 944-947 (2003).
[4] B. S. Song *et. al.*, Nature Mater. **4**, 207-210 (2005).
[5] X. Yang, *et. al.*, Opt. Express **15**, 4763-4780 (2007).
[6] Y. Taguchi *et. al.*, Opt. Express **19**, 11916-11921 (2011).

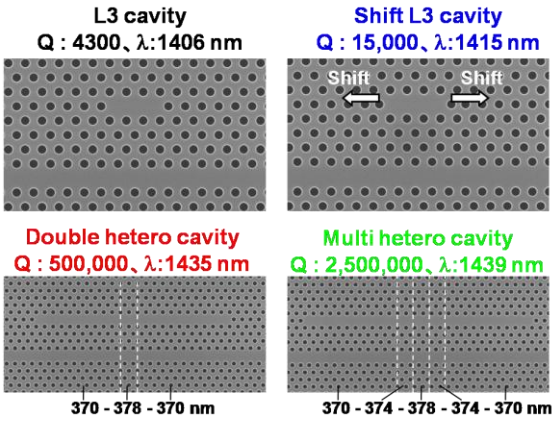

Fig. 1. SEM images for measured nanocavities with experimental *Q* factors and resonant wavelengths.

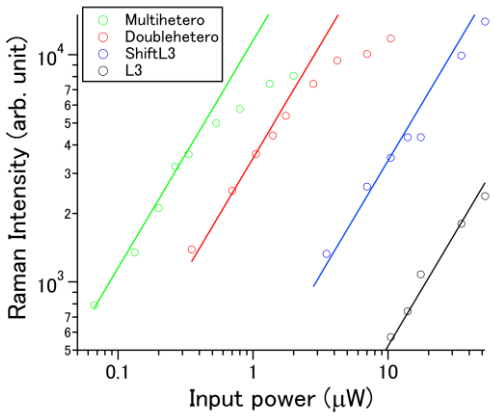

Fig. 2. Raman scattering power vs input power into the nanocavities.

Role of non-radiative relaxation process in formation of organic nano-particles by liquid laser ablation

Ikuko Akimoto[1], Masahiro Ohata[1], Nobuhiko Ozaki[1] and Gu Ping[2]
[1]Faculty of Systems Engineering, Wakayama University, Japan
[2]Faculty of Education, Wakayama University, Japan
akimoto@sys.wakayama-u.ac.jp

Usage of organic materials has been expanded to device field in these decades. However, since a fabrication process of devices from small organic molecules requires highly costed vacuum sublimation method, the application of organic materials has been limited. Many small molecules are difficult to be solved in ubiquitous polarized solvents, such as alcohol or water, without any additional aqueous moieties on the molecule or any surfactants. If aqueous solutions of plain organic molecules could be obtained, various usages would be expected; wet process in device fabrication, drag delivery system, cosmetic application, and so on. To obtain such solutions, modification of organic powders into nano-particles is one of promising technique.

A liquid laser ablation method is capable to form organic nano-particles without any surfactants. We have carried out the laser ablation method for a yellow pigment quinacridonequinone (QQ) and fullerene C_{60} in poor solvent water by 5ns-pulse laser. As a result, each precipitation was varnished with a change of solvent color, and then nano-particles of QQ or C_{60} were formed. Mean diameters of the nano-particles were estimated by a dynamical light scattering method in both solutions as a few ten nano-meters. Therefore, we obtained aqueous solution of QQ or C_{60} nano-particles by the laser ablation method.

The mechanism of the fragmentation of initial organic powders into nano-particles has been explained by rapid photo-thermal conversion on the surface layers of crystals [1]. In order to verify the expected mechanism, we focused on relaxation processes after optical excitation, because non-radiative relaxation processes such as intersystem crossing and/or internal conversion are thermal sources in the molecules. We found a transient triplet state with lifetime of 57μs by time-resolved ESR measurement in QQ as shown in Fig.1 and hardly observed radiative relaxation by photo-luminescence measurement. Such results are in line with the case of fullerene C_{60}, where the well-defined triplet state and radiative quantum yield as low as 10^{-4} have been known [2]. The existence of the transient triplet state in QQ as well as in C_{60} implies additional thermal energy conversion, because the triplet states are forbidden for radiative relaxation. The efficient intersystem conversion from singlet to triplet state after optical excitation might be a necessary condition of organic molecules for the fragmentation by the laser ablation.

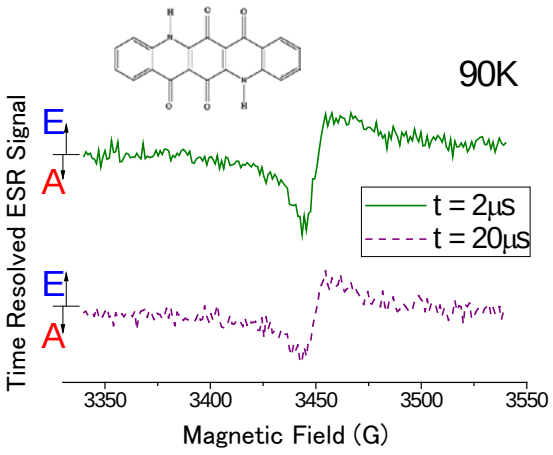

Fig.1 Transient ESR spectra of QQ delayed at 2μs and 20μs after laser pulses at 435nm, taken at 90K. Inset shows molecular structure of QQ.

[1] T.Sugiyama, T.Asahi, H.Takeuchi and H. Masuhara, Jpn.J.Appl.Phys.**45** (2006)384.
[2] M.S.Dresselhaus, G. Dresselhaus and P.C.Eklund, *"Science of Fullerenes and Carbon Nanotubes"* (Academic Press, 1996).

Structural change of single-walled carbon nanotubes induced by soft x-ray irradiation

Kunihito Asai, Toshiya Murakami, and Chihiro Itoh
Department of Materials Science and Chemistry, Wakayama Univeristy

The electronic property of single-walled carbon nanotube (SWNT) depends on its wrapping geometry. Accordingly, structural control of SWNT is a key to developing the electronic property as a nanoelectronic materials. In the nano electronic application, in-situ modification of SWNT nano structure is desirable. However, chemical and mechanical stability of SWNT hinders in structural modification of SWNTs. Electron beam irradiation has been shown to modify the nanostructure of SWNTs.[1, 2, 3] However, the primary process and dynamics are difficult to understand, because electron bombardment leads to complex effects involving knock-on, valence and inner core excitation. The complexity gives rise to difficulty of the structural control.

In the present paper, we report the results of the resonant Raman spectroscopic study on the structural change of SWNT induced by soft X-ray irradiation. The excitation process of soft X-ray is dominated by inner core excitation, which is much simpler than the electron irradiation. The SWNT films formed on CaF_2 substrates were irradiated by x-ray having a spectrum showing a peak at 277 eV with a FWHM of 210 eV. Fig.1(a) shows Raman scattering spectra of an irradiated and an unirradiated samples. Both spectra are characterized by three peaks at 1320 cm^{-1} (D band), 1560 cm^{-1} (G^- band) and 1595 cm^{-1} (G^+ band). The D band is associated with disorder of graphen surface, and the intensity ratio of the D band to G^+ band (D/G) is a good measure of the SWNT quality. The frequency of G^+ band does not vary with diameter, while G^- band gets softer in smaller diameter nanotubes.[4] The X-ray irradiation obviously enhances D/G from 0.025 to 0.097. Moreover, the irradiated SWNT shows slight high frequency shift of the G- band frequency. The results indicate that the X-ray irradiation leads to defect formation and structural change of SWNT. Figure 1(b) shows the low-frequency Raman spectra of the SWNT measured before and after the X-ray irradiation. The prominent peak around 165 cm^{-1} is ascribed to radial breathing mode (RBM). The RBM frequency, ω, has a simple relation with the SWNT diameter, d, as $\omega = 248/d$ [cm^{-1}]. Clearly, the X-ray irradiation leads to high-frequency shift of RBM by $\sim$5 %. This result demonstrates that the x-ray irradiation leads to structural change of SWNTs.

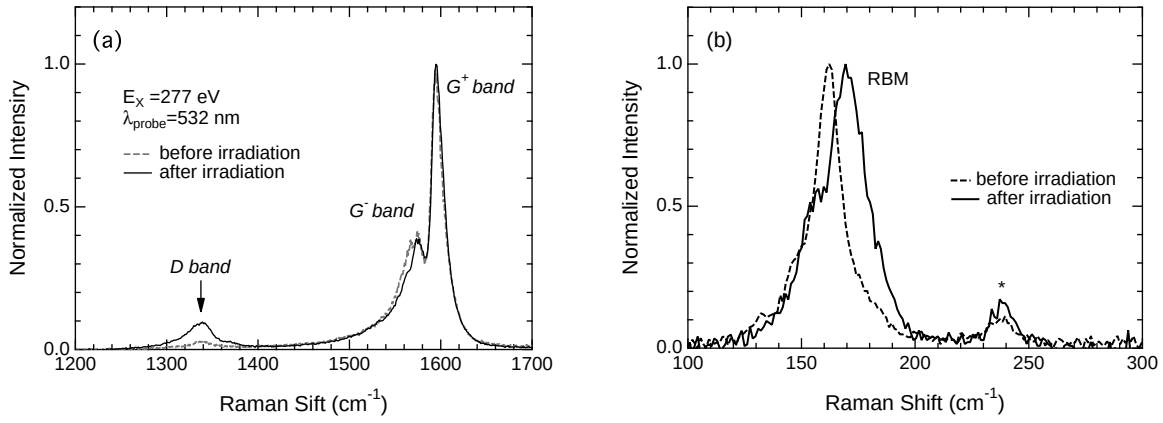

Figure 1: Resonant Raman spectra of SWNT measured before and after the 277-eV X-ray irradiation. The peak marked by * in (b) is ascribed to substrate.

References

[1] A. Hashimoto, K. Suenaga, A. Golther, K. Urita, and S. Iijima, Nature **430**(2004), 870.

[2] M. Terrones, H. Terrones, F. Banhart, J.-C. Charlier, and P. M. Ajayan, Science **288**(2000), 1226.

[3] M. Terrones, F. Banhart, N. Grobert, J.-C. Charlier, H. Terrones, and P. M. Ajayan, Phys. Rev. Lett. **89**(2002) 075505.

[4] A. Jorio et al., Phys. Rev. **B65**(2002) 155412.

[5] A. Jorio, et al., Phys Rev Lett. **86**(2001), 6.

Free exciton luminescence of anthracene nanocrystals

M. Yamashita, T. Kawai, and K. Mizoguchi
Department of Physical Science
Osaka Prefecture University, Japan
s_m.yamashita@p.s.osakafu-u.ac.jp

The physical properties of inorganic micro- and nano- crystals, such as low threshold for lasing and quantum size effect, have been investigated. However, nanocrystals of organic semiconductors are less studied. Among many organic semiconductors, anthracene crystals are an attractive material for studying optical properties related with the exciton states, because anthracene crystals have a weak exciton-phonon interaction system and show the strong free exciton luminescence. In this research, we have investigated the optical properties of thin films and nanocrystals of anthracene to reveal the effect of microcrystallinity on exciton nature in organic semiconductors.

Anthracene thin films were prepared by cell method [1]. In this method, two folded quartz plates (a cell) was immersed in the melt of anthracene. The melt penetrated into a narrow gap of the cell through capillary action and was crystallized by slow cooling. The thicknesses of the anthracene thin films prepared were about 35, 150 and 700 nm. In the preparation of anthracene nanocrystal, the cell sandwiching anodic porous alumina, which is an aluminum oxide film with regularly arranged nanoscopic pores, was used in the process of the cell method. Porous alumina was prepared by the anodization of an aluminum plate in acidic electrolyte [2]. Figure 1 shows a schematic of anodic porous alumina. The average diameter of the pores of the porous alumina is considered to be 20 nm from the conditions of the anodization. The cell sandwiching the porous alumina was immersed in the melt of anthracene and the melt percolated into the gap of the cell and the pores of the porous alumina. The melt was crystallized by slow cooling and anthracene nanocrystals were prepared in the pores of the porous alumina.

Figure 2 shows the luminescence spectra of the anthracene thin film with the thickness of 150 nm and the anthracene nanocrystals at 15 K. In the anthracene thin film, the free exciton luminescence (*b-luminescence*) from the lower Davydov state of the lowest singlet exciton and the luminescence (bound) from the bound exciton state are observed. No luminescence is observed in the higher energy side than the *b-luminescence* band, where anthracene crystals have the large absorption coefficients. In the anthracene nanocrystals, a luminescence (*a-luminescence*), which is located at the high energy side of the *b-luminescence* band observed in the anthracene thin film, is observed at 25300 cm^{-1}. The energy position of the *a-luminescence* band is close to that of the upper Davydov state of the lowest singlet exciton in anthracene crystals. From the thickness dependence of the optical properties of the anthracene thin films, the *a-luminescence* band is attributed to the radiative transition from the upper Davydov state of the lowest singlet exciton. The appearance of the *a-luminescence* band might come from the reduction of reabsorption effect. We present the optical properties of the anthracene nanocrystals and the anthracene thin films with different thicknesses.

Reference

[1] S. Hashimoto, *et al*., J. Jpn. Appl. Phys. **27**, 726 (1988).
[2] H. Masuda, *et al*., J. Electrochem. Soc. **144**, L127 (1997).

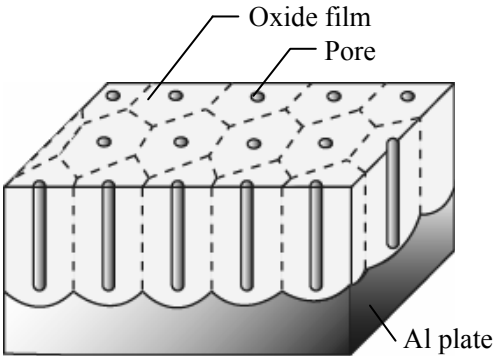

Fig. 1. Schematic of anodic porous alumina.

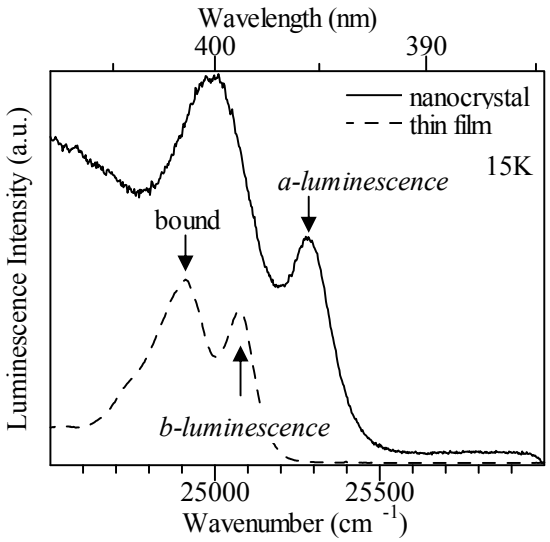

Fig. 2. Luminescence spectra of anthracene thin film and nanocrystals in pores of porous alumina.

Energy transfer from CsI host crystals to Ag^- centers in CsI:Ag^-

Satoru Nagata, Takeshi Hirai[1], and Taketoshi Kawai

Department of Physical Science, Osaka Prefecture University, Japan
[1]Department of Physical Sciences, Ritsumeikan University, Japan

Alkali halide crystals doped with Tl^+-type impurity centers have been investigated for applications to scintillator materials by many works. The Tl^+-type ions have a ns^2 electronic configuration in their ground state and a $nsnp$ electronic configuration in the first excited state. The alkali halides containing a small fraction of the Tl^+-type ions exhibit absorption bands called A, B, and C in the energy region below the fundamental absorption edge of the host crystals. When the alkali halide crystals doped with the Tl^+-type ions are irradiated by photons with energies corresponding to these absorption bands, the luminescence bands due to the radiative transitions from their relaxed excited states are observed with Stokes shifts [1]. The Ag^- centers doped in alkali halides is one of the Tl^+-type centers and have a comparatively simple absorption and luminescence feature in comparison with the other Tl^+-type centers. In this study, we prepared CsI single crystals containing Ag^- ions (CsI:Ag^-) and investigated luminescence properties under excitation above and below the band gap of CsI host crystals in order to reveal energy transfer mechanism from the CsI host crystals to Ag^- impurity centers.

In CsI:Ag^-, the C absorption band is observed at 3.76 eV and the A and C luminescence bands are observed at 2.53 and 3.45 eV, respectively [2]. When the CsI:Ag^- crystals are excited at 6.40 eV above the band edge of CsI, the off- and on-center self-trapped excitons (STEs) luminescence bands of CsI crystals are observed at 3.6 eV and 4.3 eV, respectively, in addition to the A and C luminescence bands.

Figure 1 shows the temperature dependence of the intensities of the A luminescence band of the CsI:Ag^- crystals and the STE luminescence band of pure CsI crystals. Under excitation at 3.79 eV, which corresponds to the peak energy of the C absorption band, the A luminescence (2.53 eV) intensity hardly changes in the temperature range above 20 K. On the other hand, excitation at 6.42 eV above the band gap of CsI host crystals induces the decrease of the A luminescence intensity with increasing temperature from 60 K. The temperature dependence of the A luminescence intensity is similar to that of the off-center STE luminescence intensity. This similarity indicates that the A luminescence due to the Ag^- centers is associated with the intrinsic off-center STE luminescence of CsI host crystals.

In CsI:Ag^-, the C absorption band located around 3.70 eV is covered with the off-center STE luminescence band of CsI crystals. This fact implies that the Ag^- centers are excited by the off-center STE luminescence through the reabsorption due to the C absorption band. In fact, the off-center STE luminescence band of the CsI:Ag^- crystals has a slight dent structure around 3.70 eV reflecting the reabsorption. The excited Ag^- center would radiate the A luminescence after relaxation. As a results, the intrinsic off-center STE luminescence influences the A luminescence. From various experimental results, energy transfer mechanism from the CsI host crystals to Ag^- impurity centers is discussed.

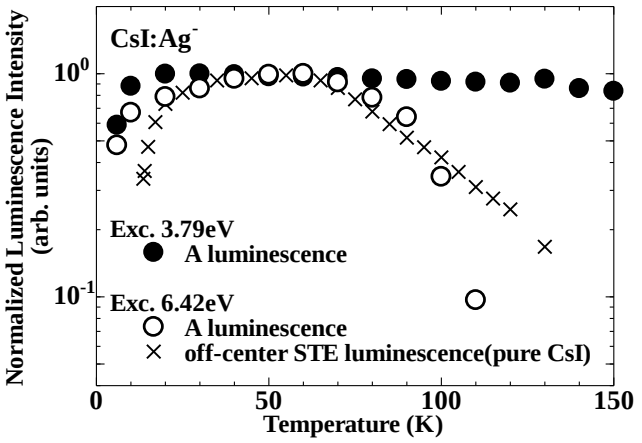

Fig. 1 Temperature dependence of the luminescence intensities of CsI:Ag^- crystals.

Reference

[1] A. Ranfagni, D. Mugnai, M. Bacci, G.Viliani, and M.P. Fontana, **32**, 823(1983).
[2] S. Shimanuki, M. Watanabe, and T. Kawai, Phys. Stat. Sol. (b) **208**, 105(1998).

Temperature dependence of optical reflectance spectrum in layered iron oxide $LuFe_2O_4$

T. Go*, G. Oohata, S. Mori[A], N. Ikeda[B], and K. Mizoguchi
Department of Physical Science, Osaka Prefecture University, Japan
[A] Department of Materials science, Osaka Prefecture University, Japan [A]
[B] Department of Physics, Okayama University, Japan [B]
*Email address: s_t.go@p.s.osakafu–u.ac.jp

Layered iron oxide $LuFe_2O_4$ is one of the multiferroic materials which have both ferroelectric and ferromagnetic properties. The ferroelectricity in $LuFe_2O_4$ originates from charge ordering of Fe^{2+} and Fe^{3+},[1] and its ferromagnetism results from the magnetic moment of Fe^{2+} and Fe^{3+}. Moreover, it is known that $LuFe_2O_4$ has the strong correlation among charge, magnetism and crystal structure. Many researchers have investigated the charge ordering and the magnetic ordering in $LuFe_2O_4$ in order to understand their relationships to phase transitions.[1–3] However, to our knowledge, there are few reports on optical properties for electronic states of Fe, though the study on the optical properties of $LuFe_2O_4$ gives us useful information about relationships among the phase transition, the charge ordering and the magnetic ordering. Then, we have investigated the temperature dependence of the optical reflectance spectrum in $LuFe_2O_4$ to clarify the relationship between the optical property and the phase transition.

The samples used were [110]– and [001]–$LuFe_2O_4$ single crystals. The optical reflectance spectra of these samples were observed at various temperatures in the range from 100 to 300 K. The observed reflectance spectra showed some peaks in the whole temperature regions, and one of the peaks was observed around 2.8 eV. According to the first principle calculation,[4] the peak around 2.8 eV is attributed to the Fe^{2+} on–site excitation.

Figure 1 shows the temperature dependence of the reflectance at 2.8 eV in the [110]– and [001]–plane crystals. In the [110]–plane crystal, the reflectance dramatically changes at 150 and 240 K. The temperatures of 150 and 240 K correspond to the temperatures of the structural phase transition (T_S) and the magnetic phase transition (T_N) obtained by the neutron diffraction, the magnetization and the x–ray scattering measurements.[2,5] In the [001]–plane crystal, the sharp change on the reflectance appears only at 150 K corresponding to the structural phase transition temperature. These results indicate that the transition probability of Fe^{2+} depends on the crystal structure and the magnetic property.

Finally, we discuss the cause of the following difference in the temperature dependence of the reflectance between the [110]– and [001]–plane crystals: the reflectance change related with the magnetic phase transition is observed only in the [110]–plane crystal, while that related with the structural phase transition is done in both the crystals. The observation of the magnetic phase transition in the [110]–plane crystal will be associated with the direction of the magnetization axis. Because the magnetic phase transition in $LuFe_2O_4$ is caused by the interlayer spin–spin interaction and the easy axis of the magnetization is parallel to the <001> axis (the c axis), the reflectance change will be observed only in the [110]–plane crystal including the c axis.

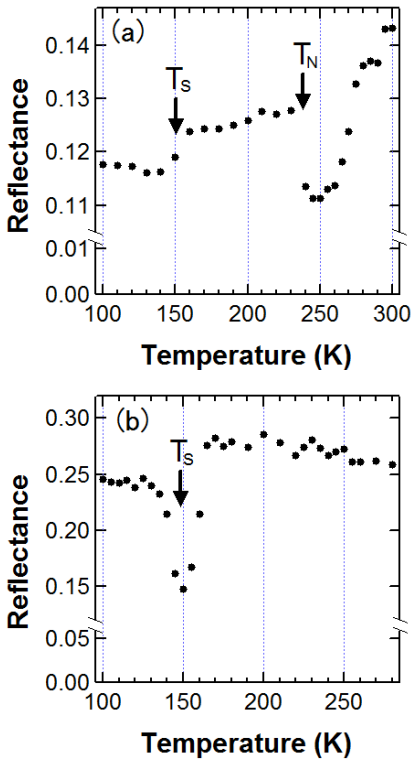

Fig. 1. Temperature dependence of the reflectance around 2.8 eV in (a) the [110]–$LuFe_2O_4$ crystal and in (b) the [001]–$LuFe_2O_4$ crystal.

Reference

[1]N. Ikeda, *et al.*, Nature (London), 436, 1136 (2005)
[2]A. D. Christianson, *et al.*, Phys. Rev. Lett. **100** 107601 (2008)
[3]A. Nagano, *et al.*, Phys. Rev. Lett. **99** 217202 (2007)
[4]H. J. Xiang and M. –H. Whangbo, Phys. Rev. Lett. **98** 246403 (2007)
[5]X. S. Xu, *et al.*, Phys. Rev. Lett. **101** 227602 (2008)

Characteristics of Cavity Polaritons in CuCl Microcavities

*S. Yoshino, G. Oohata, Y. Shim[A], H. Ishihara[A], K. Mizoguchi
Dept. Phys. Sci. and [A]Dept. Phys. and Electron., Osaka Prefecture University, Japan
*E-mail address : s_s.yoshino@p.s.osakafu-u.ac.jp

In semiconductor microcavities, the strong coupling states between excitons and cavity photons, so-called cavity polaritons, show many interesting phenomena: polariton Bose–Einstein condensation, polariton lasing, and so on. With regard to studies on cavity polaritons, it is important to control the Rabi splitting energy that is the interaction energy between the exciton and the cavity photon. Microcavities with an active layer of the semiconductor CuCl that is called "CuCl microcavities" have the potential for novel optical responses such as highly efficient generation of entangled photon[3]; besides, employment of CuCl as an active layer in a microcavity enables us to control the Rabi splitting energy in the wide range from about 20 to 135 meV[1,2]. In this report, we discuss the properties of cavity polaritons in CuCl microcavities from comparison between angle-resolved reflectance spectra and calculated reflectance spectra based on nonlocal response theory.

CuCl microcavities with distributed Bragg reflectors (DBRs) were grown on sapphire substrates by vacuum deposition method. Here, the DBRs consisted of $PbCl_2$ and NaF layers. The active layer thickness was the resonance wavelength of the Z_3 exciton λ_{ex}, where the microcavity with the active layer thickness of λ_{ex} is called "λ-cavity". The angle-resolved reflectance spectra of the λ-cavity were measured at 12 K by using a single monochromator with a spectral resolution of 0.35 nm.

In the angle-resolved reflectance spectra, several dips clearly appear. Especially, there exist the three structures which shifted to the higher energy side with an increase of incident angle. This energy shift indicates the existence of the cavity polaritons. These polaritons are named the Lower Polariton Branch (LPB), the Middle Polariton Branch (MPB), and the Upper Polariton Branch (UPB). The dip energies of these modes obtained from the angle–resolved reflectance spectra of the λ-cavity are plotted as a function of incident angle in Figure 1(a). The solid curves are the fitted results with the dispersion relation of cavity polaritons obtained by assuming the 3x3 phenomenological Hamiltonian with the two interaction energies between the cavity photon and the Z_3 ($Z_{1,2}$) exciton. The obtained Rabi splitting energies for the Z_3 and $Z_{1,2}$ excitons are 110 meV and 195 meV, respectively. In addition, we have investigated the Rabi splitting energies at various CuCl microcavities with various active layer thicknesses. The experimental results indicate that the Rabi splitting energy depends on the active layer thickness; moreover, we can control the Rabi splitting energy for the Z_3 exciton in the range from 100 meV to 135 meV by changing the active layer thickness from $\lambda_{ex}/2$ to $2\lambda_{ex}$.

In order to reveal the peculiar profile in the reflectance spectrum of the CuCl microcavity, the reflectance spectrum is calculated by nonlocal response theory at normal incidence to the λ-cavity. In Fig. 1(b), the calculated reflectance spectrum shown by the dotted curve is in good agreement with the experimental result shown by the solid curve: the calculated spectrum successfully reproduces the energy dips of all structures and Rabi splitting energies, as well as the weakly-coupled modes[2].

References

[1] M. Nakayama, *et. al*., Phys. Rev. B **83**, 075318 (2011).
[2] S. Yoshino, *et. al*., Phys. Status Solidi (c) **8**, 221 (2011).
[3] H. Oka and G. Oohata, *et. al*., Appl. Phys. Lett. **94**, 111113 (2009).

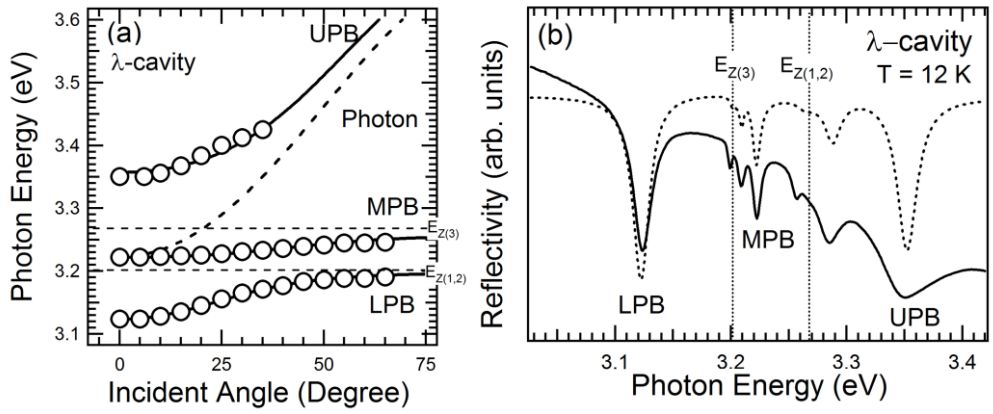

Fig. 1. (a) Incident-angle dependence of the energy of the cavity polaritons in the λ-cavity (open circles) and of cavity-polariton dispersions fitted to the experimental results (solid curves). The horizontal dashed lines show the energies of the Z_3 and $Z_{1,2}$ excitons, and the broken curve depicts the dispersion of the cavity photon.
(b) Reflectance spectrum at the normal incident to the CuCl microcavity with the active layer thickness of the resonance wavelength of the Z_3 exciton (solid curve). The dotted curve shows the calculated reflectance spectrum based on nonlocal response theory.

Observation of coherent oscillation in CuI thin film on Au nano-film

S. Isshiki, G. Oohata, and K. Mizoguchi
Department of Physical Science, Osaka Prefecture University, Japan
s_s.isshiki@p.s.osakafu-u.ac.jp

Coherent phonons generated by the irradiation of ultrashort laser pulses have been extensively investigated on various transparent and opaque materials. The enhancement of coherent phonons is an attractive object from the viewpoints of investigations of phonon dynamics and control of structural phase transitions. Recently, the enhancement of the coherent phonons in opaque cleaved graphite films with deposited Au nanostructures has been studied by Katayama, *et al*. They report that the coherent phonon corresponding to the disorder-induced mode was dramatically enhanced through surface-enhanced Raman scattering due to the enhanced electric field around the Au nanostructures.[1] In this research, we have investigated the coherent oscillations in CuI thin films on Au nano–films in order to clarify the effect of the surface enhanced electric field on the CuI thin film transparent to a pulse laser.

CuI thin films on Au nano–films were grown on sapphire substrates by vacuum deposition. The thicknesses of the CuI thin film and the Au nano–film were about 200 and 20 nm, respectively. The Au nanostructures with width of about 250 nm and height of about 1 nm were observed at the surface of the Au nano–film by atomic force microscopy. The fundamental excitonic transition energy of the CuI thin film was about 3.03 eV at room temperature. The coherent oscillations were measured at room temperature by using a transmission-type electro-optic sampling (TEOS) method with a mode-locked Ti:sapphire pulse laser delivering about 100-fs pulse.

Traces in Fig. 1 show the time-resolved TEOS signals in the CuI thin films on the substrates embedded with and without the Au nano–films. It is noted that the coherent oscillation in the CuI thin film with the Au nano–film, which is attributed to the coherent transverse optical (TO) phonon, is dramatically enhanced, while that in the CuI thin film without the Au nano–film is hardly observed. This enhancement originates from the surface enhanced electric field on the Au nano–film.

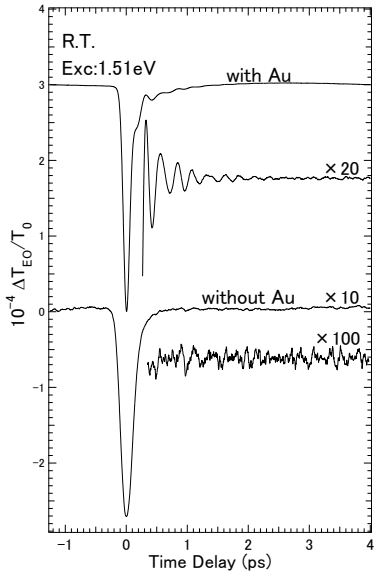

Fig. 1. Time-resolved TEOS signals in the CuI thin films on the sapphire substrate embedded with and without the Au nano-film, and oscillatory profiles extracted by subtracting a slowly varying background in the TEOS signals.

In order to reveal the properties of the enhanced coherent TO phonon in the CuI thin films on the Au nano–film, the pump-power dependence of the phonon intensity was investigated at the pump energies of 1.49 and 1.52 eV. In Fig. 2, the intensities of the coherent TO phonon are plotted as a function of pump power. At both the pump energies, the phonon intensities are proportional to the *n*th power of the pump-power. The coefficients of the exponent are about 2 and 3 at the pump energies of 1.49 and 1.52 eV, respectively. In the transparent materials, when the impulsive stimulated Raman scattering (ISRS) mechanism contributes the generation of the coherent phonon, the pump-power dependence of the phonon intensity shows square relation.[2] At the pump energy of 1.49 eV, therefore, the coherent TO phonon is generated through the ISRS process with the effect of the surface enhanced electric field on the Au nano–film. At the pump energy of 1.52 eV, because the phonon intensity is proportional to the 3rd power of the pump-power and twice the pump energy is located in the vicinity of the fundamental excitonic transition energy, we consider that the enhanced coherent phonon will be generated through the ISRS process involved with two-photon absorption.

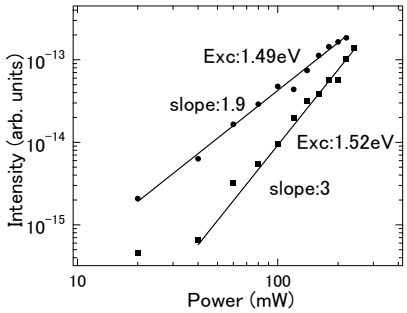

Fig. 2. Pump-power dependence of the intensity of the coherent phonon in the CuI thin film on the Au nano-fim excited at the pump energies of 1.49 and 1.52 eV.

Reference
[1] I. Katayama, *et al*., Nano Lett. **11**, 2648 (2011).
[2] Y. -X. Yan and K. A. Nelson, J. Chem. Phys. **87**, 6240 (1987).

Design of Spatiotemporal Profiles in Light Electromagnetic Field for Efficient Fluctuation-mediated Optical Transport of Nanoparticles

Mamoru Tamura[a,b], Shimpei Hidaka[a,b], Hironori Hattori[a,b], Takuya Iida[a,c,*]
[a]Nanoscience & Nanotechnology Research Center, Osaka Prefecture University, Sakai, Osaka 599-8570, Japan
[b]Department of Physics and Electronics , Osaka Prefecture University, Sakai, Osaka 599-8531, Japan
[c]PRESTO, Japan Science and Technology Agency, Kawaguchi, Saitama 332-0012, Japan
*Email address of corresponding author: t-iida@21c.osakafu-u.ac.jp

Controlling time-cycles and amplitudes of spatiotemporally asymmetric potentials is a key element for efficient transport by thermal fluctuations [1]. Previously, our group has theoretically indicated the possibility that the transport distance of nanoparticles (NPs) by light-induced force (LIF) with spatiotemporally asymmetric light standing wave under the thermal fluctuations due to collisions of solvent molecules [2]. In this contribution,we investigate the conditions for more efficient optical transport of NPs by designing spatio-temporal profiles of light field incorporating the statistical method.

In order to evaluate dynamics of NPs under the light field and thermal fluctuations, we employ "Light- induced-force nano-dynamics method" (LNDM) [2] based on the general expression of LIF from Lorentz force [3] and Langevin equation [4]. As shown in Fig.1, we assume the model that a gold NP (diameter: 40nm) is irradiated by two counter-propagating Gaussian beams (GBs) on z-axis as incident light. The amplitude of G1 is fixed and that of G2 varies proportional to $0.45(\cos[\Omega t]+1)+0.1$ ($\Omega=4\pi$), where the standing wave is spatiotemporally modulated. The difference in height of this standing wave is maximum for $\cos[\Omega t]=1$, and minimum for $\cos[\Omega t]=-1$. The time evolution of NP dynamics was repeatedly evaluated 2000 times for each power of GBs, and we take a statistical average of transport distance.

Fig.2 is one of the calculation results. In the assumed condition, while the NP continuously feel the trapping force by the standing wave, they also feel the asymmetric potentials by the effect of the light pressure by G1 pushing the NP for propagation direction with decrease of G2 intensity. Consequently, we have confirmed the prominent increase of the transport distance with the help of fluctuations. Especially, we clearly show that the transport distance is resonantly enhanced under the optimized ratio of fluctuations to optical potential depth, where the maximum intensity of GBs is within the particular range (300~500 mW). Obtained results will be foundations not only for the one-dimensional transport of NPs, but also for three-dimensional integration of NPs taking into account interparticle and interaction and highly designed light field profile.

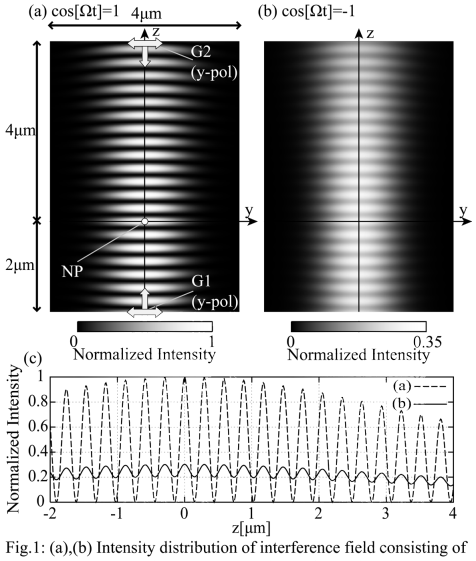

Fig.1: (a),(b) Intensity distribution of interference field consisting of two counter-propagating GBs (G1 and G2) for each value cos[Ωt] (normalized by the maximum intensity of (a)). (c) Cross-section of (a),(b) at y=0. Wavelength: 780 nm. Spot radius: 1.0 mm. The focal point is (0, 0, 0). Solvent is water with temperature of 298 K.

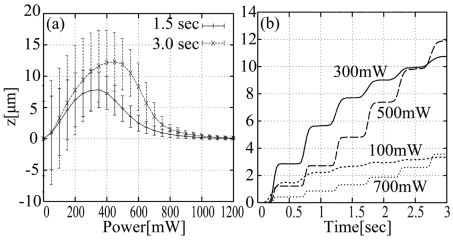

Fig.2: Dependence of the mean z-displacement of gold NP (a) on the power of GBs at 1.5 sec and 3 sec and (b) on the time for each power. Vertical bars mean deviation of z-displacement.

[1]L.Gammaitoni,*Rev Mod Phys*,**70**,223(1998)
[2]T.Iida,Technical Digest of MOC**2010**,WP123 (2010).
[3]T.Iida,H.Ishihara,*Phys.Rev,B* **77**,245319(2008).
[4]D. Ermak and J. A. McCammon, *J. Chem. Phys.* **69(4)**, 1352(1978).

Theory of Optical Response of Two-dimensional Array of High-density Metallic Nanoparticles for Optical Sensor of Organic Molecules

Kohei Yamamoto[a,b] **, Hironori Hattori**[a,b]**, Shin Tanaka**[a,b]**, and Takuya Iida**[a,c,*]
[a]Nanoscience & Nanotechnology Research Center, Osaka Prefecture University, Sakai, Osaka 599-8570, Japan
[b]Department of Physics and Electronics , Osaka Prefecture University, Sakai, Osaka 599-8531, Japan
[c]PRESTO, Japan Science and Technology Agency, Kawaguchi, Saitama 332-0012, Japan
*Email address of corresponding author: t-iida@21c.osakafu-u.ac.jp

There are many reports on the optical sensors for organic molecules and biomolecules using Surface Plasmon Resonance (SPR) in metallic nanostructures such as uniform gold thin film and gold nanoparticles (NPs) [1]. Optical biosensors using the substrate with fixed metallic NPs are also developed, where the optical properties of SPR are often analyzed with an effective dielectric constant based on Maxwell-Garnet Theory (MGT) [2]. Although high-density metallic NP-systems show various optical properties due to the strong electromagnetic interaction between them, MGT is the effective method only for dilute NP-systems. Therefore, in this contribution, we theoretically investigate the optical properties of two-dimensional array of high-density metallic NPs by considering self-consistent interaction between NPs, and explore their potential toward the highly sensitive optical sensor for the detection of organic nano-objects.

For this purpose, we employ the discretized integral method with spherical cells (DISC) [3] in order to analyze the optical response of high density metallic NPs considering the effect of adsorbed organic NPs. As shown in Fig. 1, we consider the model that organic NPs (Diameter:50nm, Number:10×10, Interval:2nm) are fixed on gold NPs (Diameter:50nm, Number:10×10, Interval:2nm) arranged on the transparent substrate in water. Taking into the account of sizes of an antigen and an antibody, we assumed that the distance between the surface of gold NPs and organic NPs is assumed to be 20nm. Here, the extinction spectra are shown in Fig. 2 for different dielectric constants of the organic NPs. In comparison with the case of gold NP-sheet only, we confirmed that the extinction spectra clearly change due to the presence of organic NPs within wavelength region 650-800nm. In addition, density dependence of gold NPs is shown in Fig. 3. When the number of NPs increases in the same area, we can confirm that the extinction spectra become broader and similar to a reflectance spectrum of a uniform gold film. This result indicates that the detection efficiency of organic NPs depends on the density of gold NPs, which implies the possibility to control the sensitivity by changing the NP arrangement and light polarization.

[1] J. Mitchell, *Sensors*,**10**,7323(2010).
[2] K. Tamada, et al. *Plasmonics* **2**, 185 (2007).
[3] C.Kojima, Y.Watanabe, H.Hattori, T.Iida, *J. Phys. Chem C*, **115**, 19091 (2011).

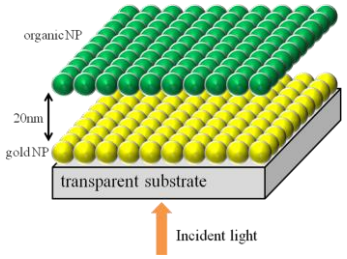

Fig. 1: Model for the calculation that organic NPs are fixed on metallic NP-sheet.

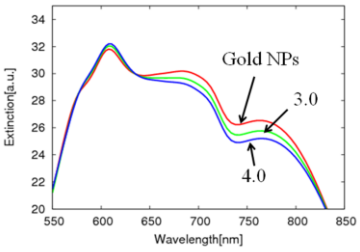

Fig. 2: Extinction spectra of coupled system of organic and metallic NPs in the geometry of Fig.1 for different dielectric constants of organic NPs.

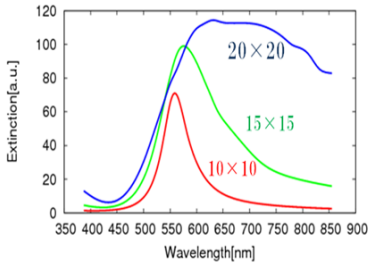

Fig. 3: Extinction spectra of metallic NP-sheet for different NP-density with equally spaced interval in the area of 1000nm ×1000nm.

Spin-polarized electronic states of $La_{1-x}Sr_xMnO_3$ studied by magnetic Compton scattering

Teruhiko Mizoroki,[a]* Masayoshi Itou,[b] Yukihiro Taguchi,[a] Toshiaki Iwazumi,[a] Yoshiharu Sakurai[b†]
[a]Graduate School of Engineering, Osaka Prefecture University, Sakai, Osaka, Japan.
[b]Japan Synchrotron Radiation Research Institute, SPring-8, Sayo, Hyogo, Japan.
[†]E-mail address: sakurai@spring8.or.jp

Perovskite manganite $La_{1-x}Sr_xMnO_3$ (LSMO) is half-metallic in a doping range of x=0.2-0.5. It is thus one of the promising materials for spintronic devices [1]. In order to investigate the effect of doping on the up-spin and down-spin electronic states in LSMO, we have carried out magnetic Compton scattering measurements for LSMO from x=0.1 to 0.5 [2]. In this experiment circularly polarized x-rays are irradiated onto the sample, Compton profiles are measured by alternating the direction of an applied magnetic field. A magnetic Compton profile, difference between profiles for up-spin and down-spin electrons, in combination with a charge Compton profile, sum of the two profiles, is used to obtain the number density of the up-spin or down-spin electrons as a function of momentum p_z projected onto the direction of the applied field [3]. In addition the spin magnetic moment of the sample is proportional to the asymmetry ratio of integrated intensities of Compton scattered x-rays for the oppositely directed fields.

The spin magnetic moment of LSMO determined from the magnetic Compton scattering measurements is larger by several percents than the magnetic moment determined from superconducting quantum interference device measurements. The spin and orbital moments are anti-parallel. The spin moment of LSMO from x=0.1 to 0.4 is nearly the same as that expected from the 3d electron number of Mn ion in the high-spin state. The holes are introduced into the up-spin states in the doping range from x=0.1 to 0.4. We have examined the difference in Compton profiles (DCP's) for each spin-subband between two adjacent dopings in order to see the change, which is induced by the hole-doping, in each spin-subband. DCP gives the Compton profile for the states where the holes enter if the holes are doped in a rigid-band manner. Up-spin DCP for (x=0.1)-(x=0.2), hereafter referred as to DCPup(0.1-0.2), shows a narrow positive peak around p_z=0 indicating that electrons decrease in those states extended in space to some extent. We have also calculated Compton profiles for the Mn 3d-O 2p molecular orbitals in a MnO_6 cluster. It is found that DCPup(0.1-0.2) closely resembles a calculated profile for the O 2p molecular orbital. This indicates that the doped holes predominantly enter the O 2p states. Although the integrated intensity of DCPdown(0.1-0.2) is almost 0, it shows a positive peak around p_z=0 similar to DCPup(0.1-0.2) in addition to negative dips around $p_z=\pm 2$ a.u. Some redistribution in momentum among the down-spin electrons takes place between the doping of x=0.1 and 0.2, where LCMO undergoes the structural and insulator-to-metal transitions. Upon doping from x=0.4 to 0.5 the spin magnetic moment abruptly decreases by about 20%. The integrated intensities of DCPup/down(0.4-0.5) represent the decrease of 0.4 up-spin electrons and the increase of 0.3 down-spin electrons per formula unit, that is, charge transfer by 0.3 electrons from the up-spin to the down-spin states. DCPdown(0.4-0.5) shows a broad negative peak around p_z=0, and it is reminiscent of a calculated Mn 3d profile indicating that the down-spin Mn 3d electrons exist at x=0.5.

*present address: Mitsubishi Electric Corp., Manufacturing Engineering Center, Amagasaki, Hyogo, Japan.
[1] Y. Tokura, Phys. Today **56**, 50 (2003).
[2] T. Mizoroki, M. Itou, Y. Taguchi, T. Iwazumi and Y. Sakurai, Appl. Phys. Lett. **98**, 052107 (2011).
[3] Y. Sakurai, Y. Tanaka, T. Ohata, Y. Watanabe, S. Nanao, Y. Ushigami, T. Iwazumi, H. Kawata and N. Shiotani, J. Phys.: Condens. Matt. **6**, 9469 (1994).

Observation of Two Raman Components in Resonant X-ray Emission Spectra of Fe Cyanides

Toshiaki Iwazumi*, Akihiro Ueno, Masayuki Tanaka, Yuuji Koga, and Takaaki Ikeuchi
Department of Mathematical Sciences, Graduate School of Engineering, Osaka Prefecture University,
1-1 Gakuen-cho, Nakaku, Sakai, Osaka 599-8531, Japan

Hiroko Tokoro and Shin-ichi Ohkoshi
Department of Chemistry, School of Science, The University of Tokyo,
7-3-1 Hongo, Bunkyo-ku, Tokyo 113-0033, Japan

Yasuhito Isozumi
Radioisotope Research Center, Kyoto University,
Yoshidakonoe-cho, Sakyo-ku, Kyoto 606-8501, Japan

*Corresponding author
Email: iwazumi@ms.osakafu-u.ac.jp

Prussian blue analogues are potential candidates for novel magnetic devices. They exhibit the valence transition induced by temperature [1], photo-irradiation [2, 3], pressure [3], and electric field [4]. For example, the valence states change from Fe(III)-Mn(II) to Fe(II)-Mn(III) with decreasing temperature in rubidium manganese hexacyanoferrate, $RbMn[Fe(CN)_6]$. Hexacyano-compounds are composed of a 3-D network structure in which the transition-metal ions are strongly bridged by cyano groups [5]. One of the characteristics of the electronic states of cyanides is π backbonding. The importance of π backbonding was confirmed both experimentally and theoretically in transition-metal 2p X-ray absorption spectra (XAS) [6, 7]. However, there are two quite different theoretical predictions about Fe 2p absorption spectra [8, 9]. In order to verify the theoretical predictions by acquiring more electronic information, we have carried out resonant X-ray emission spectra (RXES) measurements around Fe K absorption-edge for Fe cyanides, $K_4Fe(CN)_6$, $K_3Fe(CN)_6$, and $RbMn[Fe(CN)_6]$. Right figures show the obtained RXES results (right-hand side figure) with Fe K-XAS of $K_4Fe(CN)_6$. The excitation energy of RXES shown by thick lines in the right figure are indicated by white arrows in the left one. Two Raman peaks, RP1 and RP2, were observed as shown by broken lines in the right figure. Raman shift energies of RP1 and RP2 are close to those of metal-to-ligand and ligand-to-metal charge tranfers predicted by Nanba and Okada [9]. RXES data of $K_3Fe(CN)_6$ and $RbMn[Fe(CN)_6]$ will be reported in the symposium.

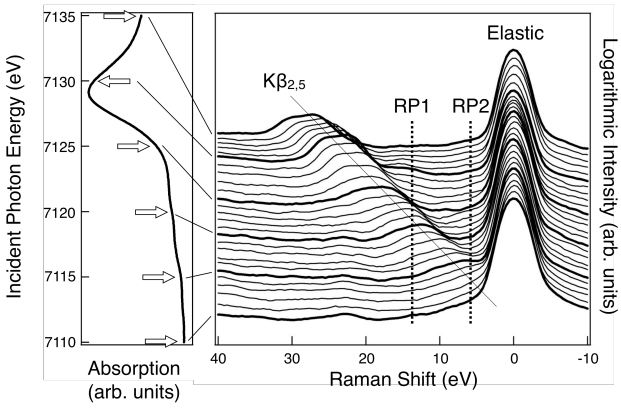

[1] S. Ohkoshi, H. Tokoro, M. Utsunomiya, M. Mizuno, M. Abe, and K. Hashimoto: J. Phys. Chem. B 106 (2002) 2423.
[2] H. Tokoro, S. Ohkoshi, and K. Hashimoto: Appl. Phys. Lett. 82 (2003) 1245.
[3] Y. Moritomo, M. Hanawa, Y. Ohishi, K. Kato, M. Takata, A. Kuriki, E. Nishibori, M. Sakata, S. Ohkoshi, H. Tokoro, and K. Hashimoto: Phys. Rev. B 68 (2003) 144106.
[4] O. Sato, T. Iyoda, A. Fujishima, and K. Hashimoto: Science 271 (1996) 49.
[5] T. Mallah, S. Thiébaut, M. Verdaguer, and P. Veillet: Science 262 (1993) 1554.
[6] N. Kosugi: J. Electron Spectrosc. Relat. Phenom. 92 (1998) 151.
[7] R. K. Hocking, E. C. Wasinger, Y.-L. Yan, F. M. F. de Groot, F. Ann Walker, K. O. Hodgson, B. Hedman, and E. I. Solomon: J. Am. Chem. Soc. 129 (2007) 113.
[8] R. K. Hocking, E. C. Wasinger, F. M. F. de Groot, K. O. Hodgson, B. Hedman, and E. I. Solomon: J. Am. Chem. Soc. 128 (2006) 10442.
[9] Y. Nanba and K. Okada: J. Phys. Soc. Jpn. 79 (2010) 114722.

Orbital Ordering in Spinel Compound CuV_2S_4 with Incommensurate Charge-Density Wave

Shogo Kawaguchi[1], Yoshiki Kubota[1], Naruki Tsuji[2], Jungeun Kim[2],
Kenichi Kato[3], Masaka Takata[3] and Hiroki Ishibashi[1]
[1] Department of Physical Science, Graduate School of Science,
Osaka Prefecture University, Sakai, Osaka 599-8531, Japan
[2] Japan Synchrotron Radiation Institute, SPring-8, 1-1-1 Kouto, Sayo-cho, Sayo-gun, Hyogo 679-5198, Japan
[3] RIKEN SPring-8 Center, 1-1-1 Kouto, Sayo-cho, Sayo-gun, Hyogo 679-5148, Japan
Email address: s_s.kawaguchi@p.s.osakafu-u.ac.jp

CuV_2S_4 has a cubic spinel structure at room temperature. It exhibits anomalies in both magnetic susceptibility and electrical resistivity accompanied by structural phase transition at T_t ~ 90 K [1]. It has been discussed that these anomalies are related to the formation of incommensurate charge-density wave (CDW) [2]. However, the origin of CDW formation in CuV_2S_4 is not understood at present. Because only the crystal system for CDW phase is reported [1] and the detailed crystal structure below T_t has not determined so far. In order to clarify the origin of CDW, we performed synchrotron powder diffraction experiments and crystal structure analysis for the low-temperature phase.

We observed peak splitting of the fundamental reflections due to crystal symmetry lowering (Fig.1-a), and weak superlattice reflections with the wave vector **q** = (1/4 - δ) [110] in the X-ray diffraction pattern at 70 K (Fig.2-b). From both the direction of modulation and lattice distortion, we determined that the low-temperature phase of CuV_2S_4 has a superspace-group of $Imm2(0\beta0)$ with an orthorhombic symmetry. We carried out incommensurate structural analysis by Rietveld method based on this superspace-group to determine the magnitude and the direction of the atomic displacement. The overall quality of fitting was fairly good (Fig.1-b). It was found that the crystal structure is characterized by the significant change of bond lengths between vanadium atoms. The V-V bond lengths at 70 K range from 3.0 Å to 4.0 Å, though those at 150 K are 3.49 Å for all bonds. We suggest that the significant change of V-V bond lengths is related to the orbital ordering of vanadium t_{2g} orbitals, which is the origin of the formation of the CDW. The details of the correlation between the crystal structure and the orbital ordering are discussed.

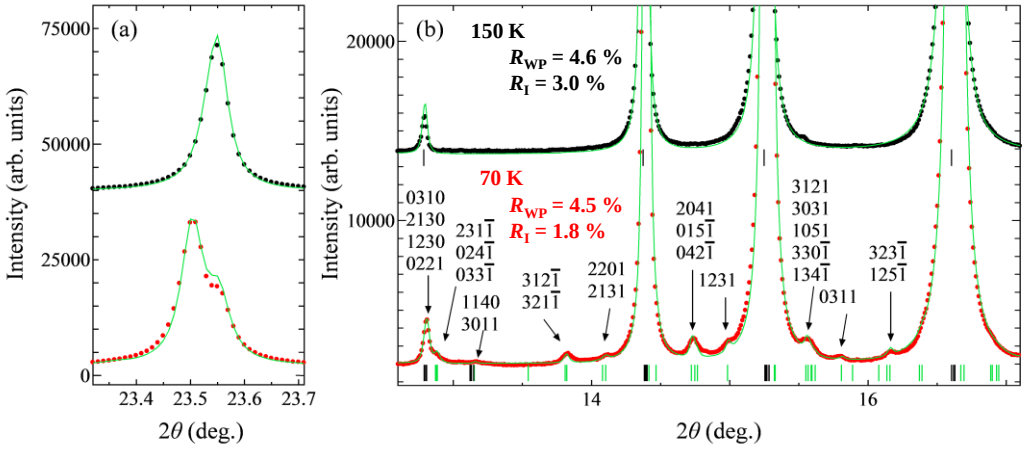

Figure 1. (a) X-ray powder diffraction of around the 800 cubic Bragg peak at 150 K and 70 K.
(b) Rietveld fitting of X-ray powder diffraction patterns at 150 K and 70 K
(arrows show superlattice reflections)

[1] H. Okada *et al.*, 2004 *J. Phys. Soc. Jpn.* **73** 3227
[2] R. M. Fleming *et al.*, 1981 *Phys. Rev. B* **24** 2850

Fe Site Substitution Effect on the Structural and Magnetic Properties in Spinel Type FeV_2O_4

Hiroki Ishibashi and Yuki Kitadai
Department of Physical Science, Graduate School of Science,
Osaka Prefecture University, Sakai, Osaka 599-8531, Japan
Email address: hiroki@p.s.osakafu-u.ac.jp

Spinel oxide FeV_2O_4 is a unique compound which has orbital degrees of freedom at both Fe^{2+} and V^{3+} ions. This compound exhibits successive structural phase transitions from cubic to tetragonal ($c < a$) at $T_{s1} \sim 140$ K, from tetragonal to orthorhombic at $T_{s2} = T_N \sim 110$ K accompanied by ferrimagnetic transition, and from orthorhombic to tetragonal ($c > a$) at $T_{s3} \sim 70$ K [1]. It was suggested that the possible scenario of the structural transitions below T_{s2} is the competition and cooperation of Fe^{2+} and V^{3+} orbitals, however, the roles of the orbital degrees of freedom of Fe^{2+} and V^{3+} ions to their phase transitions are not completely understood. In this study, we investigate the effect of substitution of Zn^{2+} for Fe^{2+} in FeV_2O_4, i.e., the structural and magnetic properties of $Fe_{1-x}Zn_xV_2O_4$ for $x \leq 0.4$ by high resolution synchrotron powder diffraction experiments and magnetization measurements.

Figure 1 shows the temperature dependence of the lattice constants and magnetization for (a) $x = 0.1$ and (b) $x = 0.3$. For $x = 0.1$, the successive structural transitions of cubic-to-tetragonal ($c < a$), tetragonal-to-orthorhombic and orthorhombic-to-tetragonal ($c > a$) are observed, which are similar to those observed in FeV_2O_4 except for the transition temperatures. On the other hand, for $x = 0.3$, the only cubic-to-tetragonal ($c > a$) structural transition is observed and both the tetragonal ($c < a$) and orthorhombic phases are absent. The result of the magnetic measurements indicates that the ferrimagnetic transitions are observed for both $x = 0.1$ and 0.3. The transition temperatures are quite close to the tetragonal-to-orthorhombic transition temperature for $x = 0.1$, and close to the cubic-to-tetragonal transition one for $x = 0.3$. These results are discussed in terms of Jahn-Teller distortions of FeO_4 tetrahedron and/or VO_6 octahedron, and spin-orbital interaction at Fe^{2+} ion.

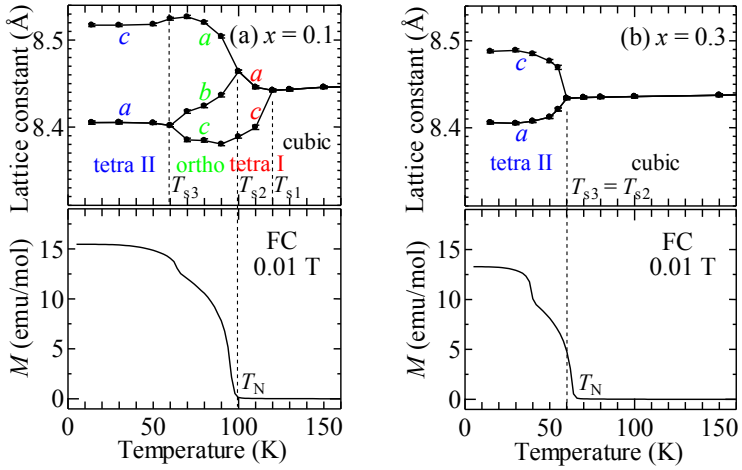

Figure 1. Temperature dependence of lattice constants and magnetization for (a) $x = 0.1$ and (b) $x = 0.3$ for $Fe_{1-x}Zn_xV_2O_4$

[1] K. Katsufuji *et al*, *J. Phys. Soc. Jpn.* **77** 053708 (2008)

Ab-initio structure determination of $[Cu(dhbc)_2(dpa)]_n$ as high CO_2 adsorption materials

Yohei Sato[1], Yoshiki Kubota[1], Yasutaka Inubushi[2], Masaki Takata[3]
[1]Department of Physical Science, Graduate School of Science,
Osaka Prefecture University, Sakai, Osaka -599-8531, Japan, [2]Synthesis Research Laboratory, Kurashiki Research Center, Kuraray Co. Ltd., Kurashiki, Okayama -710-0801, Japan, [3]Structural Science Laboratory, Harima Institute SPring-8 Center, RIKEN, Hyogo 679-5148, Japan
Email address: s_y.sato@p.s.osakafu-u.ac.jp

Porous coordination polymers $[Cu(dhbc)_2(L)]_n$ (L=bpy, dpa, dptz), where dhbc = 2,5-dihydroxybenzoic acid, bpy = 4,4'-bipyridyl, dpa = 4,4'-dipyridyl acetylene, and dptz = 4,4'-dipyridyl 1,2,4,5-tetrazine were synthesized. In the crystal structure of as-synthesized $[Cu(dhbc)_2(bpy)]_n$, two-dimensional sheets formed by dhbc molecule and bpy ligands are stacked by π-π interaction between adjacent dhbc molecules as shown in Fig.1[1]. Nanopore with the size of 3.6 Å×4.2 Å are formed. The amount of CO_2 adsorption of these materials for L = bpy, dpa, dptz is 1.97, 3.85, 3.33 in mol per unit cell, respectively. The dpa compound shows rather higher amount than that expected from the length of L ligand. To reveal this high CO_2 adsorption ability of this compound, ab-initio crystal structure analysis for the apohost compound was carried out using synchrotron powder diffraction data measured at BL02B2 SPring-8.

The initial structural model was obtained with the direct space method of simulated annealing. The reliability factors in Rietveld refinement, R_I, and R_{wp}, were 5.43 and 2.62%, respectively. The crystal structure of dpa compound was compared with that of bpy compound. The lengths of the coordination bond Cu-O and Cu-N of dpa compound is higher than that of bpy compound. The distances between two adjacent dhbc molecules bonded by π-π interaction are different (3.9 Å for bpy, 4.2 Å for dpa). The pore size and shape formed by pillar ligands also affect the amount of adsorption. The CO_2 molecules are supposed to be adsorbed with densely-packed formation. It will be found by the crystal analysis of these compounds with the adsorption of CO_2 and mechanism of high CO_2 adsorption ability will be revealed.

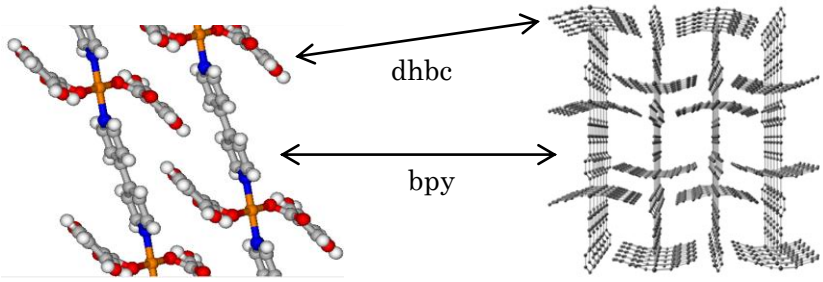

Figure1. Crystal structures of apohost(left) and as-synthesized(right) $[Cu(dhbc)_2(bpy)]_n$. Guest molecules in as-synthesized compound are omitted for clarity.

Reference
[1] Y. Inubushi et al., *Chem. Comm.*, **46**, 9229-9231(2010)

The magnetic interactions in crystals of meta- and paraphenylenebisverdazyl biradicals

K. Iwase[a], H. Yamaguchi[a], T. Ono[a], T. Shimokawa[b], H. Nakano[b],
H. Nojiri[c], A. Matsuo[d], K. Kindo[d],
T. Sakai[e] and Y. Hosokoshi[a]
[a]Dept. of Phys. Sci., Osaka Pref. Univ., Japan
[b]Dept. of Mater. Sci., Univ. of Hyogo, Japan
[c]Institute for Materials Research, Tohoku Univ., Japan
[d]The Institute for Solid State Physics, The Univ. of Tokyo, Japan
[e]JAEA,Spring-8, Japan
s_k.iwase@p.s.osakafu-u.ac.jp

A verdazyl radical is known to be stable and expected to form multi-dimensional magnetic network because of its wide spin-density-distribution within a molecule [1]. However, systematic study with their crystal structures and magnetic properties of verdazyl radicals is still limited. The meta- and paraphenylenebisverdazyl biradicals (abbreviated as *m*-Ph-V_2 and *p*-Ph-V_2, respectively, Fig.1) were first synthesizes in 1964 [2] but only the preliminary measurements of the susceptibility were reported [3]. We have first solved the crystal structures of these compounds and made the precise magnetic measurements down to low temperature and in high magnetic fields. Fig.2 shows the temperature dependence of the inverse of paramagnetic susceptibility (χ_p^{-1}) of each compound. The observed data above 200 K were reproduced by the Curie-Weiss law with the Curie constant C = 0.752 ± 0.003 emu•K /mol and the Weiss constant Θ_W = 8 ± 1 K for *m*-Ph-V_2, and C = 0.75 emu•K/mol and Θ_W = -37.3 ± 0.1 K for *p*-Ph-V_2. The positive and negative Weiss constants are attributable to the intramolecular ferro- and antiferromagnetic interactions in *m*- and *p*-Ph-V_2, respectively. The temperature dependence of χ_pT of *m*-Ph-V_2 shows a maximum at about 60 K and below this temperature the χ_pT values decreases, which suggests the existence of intermolecular antiferromagnetic interactions. The theoretical analysis of the χ_pT and magnetization curves up to 30 T revealed the two-dimensional spin network in *m*-Ph-V_2. The properties of *p*-Ph-V_2 will be also presented.

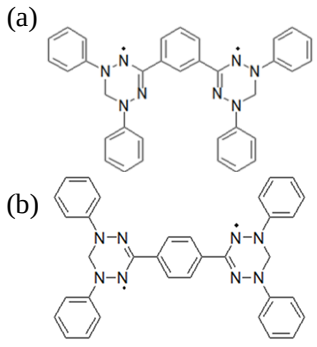

Fig.1 Molecular structures of (a) *m*-Ph-V_2 and (b) *p*-Ph-V_2.

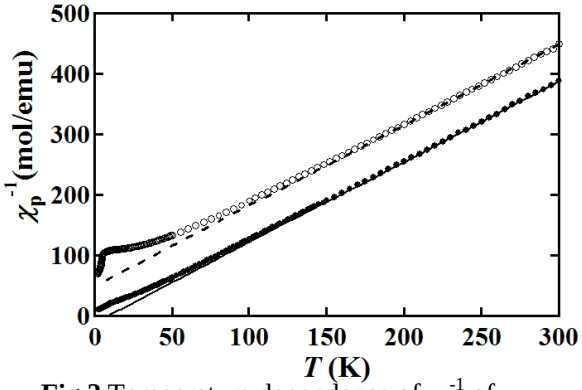

Fig.2 Temperature dependence of χ_p^{-1} of *m*-Ph-V_2 (●) and *p*-Ph-V_2 (○). Solid and broken lines represent the Curie-Weiss laws with C=0.752 K•emu/mol, Θ_W = 8 K and C= 0.75 K•emu/mol, Θ_W = -37.3 K, respectively.

[1] N. Azuma, *Bull. Chem. Soc. Jpn.*, **55**, 1357(1982)
[2] R. Kuhn et al., *Angew. Chem.*, **76**, 691 (1964)
[3] N. Azuma et al., *J. Chem. Phys.*, **61**, 2294 (1974)

Structure and magnetic properties of new verdazyl monoradical crystals

H. Yamaguchi, A. Toho, K. Iwase, T. Ono, M. Hagiwara[1], and Y. Hosokoshi
Grad. Sch. Sci., Osaka Pref. Univ., Japan; [1]KYOKUGEN, Osaka Univ., Japan
yamaguchi@p.s.osakafu-u.ac.jp

Organic radical compounds have attracted much attention since the discovery of the first organic ferromagnet in 1991. Although a large number of organic radical compounds have been synthesized during recent two decades, most of them are revealed to be one-dimensional Heisenberg chains due to the weak and local magnetic interactions between radical molecules. Verdazyl radicals are one of the stable radicals and have a delocalized π-electron system expanded over a molecule [1], which is expected to result in relatively strong and multidirectional intermolecular interactions. Actually, several verdazyl radical crystals have been reported to undergo magnetic long-range order with the aid of the intermolecular interactions [2, 3]. Most of verdazyl radical compounds have not been characterized crystallographically. It is not reliable to presume magnetic structures and explain magnetic properties without any information of packing of molecules.

We have succeeded in synthesizing new verdazyl monoradical crystals 2,3-F_2-V and 3-Cl-4-F-V. We have performed X-ray diffraction and magnetization measurements on them. The obtained crystal structures of 2,3-F_2-V and 3-Cl-4-F-V indicated one-dimensional (1D) chain and two-leg ladder, respectively. The temperature dependence of magnetization on 2,3-F_2-V showed a development of antiferromagnetic (AFM) short range order (SRO) with decreasing temperature, resulting in a broad peak around 80 K. We have explained the obtained experimental result by S=1/2 1D Heisenberg AFM chain model with a strong interchain exchange interaction of J/k_B= 115 K. In the case of 3-Cl-4-F-V, the temperature dependence of magnetization indicates the existence of the ferromagnetic (FM) inter-molecular interactions together with AFM SRO at low temperature. Experimental result is well reproduced by the model of S=1/2 two-leg ladder with AFM rung- and FM leg-interactions with the relation of $|J_{AF}/J_F| = 0.7$ (J_F/k_B = -6.8 K).

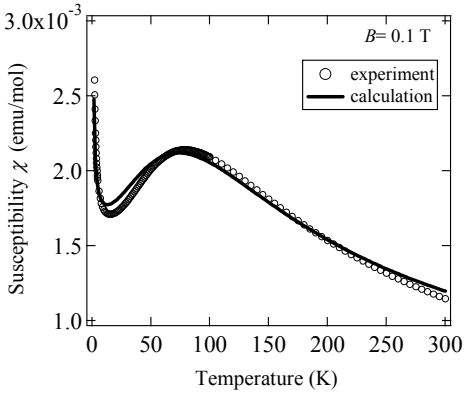

Figure 1: Magnetic susceptibility of 2,3-F_2-V

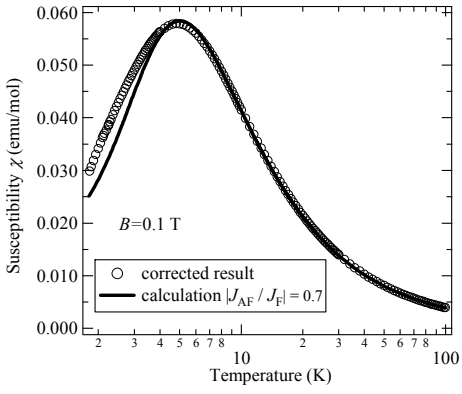

Figure 2: Magnetic susceptibility of 3-Cl-4-F-V

[1] Fischer P H H 1967 *Tetrahedron* 23 1939.
[2] Takeda K, Deguchi H, Hoshiko T, Konishi K, Takahashi, and K, Yamaguchi J 1989 *J. Phys. Soc. Jpn.* 58 3361.
[3] Kremer R K, Kanellakopulos B, Bele P, Brunner H, and Neugebauer F A 1994 *Chem. Phys. Lett.* 230 255.

Magnetic properties and crystal structure of bisverdazylbiphenyl

S. Nagata,[A] M. Tada,[A] H. Yamaguchi,[A] T. Ono,[A] T. Simokawa,[C] H. Nakano,[C]
H. Nojiri,[D] A. Matsuo,[E] K. Kindo,[E] Y. Hosokoshi,[A,B]
[A]Depertment of Physical Science, Osaka Pref. Univ., [B]INR, Osaka Pref. Univ., [C]Graduate School of Material Science, Univ. of Hyogo, [D]Institute for Materials Research, Tohoku Univ., [E] Institute for Solid State Physics, Univ. of Tokyo
E-mail address : s_sh.nagata@p.s.osakafu-u.ac.jp

We have developed two kinds of verdazyl biradicals of 4,4'- and 3,3'-bisverdazylbiphenyl (abbreviate as *p*-BIP-V_2 and *m*-BIP-V_2, respectively). Each biradical employs two spins of S = 1/2 within a molecule. The intramolecular antiferromagnetic exchange coupling in *p*- or *m*-BIP-V_2 was estimated to J_1/k_B = –5.6 K or –2.8 K, respectively, from the magnetic measurements of the solution state.

The crystal structure of *p*-BIP-V_2 shows a two-dimensional network in the *bc* plane. In fact, the almost linear field dependence of the magnetization curve suggests the two-dimensional antiferromagnetic spin lattice of this material. (Fig.1) [1] The magnetic model based on the crystal structure is shown as the inset of Fig.1. The experimental magnetization curve at T = 1.3 K is compared with the theoretical result at T = 0 K from our numerical exact diagonalization for N = 32. The intermolecular magnetic exchange couplings J_2 and J_3 were determined to be $J_2/J_1 = J_3/J_1$ = 8 with J_1/k_B = –5.0 K. We also confirm that the Monte Carlo calculation (N = 20×20) with the same parameter set well reproduces the experiments of the temperature dependence of the susceptibility (χ). Due to the weak intersheet interactions, antiferromagnetic ordering was observed at 7.5 K.

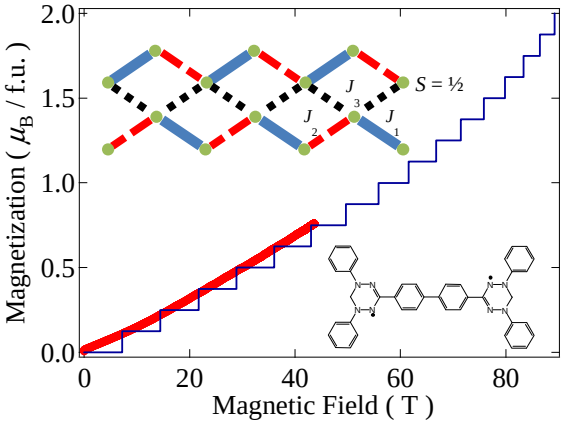

Fig.1. Magnetization curve of *p*-BIP-V_2 crystals measured at T = 1.3 K and theoretical curve at T = 0.

The biradical *m*-BIP-V_2 was newly synthesized and the crystal structure and magnetic properties were studied. Figure 2 shows the temperature dependence of the product of χ and temperature, χT, which is proportional to the square of the effective magnetic moments. The values of χT increase as decreasing temperature down to 15 K, which suggests the existence of intermolecular ferromagnetic interactions. The decrease of χT values below 15 K suggests the existence of additional antiferromagnetic interactions. The analysis by S = 1/2 ferromagnetic antiferromagnetic alternating chain model ($H = -J_1 \sum (S_{2i} S_{2i-1} - \alpha S_{2i} S_{2i+1})$) [2] gives the parameter set of J_1/k_B = –3.6 K and α = 4.1. The relation to the crystal structure will be discussed.

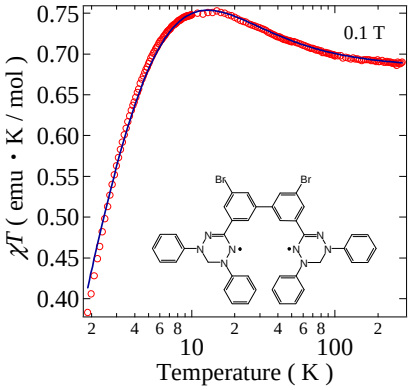

Fig.2. Temperature dependence of χT of *m*-BIP-V_2 crystals. Solid curve is the calculation. (See text)

[1] H. Yamaguchi, et al., *J. Phys. Conf. Ser.*, accepted.
[2] J. J. Borras-Almenar et al., *Inorg. Chem.* **33**(1994)5171

Magnetic properties of an antiferromagnetic alternating chain compound F_5PNN and deuteration effects

Naoki Amaya, Naoya Obata, Hironori Yamaguchi, Toshio Ono and Yuko Hosokoshi
Department of Physical Science
Osaka Prefecture University, Japan
s_n.amaya@p.s.osakafu-u.ac.jp

An S = 1/2 organic radical F_5PNN forms a uniform chain structure at room temperature and the temperature dependence of the magnetic susceptibility is well reproduced by the Heisenberg antiferromagnetic alternating chain model with $2J/k_B = -5.6$ K and $\alpha = 0.4$ in the Hamiltonian of $H = -2J\sum_{i=1}^{\frac{N_A}{2}-1}(S_{2i}\cdot S_{2i-1} + \alpha S_{2i}\cdot S_{2i+1})$ [1]. Nonmagnetic ground state with the energy gap Δ = 3 T was confirmed by the measurements of the magnetization curves. The specific heat measurements suggest the structural change occurring at about 5 K.

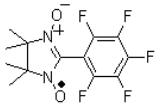
F_5PNN

Recently we found that the structural change occurs at different temperatures depending on the condition of the crystal growth. Some crystals show the structural change at about 3 K, which is detected by the sudden change of the temperature dependence of the susceptibility. Above 5 K, the calculated values of the susceptibility for uniform chain of $2J/k_B = -4.1$ K are identical with the ones for the alternating chain with $2J/k_B = -5.6$ K and $\alpha = 0.4$. The crystal which undergoes the structural change at lower temperature shows larger thermal and field hysteresis as is shown in Fig.1. The inhomogeneity of the crystal may lower the structural change. Good crystals having no hysteresis were also obtained. The magnetic properties of F_5PNN-d_{12} was studied and explained by the antiferromagnetic alternating chain model with $2J/k_B = -4.9$ K and $\alpha = 0.65$. Deuteration is considered to work as pressure.

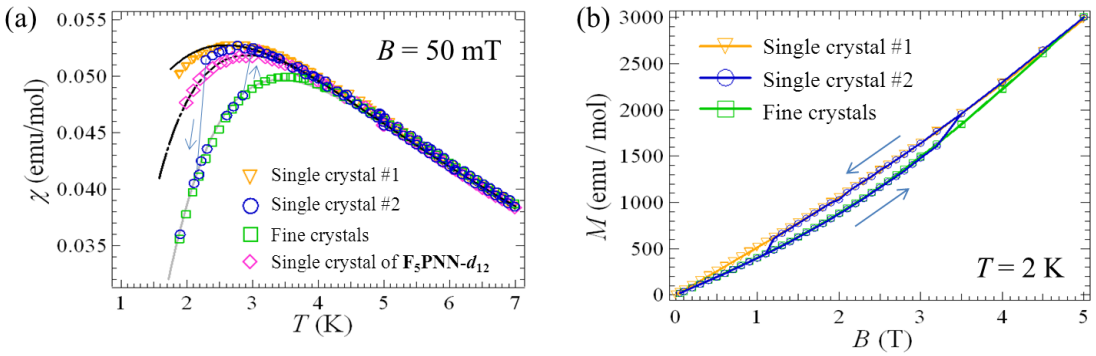

Fig.1 (a) Temperature dependences of magnetic susceptibilities of the crystals of F_5PNN and F_5PNN-d_{12}. Arrows indicate the sweeping direction. Grey solid, dot-dashed and black solid curves represent the calculation for the alternating chain with $2J/k_B = -5.6$ K and $\alpha = 0.4$, with $2J/k_B = -4.9$ K and $\alpha = 0.65$, and for the uniform chain with $2J/k_B = -4.1$ K, respectively. (b) Magnetization curves at 2 K of single crystal #1(▽), #2(○) and fine crystals(□). Solid lines are guide for eye. Arrows indicate the sweeping direction.

References

[1] a) Y. Hosokoshi, M. Tamura, D. Shiomi D, N. Iwasawa, K. Nozawa, M. Kinoshita, H. Aruga Katori and T. Goto, *Physica B*, **201** 497 (1994). b) M. Takahashi, Y. Hosokoshi, H. Nakano, T. Goto, M. Takahashi and M. Kinoshita, *Mol. Cryst. Liq. Cryst*. **306**, 111 (1997)

Low temperature magnetic properties of an organic $S = 1$ ladder BIP-TENO in magnetic fields

N. Hasegawa[A], H. Yamaguchi[A], T. Ono[A], K. Kindo[B], H. Suwa[C], S. Todo[C], Y. Narumi[D], A. Toda[E], Y. Nogami[E], Y. Hosokoshi[A,F]
[A]Dept. of Phys. Sci., Osaka Pref. Univ.,Japan [B]ISSP, Univ. of Tokyo.,Japan
[C]Dept. of Appl. Phys., Univ of Tokyo.,Japan [D]IMR, Tohoku Univ.,
[E]Grad. School of Nat. Sci. and Tech., Okayama Univ., Japan
[F]INR, Osaka Pref. Univ.,Japan
s_n.hasegawa@p.s.osakafu-u.ac.jp

An organic magnetic compound BIP-TENO is the first $S = 1$ ladder substance [1]. Theoretical calculation of $S = 1$ Heisenberg antiferromagnetic ladder by QMC method predicts that its temperature dependence of the susceptibility has a broad peak accompanied by a shoulder peak [2]. In fact, the experimental susceptibility of BIP-TENO shows such a double-peak behavior. However, its magnetization takes a constant at quarter the value of full saturation moment (1/4 magnetization plateau) in the field range of 44 ~ 66 T, which contradicts to the theoretical expectation for an $S = 1$ ladder model (Fig.1).

Recently, we did X-ray diffraction experiments at low temperature, and found the structural phase transition. In the temperature dependence of the susceptibility of BIP-TENO, a small anomaly is detected at about 90K [3], which corresponds to the structural phase transition. The crystal structural analysis at 100 K revealed the loss of the 2-fold symmetry within a molecule, which results in the nonequivalence of two $S = 1$ units within a molecule. This structural change affects the exchange coupling in legs as intermolecular magnetic interactions. Each leg has different magnetic coupling of J_1 or J_2 as is shown in Fig.2 (b). We analyzed the susceptibility data by the QMC calculations, and obtained good agreement by using the antiferromagnetic exchange couplings of $J_0 / k_B = 57$ K and $J_0 : J_1 : J_2 = 1 : 0.6 : 0.3$. This model also reproduces the spin gap, but not the 1/4 magnetization plateau. The 1/4 magnetization plateau suggests further symmetry breaking of the crystal structure and we continue to do the X-ray diffraction experiment below 100K.

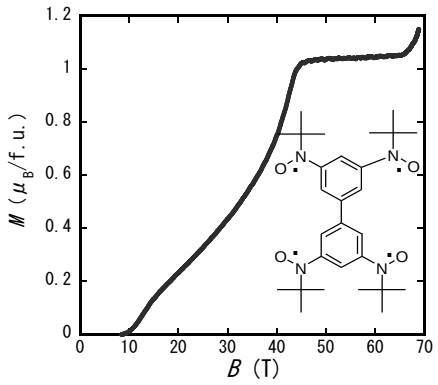

Fig.1. Magnetization curve of BIP-TENO (T=1.3 K)

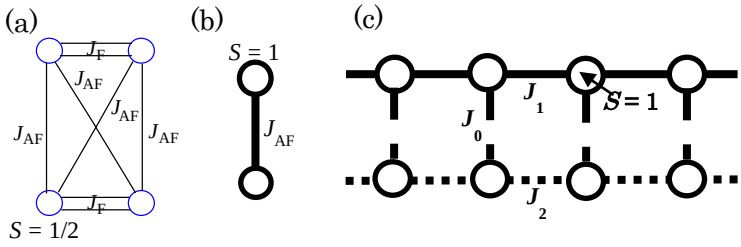

Fig.2 (a). Magnetic model of aBIP-TENO molecule. A circle represents an $S = 1/2$ and the exchange couplings are estimated to $2J_F/k_B = 590$ K and $2J_{AF}/k_B = -20.4$ K [1]. (b) In this paper, a BIP-TENO molecule is treated as a dimer of $S = 1$. (c) The spin ladder model of BIP-TENO. At room temp room temperature $J_1 = J_2$. Symmetry breaking below 100 K brings about $J_1 \neq J_2$

[1] K. Katoh et al., *J. Phys. Chem. Solids*, **63**, 1277 (2002).
[2] S. Todo et al., *Phys. Rev. B*, **64**, 224412 (2001).
[3] Y. Hosokoshi et al., *J. Mag. Mag. Mater.*, **310**, e420 (2007)

Crystal structure and magnetic properties of a new heterobiradical with a nitroxide and a verdazyl PVNO

Y.Tagawa[A], H. Yamaguchi[A], T. Ono[A], Y. Hosokoshi[A,B]
Dept. of Phys. Sci., Osaka Pref. Univ.[A] Japan, INR, Osaka Pref. Univ.[B] Japan
s_y.tagawa@p.s.osakafu-u.ac.jp

We have studied the magnetic properties of nitroxide-based organic magnets. The combination of two kinds of radical species has a benefit to design the magnetic model such as a ferrimagnet. In this study, we report the synthesis, crystal structure and magnetic properties of a new heterobiradical (PVNO, the molecular structure is shown in the inset of Fig.1) made of a nitroxide and a verdazyl radical. Each radical unit has a spin of $S = 1/2$ and a PVNO molecule is expected to form an $S = 1$ species through the strong intramolecular ferromagnetic exchange coupling between two spins of $S = 1/2$.

The X-ray structural analysis was done at room temperature and the magnetic measurements were made in the temperature range of 2 - 300 K and in the magnetic fields up to 5 T in crystalline and DMF solution states.

The crystals PVNO belong to the monoclinic system, space group $P2_1/c$, and the lattice parameters are a = 12.218(4), b = 10.993(4), c = 16.724(6) Å, β = 107.550(5) °, V = 2141.8(13) Å^3, and Z = 4. Between molecules, two kinds of short intermolecular contacts between radical parts were seen. The one is the contacts between the verdazyl radicals, which has the short interatomic distance (N···N 3.40 Å) between the molecules related by an inversion symmetry. Another is the contacts between the nitroxide and verdazyl radicals, O···N 3.44 Å between the molecules with *b*-translational symmetry.

The temperature dependence of the paramagnetic susceptibility χ_p of PVNO crystals is shown in Fig.1 The analysis of the high-temperature data above 200 K in the form of χ_p^{-1} by Curie-Weiss law gives the Curie constant C = 0.92 emu K mol^{-1} and Weiss constant θ = -28.1 K. The estimated value of Curie constant suggests that a PVNO molecule can be regarded as an $S = 1$ species. In fact, the intramolecular magnetic exchange coupling was estimated to $2J_F/k_B$ = 544 K from the magnetic measurements in solution state. The temperature dependence of χ_p of PVNO crystals shows a round peak at 33 K. Below this temperature, χ_p values decrease as decreasing temperature. The upturn below 3.8 K may come from the Curie defects. After subtracting 2.6% of Curie impurity, χ_p values go down to zero as $T \rightarrow 0$. The temperature dependence of the susceptibility was analyzed by both an $S = 1$ antiferromagnetic dimer model and an $S = 1$ Heisenberg antiferromagnetic chain model (1D-HAF) [1]. As a result, only the latter model reproduces the experiments with the intermolecular exchange coupling of $2J_F/k_B$ = -53.2 K and the calculated values are plotted as a solid curve in Fig.1. The relation of the magnetic interaction and molecular packing is discussed.

[1] J. Souletie, Phys. Rev. B 70, 054410 (2004)

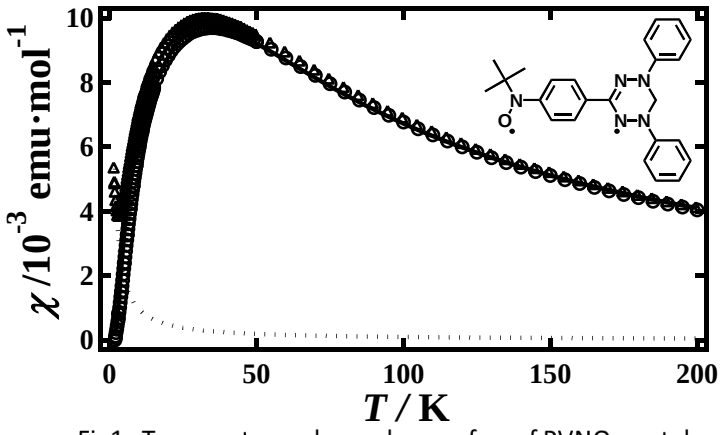

Fig1 Temperature dependence of χ_p of PVNO crystals.

The crystal structure and low-temperature physical properties of an S = 1 organic spin dimer compound Br_2Ph-BNO

K. Iwashita,[1] H. Yamaguchi,[1] T. Ono,[1] A. Matuo,[3] K. Kindo,[3] and Y. Hosokoshi[1,2]
[1]Dept. of Phys. Sci., Osaka Pref. Univ., Japan [2]INR, Osaka Pref. Univ., Japan
[3]ISSP, Univ. of Tokyo., Japan

We have succeeded in synthesizing a new organic biradical Br_2Ph-BNO. Br_2Ph-BNO has two spins of S = 1/2 in a molecule. The structural formula of Br_2Ph-BNO is shown in the set of Fig.1. It is expected that Br_2Ph-BNO molecule forms an S = 1 species by strong intramolecular ferromagnetic interaction between two spins of S = 1/2 [1]. Magnetic measurements were made by using polycrystalline samples. The temperature dependence of the static magnetic susceptibility in the temperature range of 2 - 300 K is shown Fig.1. Solid circles denote the data after subtracting the diamagnetic susceptibility. The magnetic susceptibility data between 200 K and 300 K were analyzed by Curie-Weiss law, and estimated were Curie constant C = 0.978 emu・K/mol and Weiss constant θ = -3.30 K. The estimated value of C means that a Br_2Ph-BNO molecule forms an S = 1 species. The temperature dependence of the susceptibility shown in Fig.1 exhibits a broad maximum at 8.9 K. Below this temperature, susceptibility decreases rapidly. Figure 2 shows a high field magnetization curve measured at 1.3 K. The magnetization rapidly increases at 7 T, reach half the value of full saturation at 10 T, again increases at 15 T, and saturates at 18 T to 2μ_B/f.u. The small magnetization below 7 T is attributable to the Curie defects. This behavior suggests the formation of a dimer of two S = 1 coupled with intermolecular antiferromagnetic interaction.The temperature dependence of susceptibility was analyzed by an isolated S = 1 dimer model $(H = -2J \cdot S_1 \cdot S_2)$ with Curie defects by least square technique and intermolecular interaction $2J/k_B$ = - 9.51 K and the fraction of Curie defects 3.0% were estimated. The solid curve in Fig.1 represents the calculation. The calculation for an S = 1 dimer model with $2J/k_B$ = - 9.51 K also reproduces the magnetization curve as is shown in Fig.2 by the solid curve. In the crystal structure, the short contacts between the dibromophenyl rings are seen between the neighboring molecules. The relation between the molecular packing and the magnetic exchange coupling is discussed.

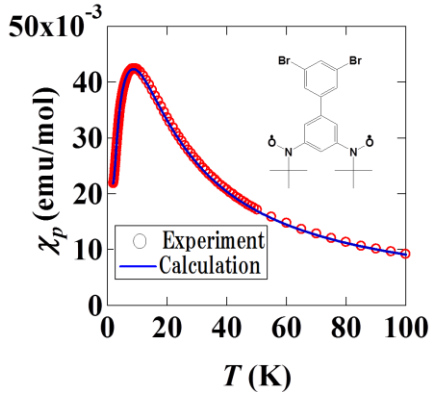

Fig. 1. Temperature dependence of the magnetic susceptibility of Br_2Ph-BNO measured at B = 1 T. The inset shows the structural formula of Br_2Ph-BNO.

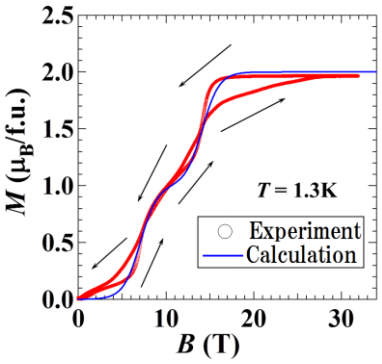

Fig. 2. Magnetization curve at 1.3 K of Br_2Ph-BNO.

[1] Y. Hosokoshi, K. Katoh, Y. Nakazawa, H. Nakano, K.Inoue, *J. Am. Chem. Soc.*, **123**, 7921 (2001).

Low temperatur magnetic properties of an organic triangular spin system, TNN･CH_3CN, in magnetic fields

K. Takada[A], S. Iisaka[A], Y. Takano[B], J.-H. Park[B], T. P. Murphy[B], H. Yamaguchi[A], T. Ono[A], Y. Shimura[C], T. Sakakibara[C], H.Nakano[D], Y.Hosokoshi[A,B]
Dept. of Phys. Osaka Pref. Univ.[A], Univ. of Florida [B], ISSP Univ. of Tokyo[C], Univ. of Hyogo[D]
E-mail address : s_k.takada@p.s.osakafu-u.ac.jp

Geometrically frustrated spin systems have no formulasic magnetic ordering state for a magnetic interaction competing against neighboring spins. One of the simplest frustrate systems is an antiferromagnetic triangular lattice. We have designed a nitronyl nitroxide triradical with threefold symmetry (TNN) as the basic unit of an isolated equilateral triangle with three spins of S = 1/2. TNN molecules crystalize with CH_3CN as solvent molecules in 1:1 ratio. In the crystal structure, the intermolecular contacts afford the triangular network of TNN molecules in the *ab* plane. The intersheet contact along the c axis is also seen. We measured the temperature dependence the magnetic susceptibility for TNN･CH_3CN from 0.1 to 300 K. The monotonous decrease of the product of susceptibility and temperature with decreasing temperature means the existence of intermolecular antiferromagnetic interactions (Fig.1). The calculation assuming the isolated equilateral triangular spin system included mean field approximation reproduced the experiments only above 2 K. The intra- and intermolecular antiferromagnetic exchanges were estimated to J / k_B = -7.93 K, 2z J' / k_B = -3.2 K, respectively, where z is the number of the neighboring spins. The susceptibility for the two-dimensional triangular spin system shown as the inset of Fig.1 was also calculated by numerical exact diagonalization up to 12 spins[1]. The calculation with J' / J = 0.09 and J / k_B = -7.9 K (J' / k_B = -0.71 K) agrees well down to 1 K.

We measured the magnetization at 0.1 K by Faraday's method. The magnetization curves show plateaus at 1/3 of the saturation value, characteristic of antiferromagnetic S=1/2 triangles. Above the plateau, the magnetization of TNN･CH_3CN rises rapidly toward saturation. This linear behavior above the plateau is reproduced by the two-dimensional triangular spin system. In Fig.2, the observed magnetization is compared with calculation by numerical exact diagonalization up to 27 and 36 spins for the parameter set of J' / J = 0.12 and J / k_B = 8.1 K.

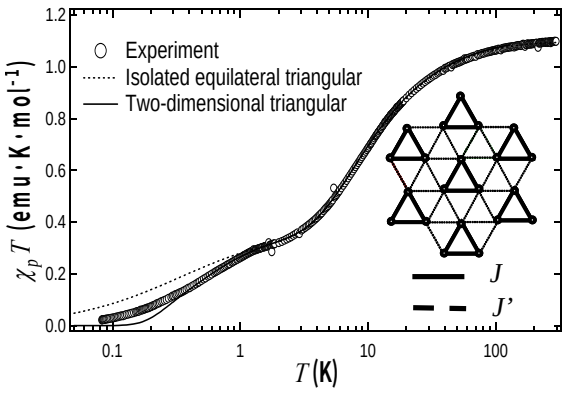

Fig 1. Temperature dependence of χT.

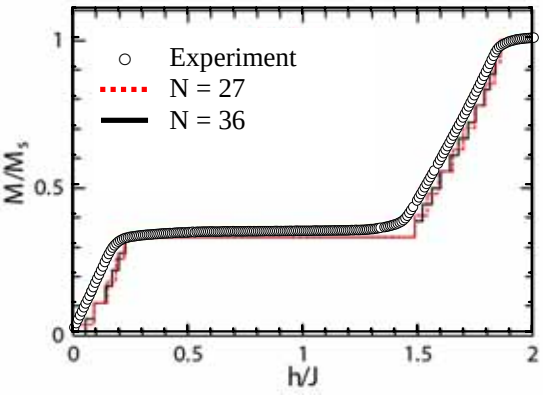

Fig 2. Magnetization curve at 0.1 K.

[1] Morita et al.: J. Phys. Soc. Jpn. 77 （2008）043707

Crystal structure and magnetic properties of organic triangular spin systems, TIM·CH_3CN and BNN·CH_3CN

A. Higashiguchi[A], K. Takada[A], S. Iisaka[A], M. Nakaji[A], H. Yamaguchi[A], T. Ono[A], Y. Takano[B], J.-H. Park[C], T. P. Murphy[C], Y. Hosokoshi[A]
Dept. of Phys. Sci. Osaka Pref. Univ.[A]
Dept. of Phys. Univ. of Florida[B] , NHMFL[C]
E-mail address: s_a.higashiguchi@p.s.osakafu-u.ac.jp

Organic triradical, TNN, TIM, BNN, which have three S = 1/2 spins were obtained. TNN has three NN radicals, TIM has three IM radicals, and BNN has two NN radicals and an IM radical (Fig.1). TNN and TIM can be translated into the same magnetic model that three S = 1/2 spins are arranged on each vertex of an equilateral triangle. BNN is considered as the magnetic model that three S = 1/2 spins are arranged on each vertex of an isosceles triangle (Fig.2). The intramolecular interaction of TNN and TIM were estimated as $2J_{AF}/k_B$ = -7.9 K and $2J_{AF}/k_B$ = -1.7 K, respectively by the magnetic susceptibility measurements with the solution state. The intramolecular interaction of TIM is smaller than that of TNN because IM radicals interact weaker than NN radicals. BNN has both NN and IM radicals and two kinds of intramolecular interactions were determined as $2J_{AF}/k_B$ = -2.1 K and $2\alpha J_{AF}/k_B$ = -5.2 K (α = 2.5). TNN, TIM and BNN are crystalized including CH_3CN as the crystal solvent. They have the isomorphous crystal structure; they construct two-dimensional spin system in the *ab* plane, coupled via inter-sheet contacts along the *c* axis. Replacement of NN radical by IM radical makes the interplanar interactions weaker and increases two-dimensionality.

The low temperature physical property of TNN·CH_3CN was studied and two magnetic ordered phases were observed below 0.25 K between zero field and B_1 = 1.24 T and below 0.34 K between B_2 = 8.45 T and B_3 = 11.28 T by specific heat, magnetocaloric effect and magnetic torque measurements (Fig.3). Recently we started studying TIM·CH_3CN and BNN·CH_3CN to examine how the difference of dimensionality they have affect the physical properties. The magnetic torque measurement of TIM·CH_3CN at 23.7mK showed the critical fields B_1 = 0.60 T, B_2 = 2.26 T and B_3 = 2.98 T, which corresponds to the phase diagram of TNN·CH_3CN. The critical temperatures of TIM·CH_3CN were speculated between 77.3 mK and 100 mK. The magnetic torque measurement of BNN·CH_3CN at 20 mK suggested magnetic ordering below about 2 T and in fields between 7 T and 9 T, but no ordering was observed down to 100 mK in specific heat.

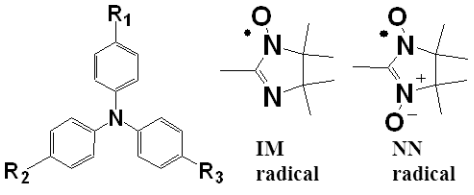

TNN : R_1=R_2=R_3=NN
TIM : R_1=R_2=R_3=IM
BNN : R_1=IM, R_2=R_3=NN

Fig.1 The molecule of TNN, TIM and BNN

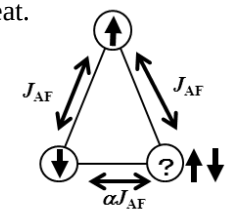

TNN : α = 1
TIM : α = 1
BNN : α = 2.5

Fig.2 The magnetic model of TNN, TIM and BNN

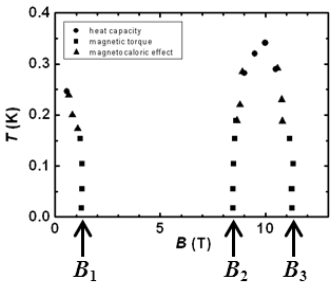

Fig.3 The phase diagram of TNN·CH_3CN

The crystal structures and the magnetic properties of trichlorophenyl nitronyl nitroxide radicals

Naoya Obata [A], Hironori Yamaguchi [A], Toshio Ono [A], and Yuko Hosokoshi [A,B]
[A]Dept. of Phys. Sci., Osaka Pref. Univ., Japan
[B]INR, Osaka Pref. Univ., Japan
s_n.obata@p.s.osakafu-u.ac.jp

The nitronyl nitroxide family is one of the most extensively studied organic radical species due to its good stability and crystallinity. The wide variety of the crystal structure has been reported by changing the substituents.[1] Recently polyfluorinated phenyl nitronyl nitroxide radicals have been reported to form similar crystal structures and a new knowledge about the correlation between the molecular packing and the magnetic exchange coupling has been obtained.[2] In this study, we report the crystal structure and magnetic properties of 2,3,5- and 2,3,6-trichlorophenyl nitronyl nitroxides, abbreviates as 2,3,5-Cl_3PNN and 2,3,6-Cl_3PNN, respectively.

Both new compounds were synthesized by conventional methods and crystal structures were solved at room temperature. Static magnetic measurements were made in the temperature range of 2 - 300 K and in the magnetic fields of up to 5 T by using single crystals.

The 2,3,5-Cl_3PNN crystals belong to a monoclinic system, space group $P2_1/n$. The temperature dependence of the product of magnetic susceptibility χ and temperature, χT, which is proportional to the square of the effective magnetic moments, is plotted in Fig.1 (a). The increase of χT value as decreasing T means the existence of the intermolecular ferromagnetic interactions. The observed data are well reproduced by the S = 1/2 dimer model with the ferromagnetic exchange coupling of $2J/k_B$ = 10.3 K adopted weak interdimer ferromagnetic interactions of $2J/k_B$ = 0.82 K by mean-field approximation.

The 2,3,6-Cl_3PNN crystals belong to a monoclinic system, space group $C2/c$. As is shown in Fig.1 (b), the gradual decrease of χT value as decreasing T means the existence of the intermolecular antiferromagnetic interactions. The observed data are well reproduced by the S = 1/2 antiferromagnetic alternating chain model with the parameter set of $2J/k_B$ = -1.2 K and alternating ratio α = 0.8.

The molecular arrangements of these compounds are compared with the ones of related compounds such as fluorinated phenyl nitronyl nitroxides. The relations between the molecular packing and the magnetic exchange coupling are discussed.

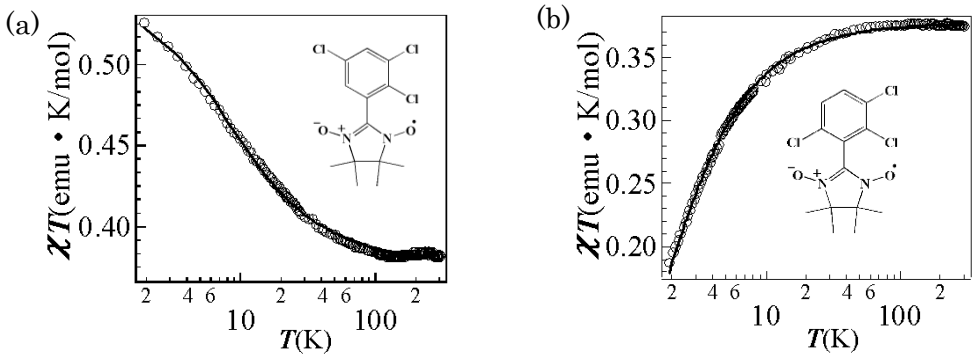

Fig.1 Temperature dependences of χT of (a) 2,3,5-Cl_3PNN and (b) 2,3,6-Cl_3PNN.
○: experiment, —: calculation

[1] Y.Hosokoshi, et al, Physica B, **201** (1994) 497.
[2] T.Kanzawa, et al, Bull. Chem. Soc. Jpn, **83** (2010) 1447.

Strong Renormalization of Spin Wave Spectrum in an $S = 1/2$ Kagome Antiferromagnet

Toshio Ono, Hironori Yamaguchi, Yuko Hosokoshi
Department of Physical Science, Osaka Prefecture University, Japan
Kittiwit Matan
Department of Physics, Mahidol University, Thailand
Nambu Yusuke, Taku J Sato, Jun-ichi Yamaura
Institute for Solid State Physics, The University of Tokyo, Japan
Hidekazu Tanaka
Department of Physics, Tokyo Institute of Technology, Japan

Kagome lattice antiferromagnet (KAFM) which is built from vertex sharing triangles is one of the most attractive spin model among the geometrically frustrated spin systems. In the classical spin model, three spins on a local triangle form a 120° structure. New degree of freedom *chirality* arise from 120° spin structure leads infinite degeneracy in the ground state of KAFM. When the degeneracy is lifted by the additional interactions such as the next-nearest-neighbor interactions or Dzyaloshinskii-Moriya (DM) interactions, the spin structure so-called $q = 0$ or $\sqrt{3} \times \sqrt{3}$ structure is stabilized. Figure 1(b) shows the spin arrangement of $q = 0$ structure.

$Cs_2Cu_3SnF_{12}$ is an $S = 1/2$ KAFM which undergoes antiferromagnetic phase transition at $T_N = 20$ K [1]. In order to investigate the ground state and magnetic excitations of $Cs_2Cu_3SnF_{12}$, we have performed elastic and inelastic neutron scattering experiments using single crystals. Figure 1 (a) shows the temperature dependence of the reflection from $\boldsymbol{Q} = (1, 1, 0)$. Magnetic Bragg reflection is clearly observed below $T < T_N = 20$ K. All magnetic Bragg reflections appear at $\boldsymbol{Q}$-positions where the nuclear Bragg reflections were observed. This result indicates that the magnetic structure is $q = 0$ structure. Within the energy range up to $E = 20$ meV, we observed three spin wave modes. When we assume the generic Hamiltonian which includes Heisenberg exchange interactions and Dzyaloshinskii-Moriya interactions, three modes can be interpreted as in/out-of plane modes and zero-energy mode as shown in Fig. 1 (c) [2, 3]. The magnitude of the nearest-neighbor interaction J estimated from the spin-wave excitation is $J = 11.5$ meV. This value is approximately one-half of $J/k_B = 240$ K (= 20.7 meV) evaluated from the magnetic susceptibility [1]. We argue that the discrepancy between these values arise from *negative* quantum renormalization of spin-wave energies which is proposed by theoretical studies for $S = 1/2$ triangular antiferromagnetic system [4].

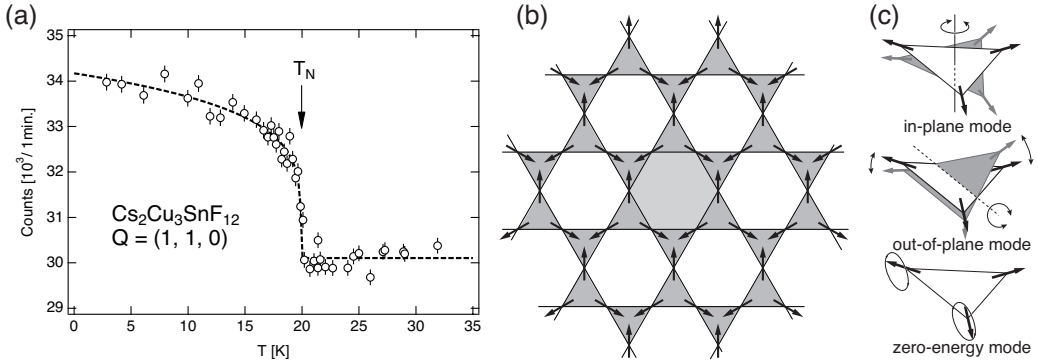

Figure 1: (a) Temperature dependence of Bragg reflection from $\boldsymbol{Q} = (1, 1, 0)$. Magnetic Bragg peak emerges at $T_N = 20$ K indicated by an arrow. (b) Spin arrangement of $q = 0$ spin structure. (c) Three kinds of spin-wave modes expected in KAFM.

References

[1] T. Ono *et al.*, *Phys. Rev. B* **79** (2009) 174407.

[2] K. Matan *et al.*, *Phys. Rev. Lett.* **96** (2006) 247201.

[3] T. Yildirim and A. B. Harris, *Phys. Rev. B* **73** (2006) 214446.

[4] A. L. Chernyshev and M. E. Zhitomirsky: *Phys. Rev. B* **79** (2009) 144416.

Construction of Low-Temperature Thermal Relaxation Calorimeter for Small Amount of Samples

Yuki, Horie, Shuhei Fukuoka, and Yasuhiro Nakazawa
Department of Chemistry, Graduate School of Science,
Osaka University, Machikaneyama 1-1, Osaka 560-0043, JAPAN
horiemon@chem.sci.osaka-u.ac.jp

Low-temperature heat capacity measurements system using handy dilution refrigerator was constructed in order to perform thermodynamic investigations on small amount of samples. We have made a relaxation calorimetry cell consisting of a small chip type thermometer and a film type heater. The thermometer used for this cell was 1kΩ ruthenium oxide. The sample stage is weakly linked to the heat sink made of Ag by thin constantan wires which are also used for lead wires for a thermometer and a heater. The calorimetry cell is mounted on small dilution refrigerator of which outer diameter of the adiabatic space is 27mm. The schematic illustration is shown in Fig.1. This dilution refrigerator is constructed for using in combination with the variable temperature insert of the supercondyuctive magnets of which maximum fields is 15 T in the vertical direction. By the combination with split pair magnet of 7T, we can also measure heat capacity in the horizontal direction.

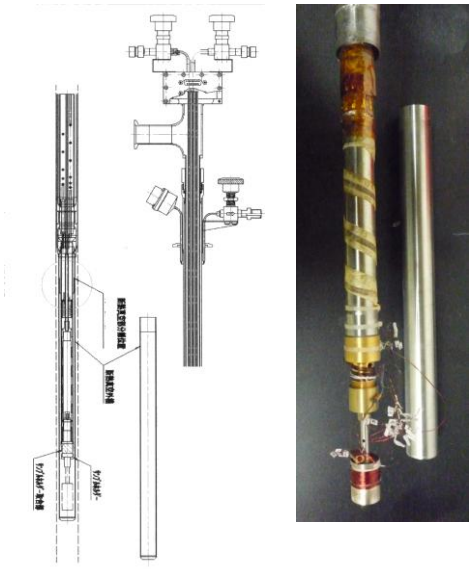

Fig.1 Schematic view of the refrigerator and a picture around the calorimetry cell.

Using this dilution refrigerator, we discuss the possibility to measure heat capacity of small amount of powder sample or microcrystal samples. We report on the heat capacity measurement results of pellet sample of intermetallic sample and nanographite sample prepared by some different heat treatment conditions[(1)]. Since the sample is air unstable, we handled them in Ar atomosphere and rapped them by thin silver foil of which heat capacity is measured by different experiment. The low temperature heat capacity results of nanographite shows that the electronic heat capacity coefficient is enhanced probably due to the interaction claims that the heat capacity of conduction electrons are enhanced probably due to the interactions with localized spins. The discussion on the electronic states is discussed including their magnetic fields dependences.

References,
(1) T. Enoki *et al*. *Diamond Related Mater.* (2007), **16**, 2029.

Thermodynamic Study of Chiral Molecule Magnets

Shuhei Fukuoka,[1] Takashi Yamamoto,[1] Yasuhiro Nakazawa,[1] Hiroyuki Higashikawa,[2] and Katsuya Inoue [2]
[1]Department of Chemistry, Graduate School of Science, Osaka University, Osaka, 560-0043, Japan
[2]Graduate School of Science, Hiroshima University, Hiroshima, 739-8526, Japan
fukuoka@chem.sci.osaka-u.ac.jp

Chirality is an important factor to control physical properties of materials. If the spin species in molecules have chiral structure, magnetic properties, especially under magnetic fields can be influenced. Chiral magnets exhibit novel magnetic properties and optical response such as giant non-linear magnetic response[1] and magneto-chiral dichroism (MChD)[2] due to the asymmetric crystal structures. When the crystal structure is chiral, it is expected that magnetic moments also form chiral magnetic ordering. The origin of chiral magnetic ordering can be ascribed to Dzyaloshinsky-Moriya (D-M) interaction and chiral arrangement of anisotropic spins. In this study, we performed heat capacity measurements for polynuclear metal complex salt $[W(CN)_8]_4[Cu(pn)H_2O]_4[Cu(pn)]_2 \cdot 2.5H_2O$ (which is abbreviated as W-Cu complex)[3] using ~10^2μg single crystal and observed unique thermodynamic behavior under magnetic fields.

As shown in Figure 1, the organic ligands of pn (=1,2-diaminopropane) have two chiral structures. Because of this structural difference around Cu^{2+}, the yielded crystals of the W-Cu complex are classified into these different compounds (*R*- and *S*-complex and racemic complex).

Figure 2 shows the results of heat capacity measurements for *R*-W-Cu complex. The large thermal anomaly was observed, which is associated with a formation of an antiferromagnetic ordering. Interestingly, when magnetic field was applied parallel to crystallographic *b*-axis, sharp anomaly appeared. On the other hand, no sharp anomaly was observed when magnetic field was applied parallel to *c*-axis. Similar behavior was also observed in *S*-W-Cu complex. From the magnetization measurements, it is known that chiral complexes form canted antiferromagnetic ordering (CAF) due to the D-M interaction and weak ferromagnetic moments exist parallel to *b*-axis for chiral complexes. These observations indicate that sharp anomaly is ascribed to a transition to an asymmetric spin structure from original CAF ordering.

[1] M Mito *et al*., *Phys. Rev. B* **79** (2009) 012406.
[2] C. Train *et al*., *Nature Mater*. **7** (2008) 729 – 734.
[3] H. Higashikawa *et al*., *Chem. lett*. **36** (2007) 1022.

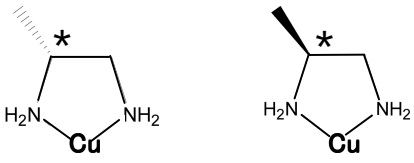

pn=1,2-diaminopropane

Figure 1 organic ligands introducing crystallographic chirality.

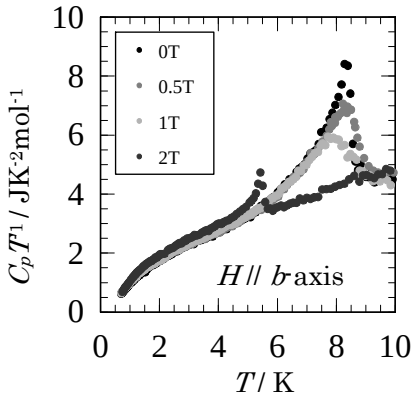

Figure 2 C_pT^{-1} vs T curves for *R*-W-Cu complex.

Fabrication and structural evaluation of Two Dimensional Polymer Sheets composed of a triangle-shape molecule connected by hydrogen/coordination bonding

○Tsuchiyama Kohei,[1] Makiura Rie[1,2]
[1]Nanoscience and Nanotechnology Research Center, [2]JST-CREST
k-tsuchiyama@pe.osakafu-u.ac.jp

Introduction

Two Dimensional Polymer Sheets (2DPSs) as shown in Fig.1 have been actively studied because of their potential applications to nanometer-scaled devices. Their properties such as conductivity, catalysis and guest molecular storage can be varied by choosing molecular components and designing structures. Methodological approaches of fabricating 2DPSs are generally categorized into two groups; top-down method and bottom-up method. We focus on the bottom-up method because it enables us to arrange the structures at the nanoscale, resulting in tuning their functionalities. Direct deposition of molecules onto a solid substrate such as chemical vapor deposition limits the substrate materials because we have to consider the interaction between the substrate and molecules. In order to freely arrange 2DPSs, it is necessary to eliminate the influence from the substrate. Therefore, we adopted liquid surfaces for assembling molecules: Langmuir-Blodgett (LB) method. Because of fabricating 2DPSs on liquid surface at first, we are able to eliminate the influence from the substrate and utilize many kinds of substrates. Furthermore, it is possible to develop 2DPSs to three dimensional frameworks by stacking them in a layer-by-layer manner.

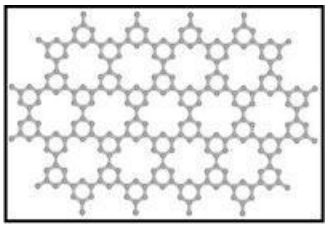

Fig.1 Two dimensional polymer sheet

Experiments

The components of 2DPSs are 1,3,5-tri(4-carboxyphenyl)-benzene (BTB) and Cu^{II} ion. We fabricated two types of 2DPS —BTB-water and BTB-Cu— on liquid surfaces by LB method and transferred them to Si(100) substrates in a layer-by-layer manner. The BTB-water sheet was fabricated on purity water subphase and BTB molecules are connected each other by hydrogen boning. On the other hands, BTB-Cu sheet was fabricated on $Cu(NO_3)_2 \cdot 3H_2O$ aqueous solution subphase and BTB molecules are connected via Cu^{II} ion by coordination bonding.

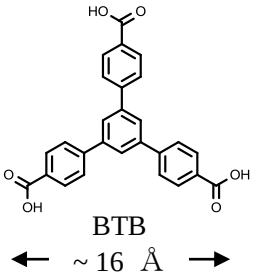

The IR spectra were collected to evaluate the layer-by-layer stacking and the chemical bonding manner. The synchrotron XRD measurements were performed to evaluate their crystal structures.

Results and discussion

In-plane XRD pattern of BTB-Cu nanoscaled sheet is shown in Fig.2. Observation of several reflections is evidential for that the BTB-Cu sheet is highly crystalline. The crystal system and lattice parameter are evaluated as orthorhombic, a = 28.86 (1) Å, b = 16.401 (7) Å, respectively. From the XRD profile and considering the size of BTB, we constructed structural model as shown in Fig.3. The calculated in-plane profile from the structure model is in good agreement with the observed profile (Fig.2), indicating that the BTB-Cu sheet is perfectly oriented.

Out-of-plane XRD patterns were also measured to evaluate stacking manners. These results and IR absorption spectra will be presented in the poster.

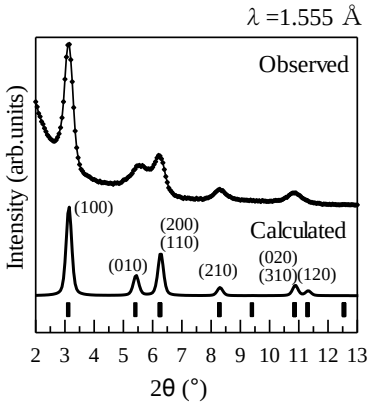

Fig.2 In-plane XRD patterns of the BTB-Cu sheet

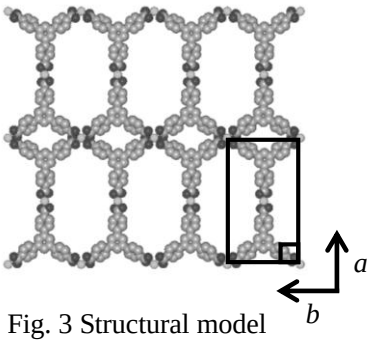

Fig. 3 Structural model of the BTB-Cu sheet
・Orthorhombic system
a = 28.7 Å, b = 16.4 Å

Control of the in-plane molecular arrangement of metal-organic framework nanofilms: application of a ditopic *trans*-coordinative porphyrin derivative

Ryo Usui[1] · Rie Makiura[1,2]
Nanoscience Nanotechnology Research Center, Osaka Prefecture University. Japan[1]
JST-CREST[2]
r-usui@pe.osakafu-u.ac.jp, r-makiura@21c.osakafu-u.ac.jp

[Introduction]

New porous materials – metal-organic frameworks (MOFs) – have been studied extensively in recent decades. These materials are composed of metal complexes and secondary building units and their structure can be controlled by the choice of building blocks. They exhibit various properties, such as gas adsorption, separation, and catalysis. Taking note of these features, many MOFs have been reported as bulk crystals. However, growing MOFs on substrates as thin films is more challenging although it is highly desirable as in this way, they can be integrated in nanodevices. MOF nanofilms consisting of tertratopic porphyrin drivatives as building blocks have been recently reported.[1],[2] In this work, we demonstrate how to exercise control of the in-plane molecular arrangement of MOF nanofilms using ditopic *trans*-substituted porphyrin derivatives.

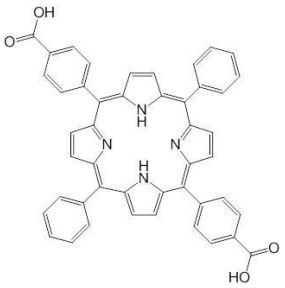

Fig. 1 *trans*-H_2DCPP

[Experiments]

In the nanofilm fabrication procedure, 5,15-diphenyl-10,20-di(4-carboxyphenyl) porphine (*trans*-H_2DCPP, Fig. 1) and $Cu(NO_3)_2 \cdot 3H_2O$ were dissolved in chloroform/MeOH mixed solvent and pure water, respectively, and films were grown by the Langmuir-Blodgett (LB) method. The single-layer LB films were transferred to substrates and multilayer films were grown following a Layer-by-Layer protocol (LbL). UV-Vis and IR absorption spectroscopic measurements were used in their characterization. Synchrotron X-ray diffraction (XRD) measurements were performed in order to establish the in-plane molecular arrangement.

[Results]

Trans-H_2DCPP-Cu films were fabricated by the LB-LbL method and transferred to a Si substrate. IR spectroscopy confirmed the formation of $Cu_2(COO)_4$ paddle-wheel bridging units. The films were also transferred to a quartz substrate and their UV-Vis absorption spectra were measured. These indicated that equal numbers of *trans*-H_2DCPP molecules were deposited on the substrate after each LB-LbL deposition cycle (Fig. 2). The measured in-plane XRD pattern of a 30-layer nanofilm allowed us to derive a structural model of the in-plane molecular arrangement by comparing the simulated and measured diffraction profiles (Fig. 3). Compared with the in-plane lattice dimensions (a= b= 16.477 Å) of NAFS-2[2] which comprises tetratopic porphyrin building units, here we find an increased size of the basal plane (a= b= 23.30(3) Å) as a result of the changed coordinative bridging network.

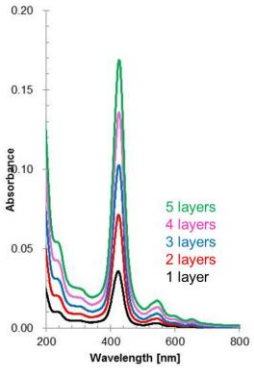

Fig. 2 (left) UV-Vis absorption spectra of *trans*-H_2DCPP-Cu films

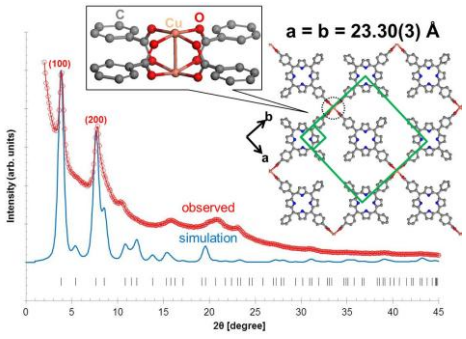

Fig. 3 (right) Measured and simulated in-plane XRD patterns (λ = 1.553 Å) of a 30-layer trans-H_2DCPP-Cu film and the proposed in-plane structural model (inset)

[Conclusion]

We fabricated crystalline MOF nanofilms by the LB-LbL method and were able to successfully control the in-plane structure by employing a ditopic *trans*-H_2DCPP-Cu building unit.

[Reference]

[1] R. Makiura, *et. al.*, *Nature Mater.*, **9**, 565 (2010)
[2] S. Motoyama, R. Makiura, *et. al.*, *J. Am. Chem. Soc.*, **133**, 5640 (2011)

Nanoparticles-Embedded and Crosslinked Hydrogels Capable of Very Slow-Release of a Model Drug

Yasutaka Watanabe[1] and Chie Kojima[2]
[1]*Department of Electronics and Physics, Graduate School of Engineering, Osaka Prefecture University, Japan,* [2]*Nanoscience and Nanotechnology Research Center, Research organization for 21st Century, Osaka Prefecture University, Japan*
E-mail (YW): y-watanabe@pe.osakafu-u.ac.jp

[**Introduction**]
Liposomes are nanoparticles with lipid bilayers and have been studied for many years as a drug carrier. Actually, hydrophilic and hydrophobic drugs can be encapsulated in the inner aqueous phase and in the lipid membrane, respectively. Liposomes are useful for reducing side effect of drug. Besides, control of the drug level in body is also indispensable. Gradual release from drug implants can achieve one-shot drug administration, which lessens some pains in patients. Thus, we attempted to construct very slow drug release system. Hydrogels take advantages of drug loading and slow release. However, the release rate of drug from hydrogel is still high. Therefore, we designed drug loading liposomes-embedded hydrogels. In this study, we used folic acid and gelatin gel as a model drug and a hydrogel, respectively. Folic acid is vitamin B9, acts as a co-enzyme and has similar structure to methotrexate, an anticancer drug. Gelatin gels are classically used as a biomaterial and are clinically approved. Crosslink of the hydrogel is important to regulate the stability as well as the size of mesh structure, which is a key factor for the controlled release. In this study, we prepared folic acid-containing liposomes and the hydrogel embedding the liposome. And, the gelatin gels were crosslinked using a condensation agent (4-(4,6-Dimethoxy-1,3,5-triazin-2-yl)-4-methylmorpholinium Chloride, DMT-MM) at different reaction ratios. The time-dependent release of folic acid from various types of gelatin gels was investigated.

[**Methods**]
Chloroform solution dissolving egg yolk phosphatidylcholine (EYPC) (10 mg) was added to glass flask. After the solvent was removed, 500 μl of folic acid aqueous solution was added and sonicated, followed by four times repeats of freeze and thaw to load folic acid into liposomes. After the centrifugation (4^{o}C, 30 min, 15,000 g), the supernatant was removed. Several times centrifugation was performed to remove free folic acid. UV-Vis spectrophotometry was performed to estimate the folic acid concentration in the presence of detergents. Gelatin (6wt%) was dissolved in water at 40^{o}C, and solution of folic acid-loading liposomes or free folic acid (1.02 mM) was added to the gelatin sol, followed by the addition of DMT-MM solution at various ratios. After the 4^{o}C incubation, drug-loading and crosslinked gelatin gels were prepared. 500μl of phosphate buffer saline (PBS) was added on the hydrogel and incubated at 37^{o}C in the dark. After 3, 12 and 24 hours, 3 days and one week, the PBS solutions on the hydrogel were collected and measured by UV-Vis spectrometry.

[**Results and Discussion**]
1.14% folic acid could be loaded in the liposome. Gelatin gels were dissolved at 37^{o}C in the absence of DMT-MM, but were stably formed in the presence. DMT-MM can link carboxyl groups and amino groups in gelatin to stabilize the hydrogels. Folic acid-loading liposomes could be embedded in the crosslinked hydrogels. The embed of liposome into the hydrogel was effective for suppressing the drug release. In addition, cross-linked gelatin gel is also effective for the slow release. Especially, more than 25wt% addition of DMT-MM to gelatin efficiently suppressed the release of folic acid. Liposome-embedded gelatin gel in the presence of 50wt% DMT-MM released less than 20% folic acid even after one week at 37^{o}C. Taken together, crosslinked gelatin gel embedding drug-containing liposomes are useful for sustained drug-release.